

Medical University of South Carolina

MEDICA

MUSC Theses and Dissertations

2012

Mitochondrial Iron Uptake Through Mitoferrin2 Sensitizes Human Head and Neck Squamous Carcinoma Cells to Photodynamic Therapy

Hsin-I (Cindy) Hung
Medical University of South Carolina

Follow this and additional works at: <https://medica-musc.researchcommons.org/theses>

Recommended Citation

Hung, Hsin-I (Cindy), "Mitochondrial Iron Uptake Through Mitoferrin2 Sensitizes Human Head and Neck Squamous Carcinoma Cells to Photodynamic Therapy" (2012). *MUSC Theses and Dissertations*. 622.
<https://medica-musc.researchcommons.org/theses/622>

This Dissertation is brought to you for free and open access by MEDICA. It has been accepted for inclusion in MUSC Theses and Dissertations by an authorized administrator of MEDICA. For more information, please contact medica@musc.edu.

Mitochondrial Iron Uptake Through Mitoferrin2 Sensitizes
Human Head and Neck Squamous Carcinoma Cells to Photodynamic Therapy

by

Hsin-I Hung (Cindy)

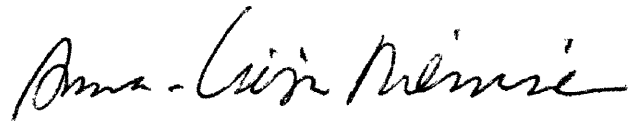
A dissertation submitted to the faculty of the Medical University of South Carolina in
partial fulfillment of the requirements for the degree of Doctor of Philosophy in the
College of Graduate Studies

Program of Molecular and Cellular Biology and Pathobiology Cancer Biology Track

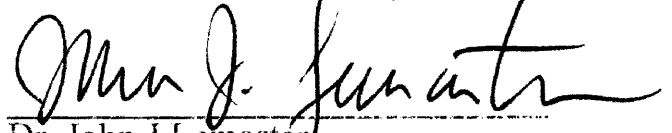
2012

Approved by


Chairman, Advisory Committee:



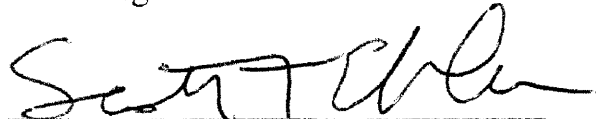
Dr. Anna-Liisa Nieminen, Advisor



Dr. John J Lemaster



Dr. Craig C Beeson



Dr. Scott T Eblen



Dr. Christina Voelkel Johnson

Dedication

This is dedicated to my parents and to the rest of my family and friends for their always support and encouragement during this time in my life.

Acknowledgement

It would not have been possible to have a small yet complete and interesting research story finished and write this doctoral dissertation without the help and support from all the kind people around me. Nevertheless, only some of whom is it possible to thank here.

First and foremost, I would like to specifically thank my advisor, Dr. Anna-Liisa Nieminen, for her endless support and guidance. Anna-Liisa gives me the freedom to explore all the possibilities of my scientific approach and learn from all the expected as well as unexpected results and findings. My scientific thinking was refined through numerous constructive discussions with her. I really appreciate her impeccable patience to lead me through this research and also through non-scientific matters. I felt so blessed to be supervised by her during my PhD training. I have learned from her and been inspired by her in all our interactions. My scientific curiosity has not only been satisfied but also has increased through my interactions with her.

I would like to thank Dr. John Lemasters, for his unlimited guidance and patience through constant and valuable suggestions and discussions. Special thanks also go to my dissertation committee members, Dr. Craig Beeson, Dr. Scott Eblen, and Dr. Christina Voelkel Johnson, for their continuous insightful suggestions and advice. I benefit every time from the discussion and questions in my committee meetings.

I would like to show my gratitude to the MUSC graduate program and all the involved faculties and staffs for expending their effort to better prepare us as future scientists. Among these, I would especially thank Dr. Perry Halushka, Dr. Cynthia Wright, Dr. Edward Krug, Dr. Thomas Smith at MUSC Writing Center, Mrs. Dodie Weise, Mrs. Marianne Rogers, and Mrs. Keisha Brown. I feel very lucky and proud to be a student at MUSC, and I hope MUSC will be proud of me in the future.

I owe sincere and earnest thankfulness to all the people I have worked with and come to know during my PhD training. I would like to thank my rotation advisors, Dr. Dennis Watson, Dr. Besim Ogretmen, and Dr. James Norris, for their guidance and support. Although the rotation time is a short period of time, I learned and gained new knowledge and skill. I am thankful to many people from both Dr. Nieminen's and Lemasters' lab--David, Venkat, Justin, Eduardo, Greg, Xun and Suparna--for their constant mental support and knowledge sharing. It is a great pleasure to work with and know all these people. Thanks to all my friends at MUSC for their kind support and inspiration.

Last but not least, I would like to thank my parents for their constant support and love through all these times. Thanks also to my government for providing me the USD 150,000 fellowship support to come to USA to learn. I hope I will be able to bring some new information to benefit my country in the future.

Table of Contents

Dedication.....	ii
Acknowledgements.....	iii
Abbreviations.....	viii
Abstract.....	x

Chapter 1: Review of Head and Neck Cancer, Photodynamic Therapy, and Iron

Physiology and Pathophysiology.....	1
1.1 Head and Neck Cancer.....	2
1.11 Epidemiology and Etiology	2
Risk factors.....	4
1.12 Pathogenesis... ..	7
1.13 Treatment Modalities for Head and Neck Cancer	10
Molecular Targeted Therapies.....	11
1.2 Photodynamic Therapy.....	14
1.2.1. Photosensitizers.....	15
Porphyrin Derived Photosensitizers.....	16
Non-Porphyrin Photosensitizers.....	22
Subcellular Localization	26
1.2.2. Photochemistry of PDT.....	26
1.2.3 Light Sources and Light Delivery.....	29
1.2.4. Role of Oxygen in Photodynamic Therapy... ..	31
1.2.5. Mechanisms of PDT-Mediated Cytotoxicity.....	31
1.2.5.1. Direct Cytotoxicity.....	32
1.2.5.2. Vascular Effects.....	35

1.2.5.3. Immune Responses.....	36
1.2.6. Combination of PDT with Other Therapies.....	37
1.3 Iron Physiology and Pathophysiology.....	39
1.3.1. Cellular Iron Regulation.....	41
Mitochondrial Iron Regulation.....	45
1.4 Aim and Outline of the Project.....	47
Chapter 2: Role of Iron in Pc 4-PDT-Treated Head and Neck Cancer Cell Lines	48
.....	48
Introduction.....	49
Materials and Methods.....	52
Results.....	57
<i>Cellular uptake and subcellular localization of pc 4 in head and neck cancer cells.....</i>	<i>57</i>
<i>Head and neck cancer cells respond differently to PDT.....</i>	<i>57</i>
<i>Bafilomycin enhances PDT killing in both resistant and responsive cell lines.....</i>	<i>58</i>
<i>Iron chelators and ru360 protect against bafilomycin-enhanced PDT killing.....</i>	<i>61</i>
<i>Lysosomal iron augments bafilomycin plus pc 4-PDT-mediated cell killing.....</i>	<i>62</i>
<i>Bafilomycin enhanced pc4-PDT killing through lysosomal iron release without causing lysosomal membrane permeability.....</i>	<i>63</i>
<i>Ferristatin protects cells against bafilomycin-mediated PDT toxicity</i>	<i>65</i>
<i>Chloroquine retards regrowth of tumors after PDT.....</i>	<i>66</i>
Discussion.....	67
Chapter 3: Role of Mitochondrial Iron Transporter Mitoferrin2 in Pc 4-PDT Treatment.....	85
Introduction.....	86
Materials and Methods.....	89

Materials and Methods	89
Results	93
<i>Differential endogenous Mfrn-2 gene and protein expression in head and neck cancer cells</i>	93
<i>Downregulation of Mfrn2 results in decreased mitochondrial Fe²⁺ uptake</i>	94
<i>Downregulation of Mfrn2 delays mitochondrial depolarization and cell death after PDT plus bafilomycin</i>	95
<i>Increased expression of Mfrn2 enhances cell death in resistant head and neck cancer cells after PDT plus bafilomycin</i>	96
Discussion	97
Chapter 4: Summary and Future Directions	108
<i>Role of DMT1 in lysosomal iron release after bafilomycin</i>	109
<i>Mitochondrial iron regulation</i>	109
<i>Signaling pathways induced by bafilomycin-enhanced Pc 4-PDT</i>	111
<i>In vivo studies</i>	111
<i>Nanoparticles</i>	112
Significance and Conclusion	114
References	115

Abbreviations

5-ALA	5-Aminolevulinic acid
DFO	Desferrioxamine
DMEM	Dulbecco's modified eagle's medium
EBV	Epstein-Barr virus
EGF	Epidermal growth factor
EGFR	Epidermal growth factor receptor
EPO	Erythropoietin
FBS	Fetal bovine serum
FDA	Food and Drug Administration
HBO	Hyperbaric Oxygen
HDL	High-density lipoprotein
HPD	Hematoporphyrin derivative
HPV	Human papillomavirus
ICB	Intracellular buffer
IL	Interleukin
ITX	Insulin-transferrin-selenium-X
LDL	Low-density lipoprotein
mAb	Monoclonal antibody
MCF	Mitochondrial carrier family
MCU	Mitochondrial calcium uniporter
Mfn1	Mitoferrin1
Mfn2	Mitoferrin2
NNK	4-(methylnitrosamino)-1-(3-pyridyl)-1-butanone
NNN	N'-nitrosonornicotine
NPC	Nasopharyngeal carcinoma
OH•	Hydroxyl radical
OSCC	Oral Squamous Cell Carcinoma
PAHs	Polycyclic aromatic hydrocarbons
PBS	Phosphate buffered saline
Pc	Phthalocyanine
PDT	Photodynamic therapy
PEG-PCL	Polyethyleneglycol–polycaprolactone
PI	Propidium iodide
PI3CA	Phosphatidylinositol 3-kinase p110 alpha
Rh123	Rhodamine 123

RIP1	Receptor-interacting protein 1
ROS	Reactive oxygen species
RT PCR	Real time PCR
Ru360	Ruthenium 360
sDFO	Starch-desferrioxamine
SDS	Sodium dodecyl sulfate
TGF- β	Transforming growth factor beta
TMRM	Tetramethylrhodamine methyl ester
UADT	Upper Aero-Digestive Tract

Abstract

Photodynamic therapy (PDT) is an FDA-approved, minimally invasive treatment modality that utilizes light in the presence of oxygen to activate photosensitizing agents to produce cell death. Phthalocyanine 4 (Pc 4), a second generation photosensitizer has shown efficacy *in vitro*, *in vivo* and in a phase I clinical trial. Pc 4 localizes primarily to mitochondria and endoplasmic reticulum, where it causes apoptotic cell death during PDT. Previously, our laboratory showed that photosensitizers that localize to lysosomes are more effective in killing cancer cells than ones directed to mitochondria after PDT. Here, we investigated the interactions between lysosomes and mitochondria in promoting the efficiency of PDT cell killing efficiency. Three head and neck cancer cell lines (UMSCC1, UMSCC14A and UMSCC22A) were exposed to Pc 4-PDT. The 3 cell lines responded differently: UMSCC1 and UMSCC14A cells were more resistant, whereas UMSCC22A cells were more sensitive to Pc 4-PDT. In non-erythroid cells, the mitochondrial iron transporter mitoferrin2 (Mfrn2) localizes on the mitochondrial inner membrane and transports iron from the cytosol into the mitochondria. PDT-sensitive cells expressed higher Mfrn2 mRNA and protein levels compared to PDT-resistant cells. High Mfrn2 expressing cells showed higher rates of mitochondrial Fe^{2+} uptake compared to low Mfrn2 expressing cells. Bafilomycin, an inhibitor of the vacuolar proton pump of lysosomes and endosomes that releases lysosomal iron to the cytosol, enhanced PDT-induced cell killing of both resistant and sensitive cells. Inhibition of the divalent metal transporter 1 (DMT1) on lysosomal membranes by ferristatin markedly protected high Mfrn2 expressing cells against bafilomycin-enhanced PDT toxicity, suggesting that iron

release after bafilomycin occurs *via* DMT1. Iron chelators and the inhibitor of the mitochondrial Ca^{2+} (and Fe^{2+}) uniporter, Ru360, protected against PDT plus bafilomycin toxicity. Knockdown of Mfrn2 in UMSCC22A cells decreased the rate of mitochondrial Fe^{2+} uptake and delayed PDT plus bafilomycin-induced mitochondrial depolarization and cell killing. Conversely, increased expression of Mfrn2 in low Mfrn2 expressing UMSCC1 cells increased PDT plus bafilomycin-induced killing. Chloroquine, which also releases iron from lysosomes, significantly delayed tumor regrowth in high Mfrn2 expressing tumors after PDT. Taken together, the data suggest that lysosomal iron release and mitochondrial iron uptake through Mfrn2 act synergistically to induce PDT-mediated and iron-dependent mitochondrial dysfunction and subsequent cell killing. Furthermore, Mfrn2 expression levels in tumors might be utilized as a biomarker predicting response to PDT in head and neck cancers.

Chapter 1

Review of Head and Neck Cancer, Photodynamic Therapy, and Iron Physiology and Pathophysiology

1.1. Head and Neck Cancer

1.1.1. Epidemiology and Etiology

Head and Neck Cancer (HNC) covers a broad spectrum of soft tissue malignant neoplasms of the tongue, lips, nasal and oropharyngeal cavities, paranasal sinuses, major and minor salivary glands, larynx, and the lymphatic tissues of the neck (Fig.1). It is the 6th most common cancer worldwide and accounts for approximately 6% of all cases of cancers [1-3]. Each year, over 650,000 new cases are diagnosed worldwide, and 350,000 patients die from this disease [3]. More than 90% of the cancers are squamous cell origin from the epithelium of the mucous-lining membrane of the upper aerodigestive tract (UADT) [4], and therefore squamous cell carcinoma (SCC) represents the majority of head and neck cancers. Head and neck cancers with adenocarcinoma origins from associated secretory glands are rare. Early stages (stage I/II) of head and neck cancer have good prognosis after surgery or radiotherapy, with 75% overall 5-year survival rate [5]. However, approximately 66% of patients diagnosed with head and neck cancer are already in stages III and IV, for which the prognosis is poor, and the overall 5-year survival rate is 35% [6, 7].

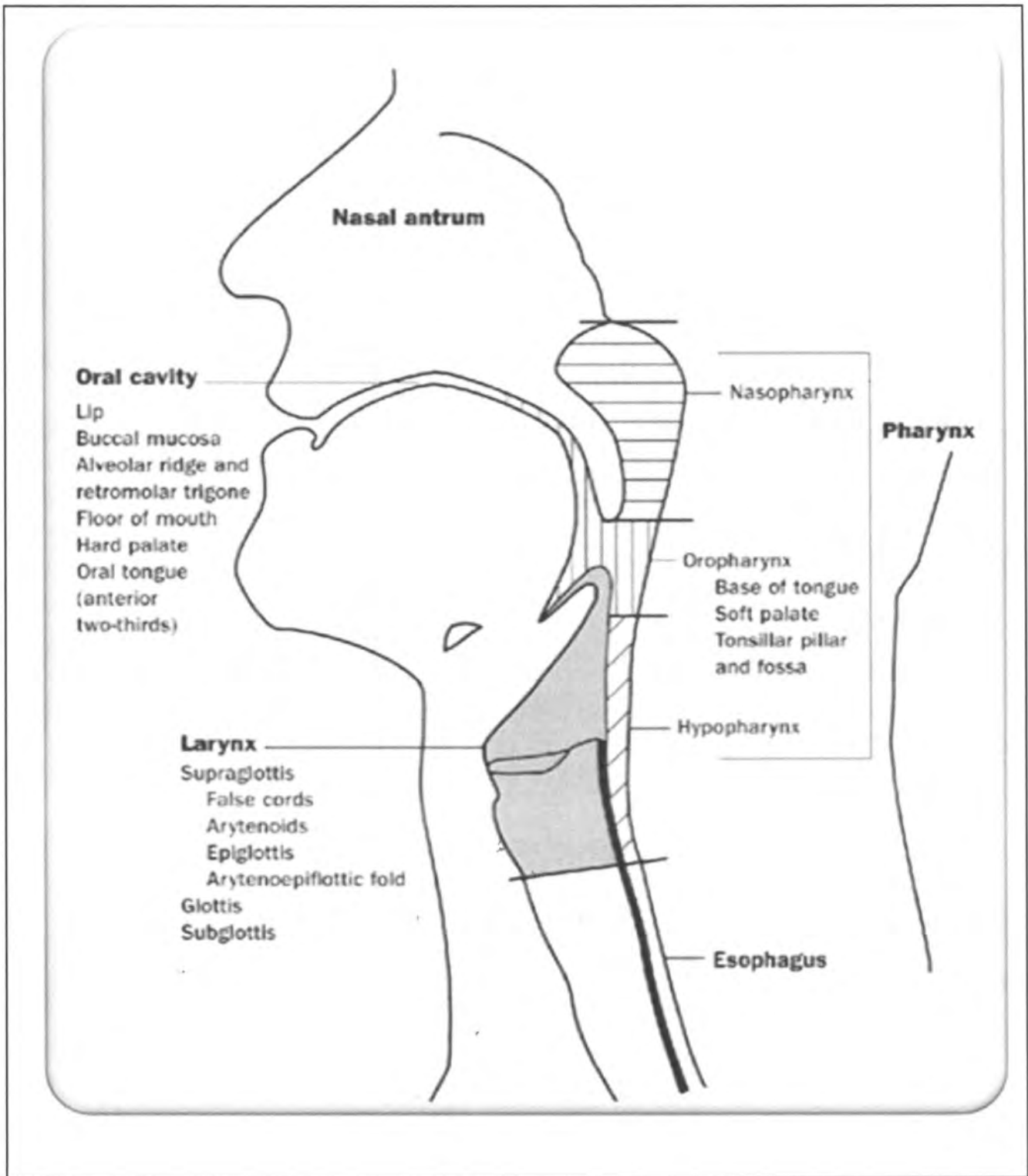


Figure 1. Anatomic sites and subsites of the head and neck cancer. Approximate distribution of head and neck is 44% oral cavity, 31% larynx and 25% of pharynx. *Adopted from CANCER MANAGEMENT: 13TH EDITION, March 25,*

Risk Factors

Head and neck cancer is strongly associated with environmental and lifestyle risk factors. Tobacco (including smokeless), alcohol, poor diet, UV radiation, and virus infection are the most important risk factors for head and neck cancers. Nearly 80% of head and neck cancers are tobacco and alcohol related [8]. More than 60 carcinogenic combustion products have been found in tobacco smoke, and therefore tobacco is a major risk factor for the susceptible epithelial mucous-lining membrane in which head and neck squamous cell carcinoma arises. Oral and pharyngeal sites, as well as the upper aerodigestive tract, are especially vulnerable to smoke insult. Smoke contains carcinogenic materials like 4-(methylnitrosamino)-1-(3-pyridyl)-1-butanone (NNK), N-nitrosornicotine (NNN), and polycyclic aromatic hydrocarbons (PAHs), which have been linked to UADT cancer through their activity producing DNA adducts [9]. In addition to this mutagenic effect, tobacco also causes oxidative stress to the exposed tissues through reactive oxygen species (ROS). ROS can damage proteins, lipids, carbohydrates and DNA, which also results in mutation and increases malignant transformation.

Alcohol promotes oncogenesis through increased permeability of cell membranes by damaging their phospholipid components to enhance the penetration of tobacco-containing carcinogens across oral mucosa. Impaired DNA repair mechanisms activate carcinogens and decrease activity of the detoxification enzymes (glutathione-S-transferases and cytochrome P₄₅₀) in the liver [10, 11]. Some alcoholic beverages contain carcinogenic impurities or contaminants, such as N-

nitrosodimethylamine [12], which is present in some beers and whisky and has been linked to the increased risk of oral cancer. Thus, smoke and alcohol are the major risk factors for head and neck cancer.

In Western Countries, dietary factors are estimated to account for 30% of all cancers [13]. Poor diet has been reported as a significant risk factor for head and neck cancer and is second to tobacco and alcohol as a cause of oral cancer worldwide [14]. According to the World Health Organization (WHO), dietary deficiencies or imbalances contribute to approximately 15% oropharyngeal cancers [15]. Since oxidative stress is one of the major factors to induce transformation of normal cells into malignant cells, vitamins with antioxidant activity, such as vitamins A, C, and E, and selenium have been reported to provide protection against most epithelial cancers by reducing the generation of free radicals that can cause DNA mutations and cellular membrane peroxidation [16-18]. Additionally, micronutrient diets also protect against cell malignancy by modulating cellular carcinogen metabolism, maintaining proper cell differentiation and immune function, and inhibiting cell proliferation and oncogene expression [19]. Therefore, a diet with excess preserved food (*e.g.*, nitrates and nitrites) that increases cellular oxidative stress or a diet lacking in fresh fruits and vegetables elevates the risk for head and neck cancer [20-22].

Prolonged exposure to sunlight (*e.g.*, UV light) increases the risk to develop lip cancer [23]. People with outdoor occupations are particularly more susceptible to lip

cancer. Radiation exposure has also been reported to increase the risk of thyroid cancer and has been associated with cancer of the salivary glands [24, 25].

The growing incidence of oropharyngeal cancer among younger head and neck cancer patients is related to human papillomaviruses (HPVs) infection [26-30]. To date, more than 200 different types of HPVs have been isolated and categorized into different groups according to their infection sites (cutaneous or mucosal) or risk for malignancy (high, intermediate, or low) [31, 32]. HPVs with low risk induce benign hyperplasias, like papillomas or warts, whereas HPVs with high risk are strongly associated with malignancy and carcinogenesis [33]. People with HPV infection in oral mucosa and showing HPV in the serum are at high risk for developing an oral squamous cell carcinoma (OSCC) [34-36].

For head and neck cancer, the HPV types of most concern are those capable of infecting the epithelial mucosal lining of the aerodigestive tract. HPV 16 and HPV 18 are strongly associated with head and neck carcinogenesis, particularly of the oral cavity and oropharynx (tonsil and tongue base) [37-39]. HPV-positive head and neck cancers are different from HPV-negative tumors, both clinically and biologically [40, 41]. Interestingly, HPV-infected OSCC patients tend to have better outcomes, greater treatment responses, and less chance of relapse compared to those with HPV-negative head and neck cancers [42-44]. The response to treatment is linked to functional p53. Indeed, a decreased number of p53 mutations have been reported in HPV-

positive cancers [45-48]. In addition to HPV, Epstein-Barr virus (EBV) has been strongly linked to nasopharyngeal carcinomas (NPC) [49, 50].

1.1.2. Pathogenesis

Head and neck squamous cell carcinoma results from successive accumulation of somatic gene alterations in the squamous epithelial lining of the upper aerodigestive tract [51, 52]. The progression of head and neck cancer from normal histologic features to hyperplasia, mild, moderate, and severe dysplasia, carcinoma in situ, invasive carcinoma, and metastasis is accompanied by multiple gene mutations and gains and losses of chromosome functions [53]. Down-regulation of tumor suppressor proteins (p53, Rb, Notch1), up-regulation of oncogenic proteins (Epidermal growth factor receptor [EGFR]), Phosphoinositide-3 kinase catalytic subunit (PI3CA), c-Met ligands, or hepatocyte growth factors (HGF)) and chromosomal gain and loss function on 3p14, 9p21, 17p13, 8p, 11q, 13q, 14q, 6p, 4q27, and 10q23 have been observed in head and neck squamous pathogenesis (Fig. 2) [53-57].

In head and neck cancer, a loss of tumor suppressor gene activity has been frequently observed rather than a gain or activation of oncogene function. The somatic TP 53 mutation represents 60-80% of head and neck cases [58-60]. Among head and neck cancers, approximately 80% were HPV-negative, with a large proportion of cases harboring the TP53 mutation, while 20% of HPV-positive cases had decreased p53 levels but intact p53 function [57, 61]. This finding points to the important role

of p53 in head and neck cancer therapy. At the same time, it makes a pharmacological treatment difficult, since regaining tumor suppressor gene function is more challenging than inhibiting oncogene activity.

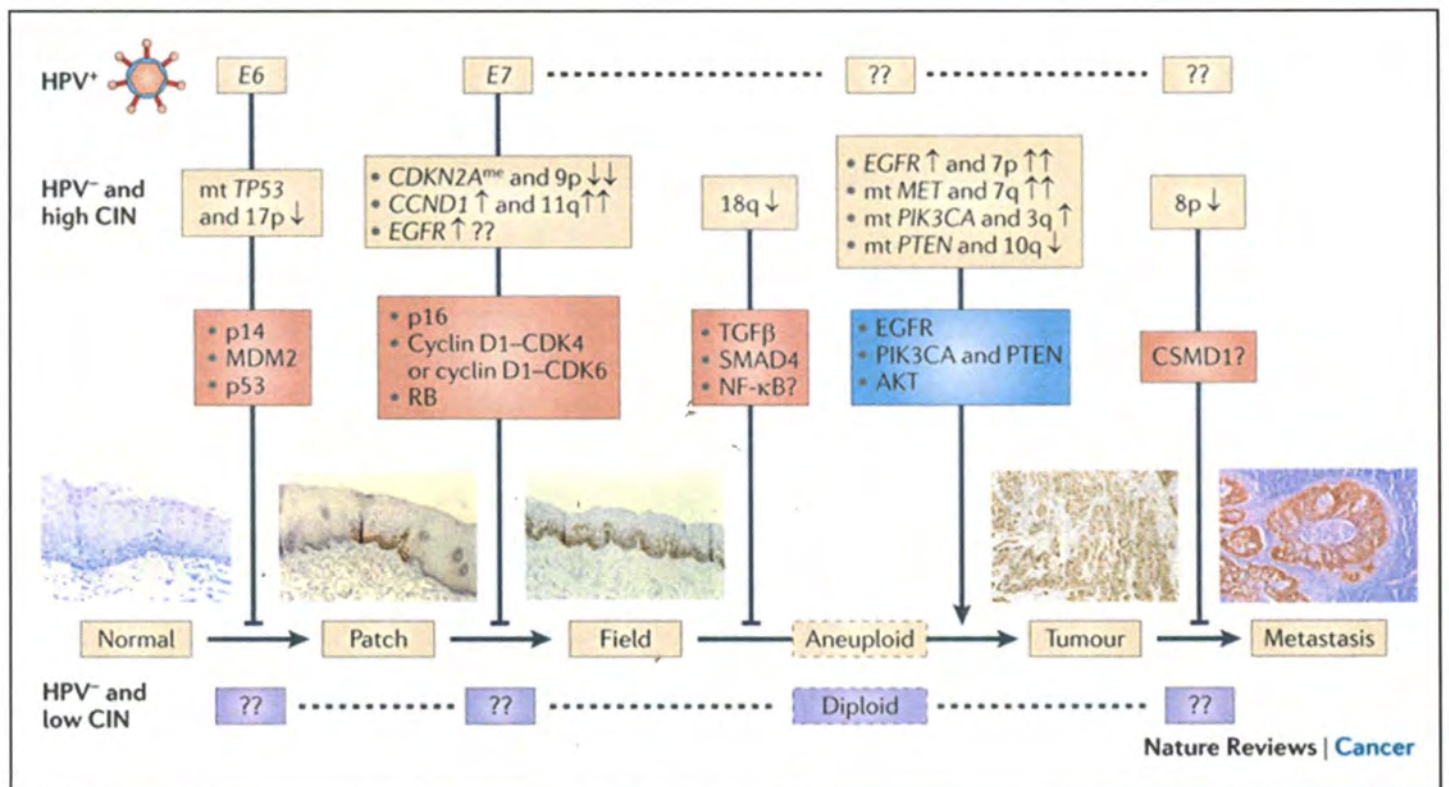
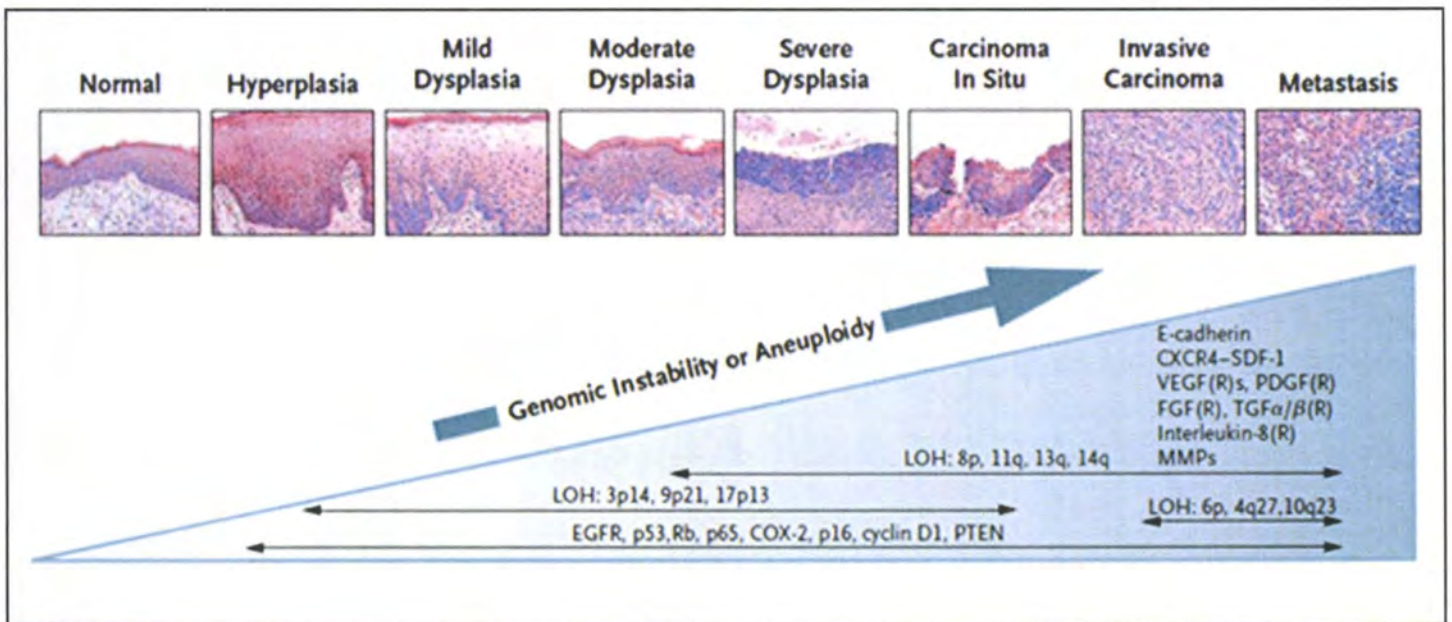


Figure 2. Progression of the head and neck squamous cell carcinoma and involved genetic alterations. Adopted from *Nat Rev Cancer*, 2011. 11(1): p. 9-22

1.1.3. Treatment Modalities for Head and Neck Cancer

For head and neck cancer, traditional treatment options are surgery, radiotherapy, chemotherapy, and any combination of these therapies. Surgery is carried out when the tumor is resectable, without organ function compromise, and the patient is able to tolerate the surgical procedure. Surgery is generally recommended for patients with early stages (I/II) of head and neck cancer [62]. However, when the tumor is not resectable or organ function loss is a concern, single modality radiation therapy may become an alternative treatment for early stage patients [62]. For patients with advanced stages status (above III), surgery alone is considered only appropriate in the absence of nodal spread. When patients present with nodal disease (N1-2), multiple modalities are applied, with resection of the primary tumor by surgery followed by radiation therapy or chemoradiotherapy [62]. The goal of radiotherapy is to intensify and focus the treatment dose in the cancerous area while saving the normal tissue from radiation damage.

Single drugs cannot cure most cancers. Therefore, chemotherapy is executed as a combination with multiple drugs or combined with surgery and radiotherapy. Historically, first-line chemotherapy for recurrent and metastatic head and neck cancer has been cisplatin [63]. Currently, however, the most frequently used chemotherapeutic drugs for head and neck cancer patients are platinum compounds (5-fluorouracil, methotrexate, and cetuximab). Chemotherapy is often combined with radiotherapy. Radiotherapy with platinum-based chemotherapy is a common cancer

treatment regimen and has become an alternative treatment modality for surgery in the treatment of locoregional advanced head and neck cancer [64-66].

Molecular Targeted Therapies

Molecular targeted therapies have been developed to maximize delivery of therapeutic doses to the cancer cells while minimizing side effects and toxicity in the normal cells. Epidermal growth factor receptor (EGFR) is frequently up-regulated in head and neck cancers. Thus, cetuximab, which is an anti-EGFR monoclonal antibody (mAb) and targets EGFR, has been effective against unresectable laryngeal, oropharyngeal, or hypopharyngeal carcinomas when combined with platinum-based chemotherapy or radiotherapy [64-67].

Genetic events frequently observed in head and neck cancer are tumor suppressor gene (*e.g.*, p53, p16, p21) loss of function and chromosome (*e.g.*, 3p, 9p and 17p) loss of heterozygosity [68]. Mutations of p53 have been found ranging from 40 to 70% in head and neck cancer, and 20% in the premalignant lesion areas [69, 70]. Mutation of p53 is associated with more aggressive cancer status, poor prognosis, poor survival rate, and higher local recurrence in head and neck cancer patients [71-73]. P53 regulates genes involved in cell cycle control and apoptosis. Head and neck cancer patients with a long history of tobacco and alcohol use are more frequently found with a p53 mutation in their tumor samples. Most p53 mutations are

guanidine transversions thymidine mutations, with less extent of missense mutations on exon 5 and 9.

Currently, there are three ways to restore wild type p53 function in cancer patients. The first is application of antagonists of p53-negative regulators (*e.g.*, murine double minute 2) in patients with wild type p53 whose p53 function is limited by these negative regulators [74]. The second is reactivation of mutated p53 by either applying small molecules, an antibody (*e.g.*, antibody 421), a heat shock protein (*e.g.*, chaperone protein dnaK), or artificial high-affinity DNA-binding sequences of p53 to assist p53 refolding and rescue p53's biological function. The third is exogenous expression of wild type p53 in tumors by adenovirus-mediated gene therapy [75]. Data from clinical trials of Ad-p53 delivery to 445 patients with advanced squamous cell carcinoma, lung cancer, colon cancer, and prostate cancer showed that Ad-p53 gene therapy was a safe and well-tolerated therapy [75]. Many clinical trials with Ad-p53 are ongoing on head and neck cancer patients [75].

Photodynamic Therapy (PDT)

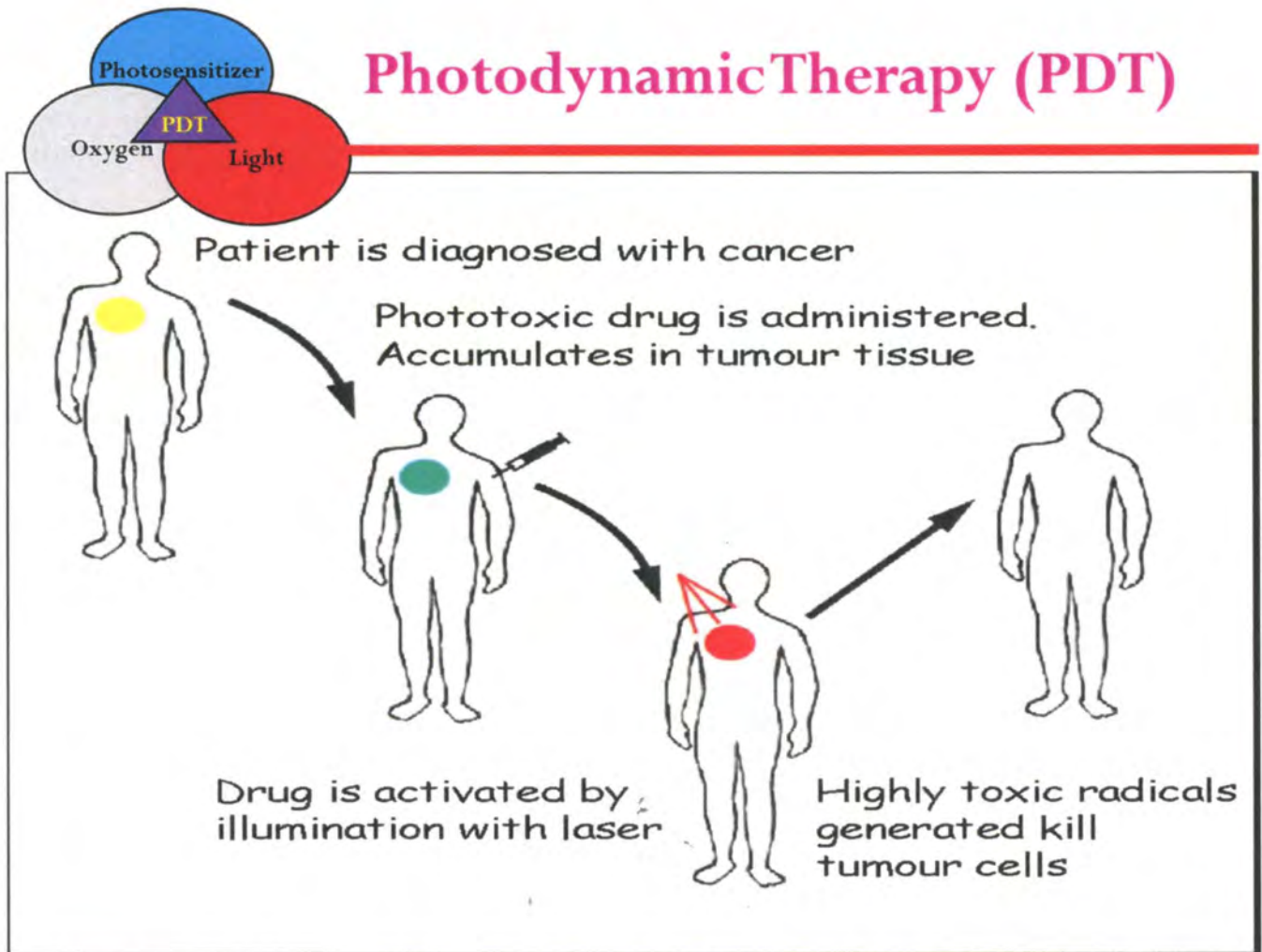


Figure 3. Photodynamic therapy simplified schematic which shows the three major components of the PDT therapy: light, photosensitizer, and oxygen.

1.2. Photodynamic Therapy

PDT is a US Food and Drug Administration (FDA)-approved, minimally invasive treatment modality that utilizes light in the presence of oxygen to activate photosensitizing agents to produce cell death (Fig. 3) [76]. Absorption of a photon activates the photosensitizer to an excited singlet state that can then undergo intersystem crossing to the triplet state. The triplet transfers energy to molecular oxygen to generate singlet oxygen ($^1\text{O}_2$). This is referred to as a Type II photochemistry [77]. Oxidation-reduction reactions also occur to generate other reactive oxygen species (ROS) [77]. PDT has various clinical applications; among these, PDT as a treatment of cancer is especially promising and attractive.

PDT has many advantages. The photosensitizers do not accumulate in the nuclei and therefore do not induce DNA damage or mutagenesis or generate resistance to the therapy, which commonly occurs after chemotherapy or radiotherapy. PDT can be applied as a combination therapy either prior to or after other treatments (*e.g.*, chemotherapy, radiation, surgery) without compromising the therapeutic effects of those modalities. PDT is a non-invasive treatment modality, and treatment can be repeated on patients. Currently, PDT is under intensive investigation for treatment of various forms of cancers [77-87].

1.2.1. Photosensitizers

Photosensitizers are the key components in PDT. The ideal photosensitizer would have the following characteristics. It would be present as a pure single compound of known composition and stable at the room temperature. It would not induce dark toxicity and would have more rapid clearance from normal cells and tissues than tumor cells. It would not yield any toxic metabolites. Its absorption wavelength would span from red to deep red (600-800 nm). The longer the absorption wavelength, the deeper the photosensitizer can penetrate into tissues. Therefore, photosensitizers with absorption peaks at longer wavelengths are more favorable for clinical applications. However, above 800 nm, the energy is insufficient to excite oxygen to generate $^1\text{O}_2$ and yield PDT's intended effect. Thus, the ideal absorption wavelength for the photosensitizers is 600-800 nm.

Photosensitizers can be administered through numerous routes (*e.g.*, oral, intravenous, topical, intratumoral, inhalational). The ideal photosensitizer would have a good pharmacokinetic profile, high quantum yield to produce $^1\text{O}_2$, inexpensive, and would not target the nucleus as a possible mutagenic agent [77, 88, 89]. Photosensitizers are generally categorized into porphyrin or non-porphyrin groups, as show in (Fig. 4 A-B) [88]. Porphyrin-derived photosensitizers are further classified into first, second, and third generation based on their improved characteristics and modifications. Most photosensitizers used in cancer therapy are porphyrin-related, meaning they have a hetero-cyclic ring and tetrapyrrole structure that resembles that of the

protoporphyrin present in chlorophyll, hemoglobin, or hematoporphyrin (Fig. 5) [77]. Structures of porphyrin molecules have a 22π electron system which confers a long wavelength absorption [88].

Porphyrin Derived Photosensitizers

First Generation Photosensitizers

The first clinically applied photosensitizer for cancer treatment was a water soluble, porphyrin-derived molecule named hematoporphyrin derivative (HPD), which was later called Photofrin™ (porfimer sodium) [90]. Although Photofrin is one of the most widely used photosensitizers, it has some unfavorable characteristics, such as low cellular uptake, low molar extinction coefficient ($1170 \text{ M}^{-1} \text{ cm}^{-1}$) that results in a poor therapeutic effect, and long-lasting photosensitivity caused by a long half-life of 452 h [88, 91]. Because of these limitations, second generation porphyrin-derived photosensitizers have been developed.

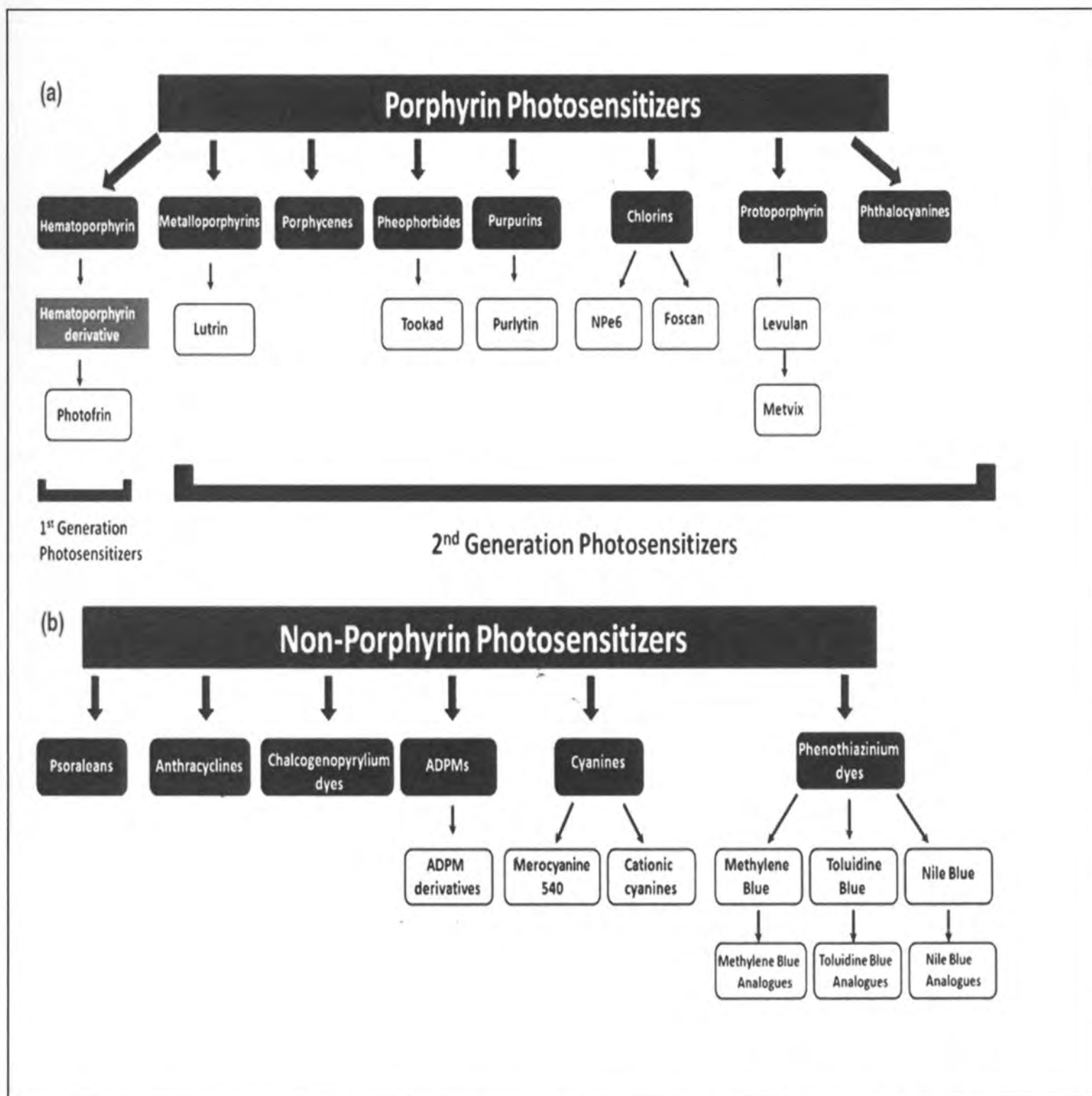
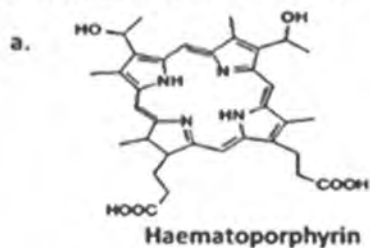
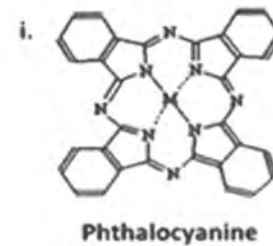
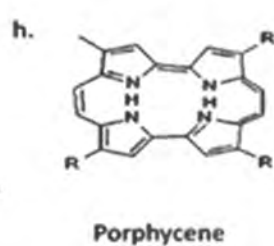
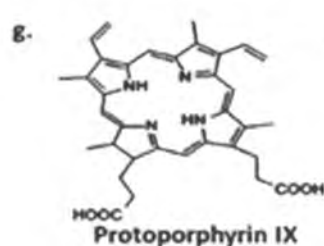
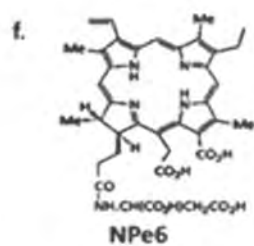
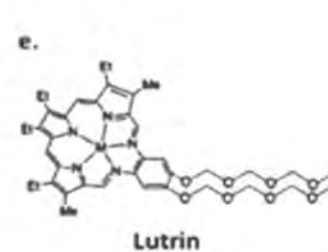
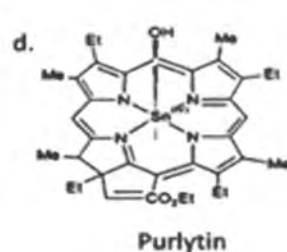
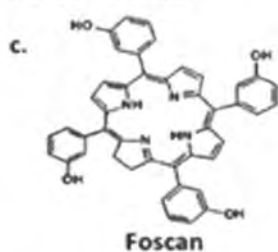
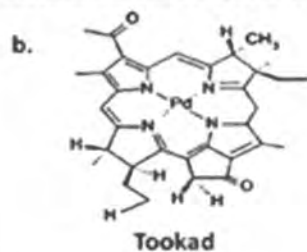


Figure 4. Categories of porphyrin-derived (a) or non-porphyrin-derived (b) molecules. *Adopted from Photochemistry and Photobiology, 2009, 85: 1053–1074*

First generation porphyrin photosensitizer



Second generation porphyrin photosensitizers



Non-porphyrin photosensitizers

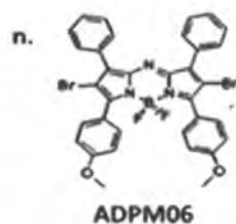
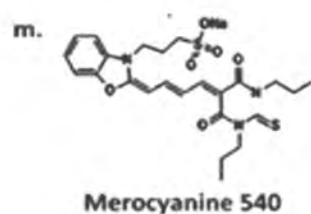
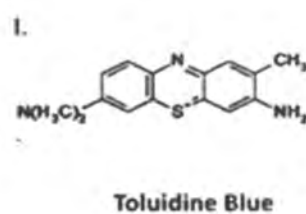
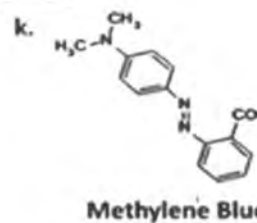
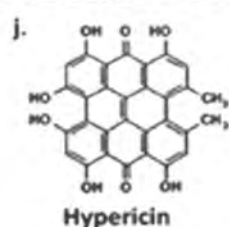


Figure 5. Chemical structure of the common photosensitizers for cancer treatment.
Adopted from Photochemistry and Photobiology, 2009, 85: 1053–1074

Second Generation Photosensitizers

The second generation photosensitizers attempted to improve PDT efficacy and reduce unfavorable characteristics of the first generation photosensitizers. Second generation photosensitizers have several advantages: 1) reduced skin photosensitization after treatment; 2) absorption at longer wavelength to facilitate deeper tissue penetration; and 3) increased cellular uptake. Phthalocyanine (Pc), chlorin, protoporphyrin IX, and foscan are currently under intensive investigation for cancer treatment (Fig. 4 and 5) [81, 92-95].

The **Phthalocyanine** (Fig. 5i) family, derived from porphyrin as a second generation photosensitizer, has high quantum yield to generate $^1\text{O}_2$ and has a strong absorption peak at 670-770 nm. This long wavelength allows penetration into deep tissue. Pc has a central metal atom (M), either zinc, aluminum, or silicon, which stabilizes the Pc structure and also yields long-lived triplet state $^1\text{O}_2$, enhancing PDT's effect (Fig. 5i) [96].

Phthalocyanine 4 (Pc 4), one of the most studied phthalocyanines, localizes to the membranes of the mitochondria, endoplasmic reticulum and Golgi and has shown promising in vitro and in vivo results [92, 97, 98]. Pc 4 has a dimethylaminopropyl siloxy ligand on its central silicon. It is a hydrophobic molecule and binds to lipoproteins and serum albumin, which delivers it into cells [99]. Pc 4 causes mitochondria-mediated apoptotic cell death [92, 97]. A Phase I clinical trial of Pc

4-PDT has been completed for cutaneous neoplasms [98], and it is currently in a Phase I trial for psoriasis. In addition, over 250 analogs of Pc 4 have been synthesized, some of which have been further investigated for their potential in PDT [100-102]. Results showed that Pc 4 analogs with two axial ligands increased Pc monomerization, which improved Pc cellular uptake. Pc 4 analogs such as Pc 181, with hydroxylated ligands, preferentially localize to lysosomes. Pc 181 was found to be more effective in killing cancer cells than Pc 4 from in vitro study [97].

Foscan (Fig. 5c) is a single pure chlorine derivative that absorbs light at 652 nm. It has a long plasma half-life (45-65 h) and is a very potent photosensitizer [88]. Due to its superior photophysical properties and high $^1\text{O}_2$ yield, a small drug dose (0.1 mg/kg) and light intensity (10 J/cm^2) are needed to obtain a robust PDT effect [91]. Currently, foscan has been approved in Europe to treat head and neck cancer. Foscan accumulates preferentially in brain tumors, with the ratio of tumor to normal cells as 100:1; which makes foscan a superior cancer targeting photosensitizer [103-105]. A nonrandomized phase II study of foscan-PDT on lip cancer showed complete response, which is just as good as patients treated with surgery or radiotherapy [106]. Presently, foscan is one of the photosensitizers that have been intensively applied to head and neck cancer because of its high efficacy. However, a long plasma half-life of foscan causes prolonged photosensitivity.

Protoporphyrin IX (Fig. 5g) is a second generation porphyrin derived photosensitizer that is activated by light to initiate the PDT reaction. Protoporphyrin IX is converted from its hydrophobic precursor 5 aminolevulinic acid (5-ALA), which is involved in heme biosynthesis (Fig. 6). After conversion of 5-ALA into protoporphyrin IX by mitochondrial enzymes, it can be activated by light at 630 nm to cause a PDT effect [107]. Since protoporphyrin IX is localized to mitochondria, the main PDT effect occurs on mitochondria. Tumor cells tend to accumulate 2 fold more on protoporphyrin IX-treated as compared to normal cells. [88]. Thus, increased accumulation of protoporphyrin IX can be an advantage for cancer therapy. Protoporphyrin IX has been applied with PDT to treat superficial basal and in situ squamous cell carcinoma and actinic keratosis [108, 109].

Researchers are trying to improve protoporphyrin IX PDT efficacy by increasing ALA metabolism into protoporphyrin IX or decreasing protoporphyrin IX conversion into heme. One way to enhance protoporphyrin IX-PDT is to apply iron chelators, which block incorporation of iron into protoporphyrin IX and heme biosynthesis, resulting in protoporphyrin IX accumulation [110].

Third Generation Photosensitizers

Third generation porphyrin-derived photosensitizers have been improved by increased tumor targeting specificity, photosensitizer stability, cellular uptake, and efficacy by formulating photosensitizers with liposomes, nanoparticles, and poly-

mers [88]. Tumor oncogenes such as EGFR have been utilized for micelle-formulated nanoparticles Pc 4 with GE11 peptide ligands to enhance photosensitizer delivery to EGFR-overexpressed cancer cells [111]. In addition, poly (ethylene glycol)–poly (ϵ -caprolactone)–poly (ethylene glycol) (PEG-PCL) micelle nanoparticles have been applied to improve the delivery of the highly hydrophobic photosensitizer Pc 4 into cells and increase its bio-distribution. Pc 4 PEG-PCL shows intracellular uptake and improved cytotoxicity [112].

Non-Porphyrin Photosensitizers

Non-porphyrin photosensitizers have been considerably less studied due to a lack of encouraging clinical results [88]. Most of the non-porphyrin photosensitizers are cationic dyes that selectively accumulate into mitochondria with negative membrane potential [88]. Hypericin, which has shown good tumor selectivity and in vitro efficacy, is considered as a potential candidate for the clinical application, but it has not been successful in clinical trials thus far [88].

Results from several institutions have shown that PDT can successfully treat early carcinomas in the head and neck regions, including the oral cavity, pharynx, and larynx, and at the same time preserve the organs and their vital functions of speech and swallowing [113, 114]. In one small randomized clinical trial which compared patients treated with porfimer sodium-PDT (foscan-PDT) to patients treat-

ed with chemotherapy (5-FU and cisplatin) in nasopharyngeal carcinoma, PDT demonstrated better clinical outcomes.

In a 15 year accumulating clinical research with more than 300 patients who were treated with the porfimer sodium-PDT with a single PDT procedure, showed that in the laryngeal carcinoma group (133 patients) after average 8 year follow up, the 5 year cure rate was 90%, and in the oral cavity group (138 patients), after up to 211months follow up, the 5 year cure rate was 100% with a totally complete pathological and clinical response in patients [115]. The protocol used in this study was following of 2.0 mg/kg of porfimer sodium IV administration for 48 h, then irradiated with 630 nm of light from a neodymium yttrium aluminum garnet (Nd:YAG) pumped dye laser with 50-75 J/cm² fluences for oral cavity, nasopharyngeal, and 80 J/cm² fluences for laryngeal tumors.

Currently, over 500 head and neck cancer patients with early stage oral cavity, larynx, pharynx, and nasopharynx lesions were treated with porfimer sodium-PDT worldwide and showed similar success [116-118]. From these studies, only a small number of patients experienced recurrence and were treated either with surgery or repeated PDT. The only complaints from these patients were photosensitivity of skin and local pain, which can be controlled with oral analgesics.

In addition to the porfimer sodium-based PDT, 5-ALA and foscan have also been applied to treat head and neck cancers. Currently, foscan is the most widely applied second generation photosensitizer used in head and neck cancer treatment and has shown impressive results. In a study of foscan-treated head and neck cancer patients (n=27), results showed the cure rates for stage I were 85%, with a 38% rate for stages II and III [119]. In another foscan based PDT treatment with patients who had been treated unsuccessfully with traditional cancer therapies or were unable to go through the traditional therapies, results from 96 h post-foscan PDT found that 43% of the lesions showed 100% tumor mass reduction, and 57% of lesions showed at least a 50% tumor mass reduction [120]. However, researchers pointed out that, when the total surface area of the tumor could be illuminated or the tumor depth was less than 1 cm to allow light penetration into the whole tumor, treatment success significantly increased.

For 5-ALA-based PDT treatment in head and neck cancers, fewer reports showed less successful rates in terms of clinical outcome compared to either the porfimer sodium or the foscan [121, 122]. In conclusion, results from current phases I/II head and neck cancer trials strongly demonstrated that PDT is an effective cancer treatment modality either as primary or alternative therapy. In addition, patients who received PDT treatment also benefitted from organ preservation, a lack of systemic toxicity, and better quality of life.

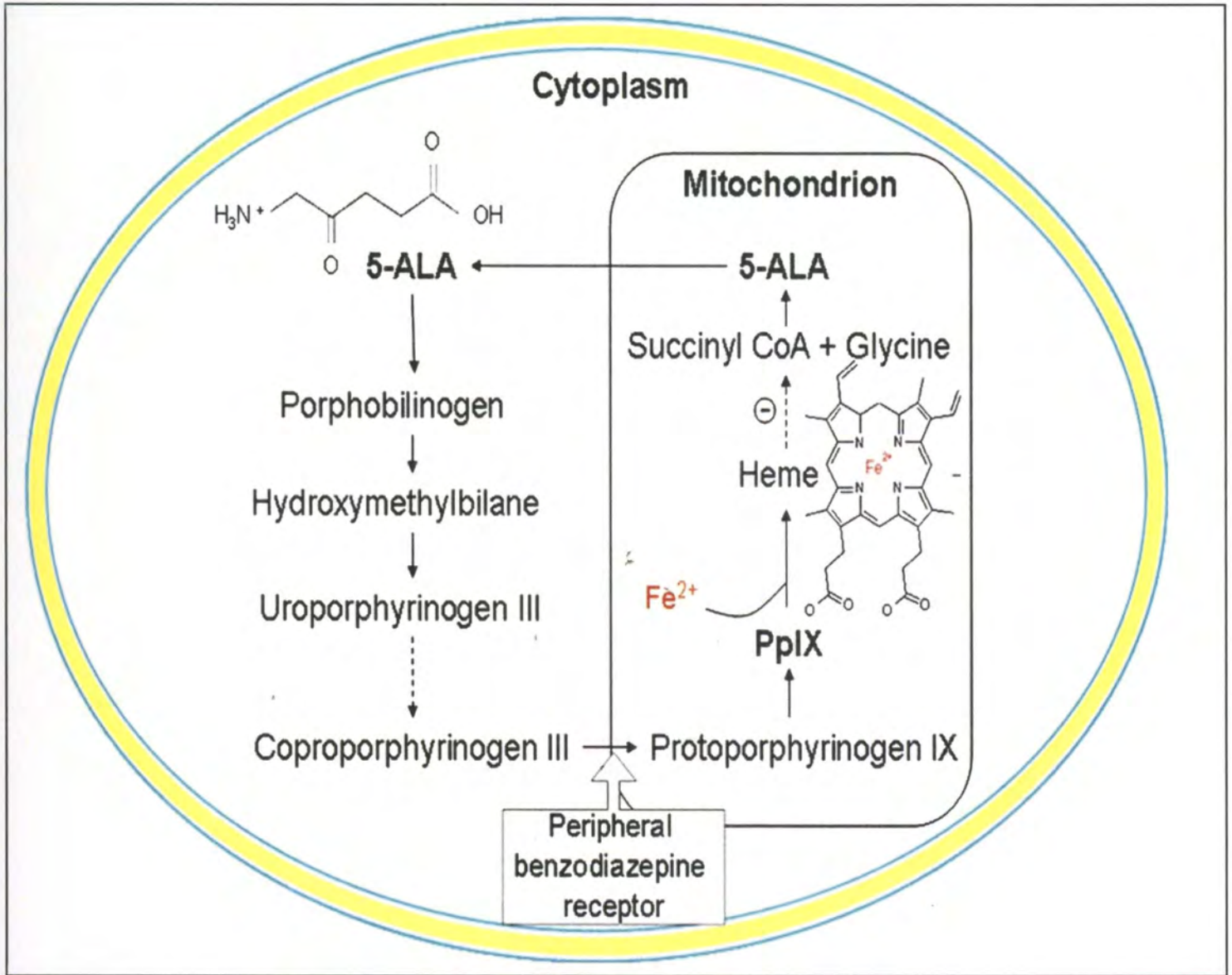


Figure 6. Intracellular 5-aminolevulinic acid metabolism. *Adopted from J Am Acad Dermatol 2010;63:183-93.*

Subcellular Localization

Subcellular localization of the photosensitizer is a main factor to determine site of $^1\text{O}_2$ generation and initial photodamage [123]. Many organelles (*e.g.*, mitochondria, lysosomes, endoplasmic reticulum, Golgi apparatus, and plasma membrane) have been studied as cellular targets for photosensitizers [124]. The important factors determining cellular localization of the photosensitizer are 1) net ionic charge of the photosensitizer that can range from (-4) anionic to (+4) cationic; 2) hydrophobicity of the photosensitizer; and 3) degree of asymmetry of the photosensitizer. Hydrophobic photosensitizers with net charge less than two negative charges (≤ -2) freely diffuse across the plasma membrane and then redistribute to intracellular membranes of other organelles, resulting in high cellular uptake. Less hydrophobic photosensitizers with less than two negative charges are too polar to diffuse across the plasma membrane, and therefore they are taken up by cells through endocytosis/pinocytosis [89].

1.2.2. Photochemistry of PDT

Light absorption and energy transfer are the two main photochemical/photophysical events during PDT (Fig. 7). In the ground state, the photosensitizer has two electrons with opposite spin in an energy most favorable low molecular orbital as the singlet state. When the photosensitizer is activated by light, one electron is boosted into a higher energy orbit but maintains its original spin direction. This state is unstable and emits extra energy as either fluorescence or heat. Alternatively,

the excited photosensitizer may undergo intersystem crossing to form a more stable high energy state that has one electron inverted to form a parallel spin of electron conformation [125].

The triplet state of a photosensitizer can transfer its energy to other molecules through either type I or type II reactions (Fig. 7). Most PSs are believed to undergo type II reactions during PDT [77]. In a type II reaction, the triplet state of the activated PS transfers its high energy to the adjacent molecular oxygen (O_2) to form highly reactive 1O_2 . Alternatively, in a type I reaction, the triplet state of the activated photosensitizer transfers its high energy to the substrates and organic molecules other than O_2 through proton or electron transfer and forms a radical anion or cation, respectively. These radicals can further interact with O_2 to generate ROS, such as superoxide anion radical ($O_2^{\bullet-}$), hydrogen peroxide (H_2O_2), and a hydroxyl radical ($OH\bullet$). The type of photosensitizer, biological substrates, and the level of O_2 all determine what type of reaction occurs during PDT [126]. Since 1O_2 and ROS (except H_2O_2) are highly reactive and short lived, they interact with biomolecules on the sites where ROS are formed. Thus, PDT's effects occur in close proximity to the photosensitizer.

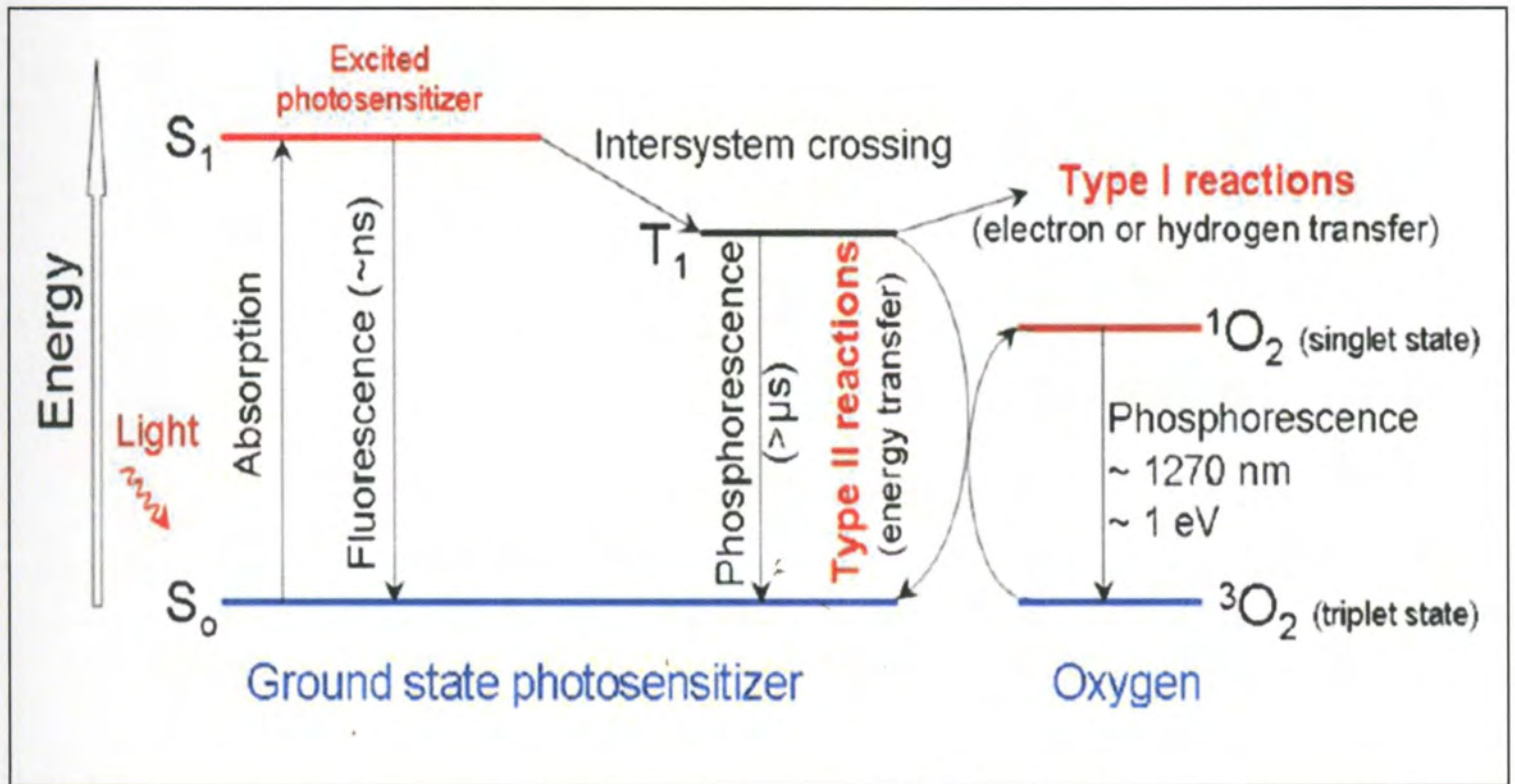


Figure 7. Photochemical reactions during PDT. *Adopted from CA Cancer J Clin 2011;61:250-281.*

1.2.3. Light Sources and Light Delivery

In PDT, light is also a crucial factor to determine outcomes since precise light delivery can activate the PS in tumor areas and selectively destroy the cancer. Inside the tissue, light can be either absorbed or scattered. Therefore, one way to improve PDT efficacy is to focus the light on targeted areas. Red and infrared light has the deepest penetration (up to 1 cm into tissue) whereas blue light penetrates least efficiently into tissue (Fig. 8) [127]. The light region between 600 and 1200 nm is often called the optical window of the tissue [77]. Above 800 nm, however, the energy of the light is insufficient to activate PS and cause a PDT response.

No single light source is ideal for all PDT applications. Depending on the photosensitizer used, a light source with specific wavelength needs to be applied to obtain maximal photosensitizer activation. The efficacy of the PDT is dependent on complex dosimetry, which is determined by total light dose, total light exposure time, and the mode in which light is delivered (*e.g.*, single or fractionated mode). Both lasers and incandescent light sources are applied for PDT and show equivalent efficacies [128, 129]. The diode laser is the most commonly used PDT light source, but some researchers have used LED as an alternative source. Since laser light is coherent, the laser is coupled with a fiber to transfer consistent and stable light deep into tissue maximally [130].

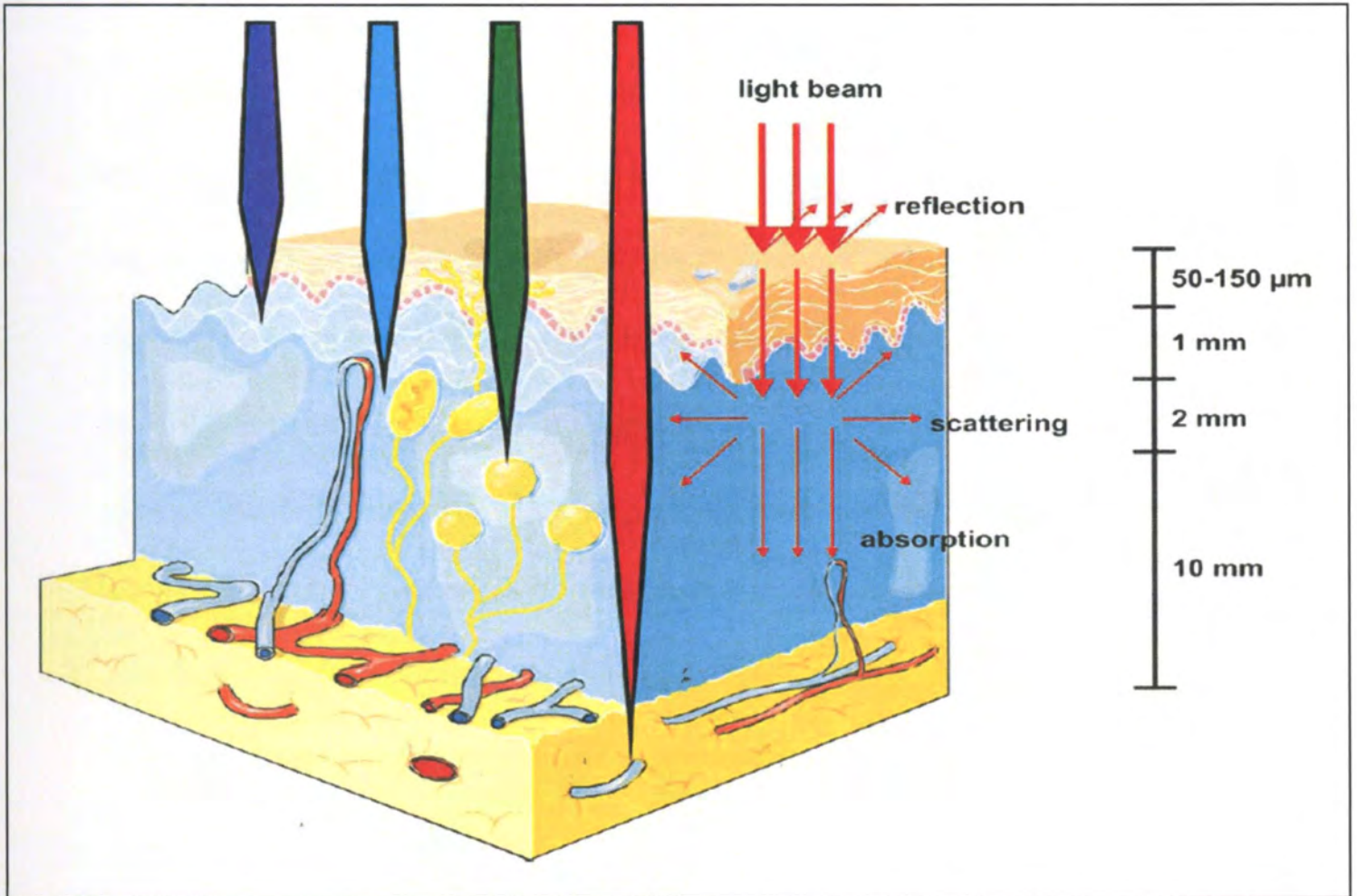


Figure 8. Penetration of light into tissue. *Adopted from CA Cancer J Clin 2011;61:250-281.*

1.2.4. Role of Oxygen in Photodynamic Therapy

Besides the photosensitizer and light, oxygen is an important factor in determining PDT outcomes. Using PDT in solid tumors is challenging. Decreased oxygen tension deep in poorly vascularized tumors can result in decreased formation of $^1\text{O}_2$ and other ROS, thereby diminishing the therapeutic effect. $^1\text{O}_2$ generation during PDT treatment can induce local hypoxia in tissue [131]. In order to overcome these challenges and improve PDT efficacy in hypoxic solid tumors, several strategies have been developed, such as using fractionating light for irradiation and allowing tissue reoxygenation during intervals between PDT treatments [132]. PDT has also been administered to patients in hyperbaric oxygen (HBO) environments to provide a continuous oxygen supply. Hyperoxygenation of tissue has successfully extended the survival period in patients with esophageal carcinomas [133, 134] although this application requires a pressurized chamber, which is not widely available. Strategies to overcome these oxygen-related PDT limitations are still under investigation.

1.2.5. Mechanisms of PDT-Mediated Cytotoxicity

PDT is a cancer therapy modality that causes cytotoxicity by direct cell killing through apoptosis, necrosis, and autophagy pathways. PDT can also target tumor vasculature to block nutrient supply in tumors and thus inhibit tumor survival. PDT can also boost host immunity, which helps to combat cancer [77]. Mechanisms of PDT induced cancer cell death are addressed below.

1.2.5.1. Direct Cytotoxicity

Due to the very short half-life of the $^1\text{O}_2$ (approximately 10-320 nanosec), it can only interact with biomolecules within 10 nm to 55 nm after its generation [135]. Therefore, cellular sub-organelle localization of photosensitizers plays an important role in determining mechanisms involved in photodamage-caused cell death. PDT can cause direct cytotoxicity through three main cell death pathways: apoptosis, necrosis, and autophagy, among which apoptosis is generally the major cell death pathway involved after photosensitizer-induced photodamage [136]. In general, it is commonly agreed that lower doses of PDT lead to more apoptotic cell death while higher doses of PDT tend to cause more necrotic cell death proportionately [137]. However, cell death pathways that occur are determined by cell type, cellular localization of photosensitizer, PDT dose (photosensitizer concentration, light dosimetry), and protocols applied.

Photosensitizers mainly localized to the mitochondria, such as Pc 4 [92], cause cell death through the mitochondria-mediated apoptotic cell death pathway. After Pc 4 is irradiated by light at the red wavelengths, it initiates mitochondrial depolarization, followed by cytochrome *c* release, and caspase 3/7 activation to cause apoptotic cell death [160]. Researchers have reported that, for mitochondria localized photosensitizers, Bcl-2 dissipation is the initiation step to trigger mitochondrial outer membrane permeabilization and mitochondrial membrane potential loss, which in turn leads to downstream caspase 3/7 activation and eventually apoptotic cell death [138-140].

In addition to apoptosis, phototoxicity can lead to cell death through nonapoptotic pathways, which include autophagic and necrotic pathways [141]. Generally, in the event of caspase-deficient conditions such as caspase genetic knockout or caspase inhibitor administration, cells delay their response to phototoxicity and shift to necrosis [142]. Although the molecular mechanisms of necrosis are still not well understood, researchers have reported some events that lead to necrosis, including receptor interacting protein 1 (RIP1) activation, lysosomal damage, block of ATP synthesis, intracellular Ca^{2+} overload, and an excess of mitochondrial ROS generation [143, 144].

Autophagy occurs through a lysosome mediated cellular pathway to recycle cellular components. Various stress signals can induce autophagy, including oxidative stress [145]. Researchers have reported that some photosensitizers induce autophagy during the PDT process, although the role of the autophagy process could be either cytoprotective or pro-death [145]. Currently, a general conclusion from all the present findings is that autophagy induces cell death and plays a pro-death role under situations when the apoptosis pathway is defective or when the autophagy recycle mechanism is impaired due to overwhelming stress conditions [146, 147]. Alternatively, autophagy plays a prosurvival role and rescues the cells when the cells are under low stress conditions (low-dose PDT) where autophagy can repair cell damage [148]. Similar to necrosis, when cells are under stress but the apoptosis pathway is

inhibited due to caspase deficiency, autophagy can also serve as an alternative cell death pathway.

Studies from Bax-deficient DU145 human prostate cancer cells and Bax knock-out HCT116 human colon cancer cells showed that, although these cells have deficient apoptosis pathways, cells still retain a similar degree of cell killing under Pc 4-PDT treatment [203, 204]. These findings suggest the possibility of another bax-independent cell death pathway. In addition, researchers found vacuole formation in these cells under electron microscopy and the conversion of LC3-I to LC3-II after Pc 4-PDT treatment [149]. After applying the autophagy blockers 3-methyladenine and wortmannin, which inhibit Pc 4-PDT-induced cell death in these bax deficient cells, researchers concluded that cells deficient of bax underwent autophagy-mediated cell death [150].

Additionally, it has also been reported that PDT induces both autophagy and apoptosis concurrently using the CPO photosensitizer in murine leukemia L1210 cells. These photodamaged cells showed both apoptotic and autophagic characteristics, including chromatin condensation, mitochondrial depolarization, phagolysosome formation, and conversion of LC3-I to LC3-II [149].

1.2.5.2. Vascular Effects

Since blood supply supports tumor growth, one strategy for cancer therapy is to target tumor vasculature with anti-angiogenic agents that inhibit neovascularization in solid tumors. Besides causing cytotoxic effects, PDT concurrently may cause vascular damage that leads to ischemic cell death in tumors [151, 152]. These findings suggest that targeting tumor vasculature provides another mechanism to treat solid tumors. Since photosensitizers are bound to cellular lipoproteins (high-density lipoprotein [HDL] and low-density lipoprotein [LDL]) and serum proteins (*e.g.*, albumins) to be carried into cells, endothelial cells that express receptors for serum proteins and lipoproteins are primary targets for vascular approaches to PDT [153].

Typically, PDT procedures with shorter photosensitizer-light intervals restrict photosensitizers in the blood circulation and accumulate in endothelial cells or are bound to vessel walls to cause vascular targeting effects whereas longer photosensitizer-light waiting periods following PS administration lead to cellular organelle distribution of the photosensitizers and induce more tumor cell damage. PDT with short photosensitizer-light intervals result in damage to the endothelial cells through loss of tight junctions between cells and leads to blood cell adherence to vessel walls. This damage induces the formation of thrombogenic sites with physiological cascade of reactions including platelet aggregation, vasoactive molecules release, leukocyte adhesion, increased vascular permeability and vessel constriction. Vasculature-targeting PDT causes microvascular collapse, blood flow stasis, and tissue hemor-

rhage that eventually leads to persistent post-PDT tumor hypoxia and nutrient deficiency, resulting in long-term tumor control [154, 155].

1.2.5.3. Immune Responses

PDT frequently triggers a strong acute inflammatory reaction as localized edema, which is recognized by the host as an acute trauma. This recognition launches an acute inflammatory response as a protective action to remove damaged cells in affected sites and promote local healing to restore tissue function, integrity, and cellular homeostasis [156]. PDT-provoked inflammation increases the permeability of the tumor vasculature, which induces inflammatory cells (*e.g.*, neutrophils, monocytes and macrophages) to invade the affected areas rapidly [156, 157]. Subsequently, dead and injured cells and PDT-damaged vasculature that forms occlusions are eliminated by inflammatory cells. Inhibition or depletion of the activity of these inflammatory cells as well as their regulatory cytokines interleukin (IL)-1 β and IL-6 reduce PDT efficacy [158-161]. In contrast, diminishing the anti-inflammatory cytokines such as IL-10 and transforming growth factor- β (TGF- β) significantly improves PDT effects [156]. Increased CD8⁺ levels, T cell activation, and tumor infiltration have also been linked to PDT efficacy [162, 163]. Therefore, effort has been focused on mechanistic studies to potentiate CD8⁺ and T cell activation.

1.2.6. Combination of PDT with Other Therapies

Most cancers are not curable through treatment with single drugs. This limitation applies to PDT as well. Thus, combining PDT with other modalities to improve the therapeutic index has received much interest. In general, therapies with different mechanisms or targets can be combined together to achieve either additive or synergistic effects. PDT can be safely combined with other cancer therapy modalities without compromising therapeutic outcomes or inducing cross-resistance between the therapies [164]. PDT has been successfully combined with surgery, radiotherapy, and chemotherapy [165-167]. The purpose of PDT in combination therapy is either to further sensitize tumor cells and enhance overall tumor killing effects or to maintain therapeutic effects but significantly reduce systematic toxicity or adverse side effects by reducing the treatment dose of other therapy. PDT can be combined with other mechanism-driven drugs or modalities with further enhancement of therapeutic outcomes. PDT has been combined with radiotherapy [167], chemotherapeutic drugs such as platinum compounds and proteasome inhibitors [168], and overexpressed EGFR and folic acid receptor [169].

PDT has also been combined with erythropoietin (EPO) and hyperbaric oxygen to increase oxygen in the tumor cells [170]. In addition, two different mechanism-driven photosensitizers can be combined in PDT treatment to obtain better outcomes [171]. Combination PDT with other therapy enhances treatment efficacy without affecting normal cells and tissues, and in some cases can also reduce system-

ic toxicity. Therefore, PDT combination therapy is of great interest and is a major focus in clinical research.

1.3. Iron Physiology and Pathophysiology

Iron is essential for the biological system. In eukaryotic cells, iron participates in several cellular processes, including oxygen transport, oxidative phosphorylation, DNA biosynthesis, and xenobiotic metabolism [172]. In addition, iron is a constitutive part of physiologically important proteins, such as hemoglobin, cytochromes, oxygenases, flavoproteins, and redoxins [173].

Iron exists either in reduced ferrous (Fe^{2+}) or oxidized ferric (Fe^{3+}) form and recycles between these two forms based on environmental conditions [174]. Depending on its oxidative status, iron is utilized by biological systems and integrated into vital biologic processes that require transfers of electrons (*e.g.*, respiration and oxidative phosphorylation processes) [175, 176]. Inside the cytoplasm, iron mainly exists in Fe^{2+} , which is very active and rapidly reacts with O_2 to form ROS. Especially when Fe^{2+} interacts with H_2O_2 , it generates highly reactive and toxic $\text{OH}\cdot$ through the Fenton reaction to damage macromolecules, including DNA, lipid membranes, and proteins [177]. Therefore, in the biological system, free iron levels are regulated in a tightly controlled manner. Iron is always carried with proteins or iron transporters to reduce the level of free redox-active iron and prevent cell damage and toxicity.

Considering the important biological role of iron, either iron overload or iron deficiency causes dysregulation of biological systems and damages the organism. Iron deficiency decreases heme synthesis and disturbs iron-regulated biological reac-

tions, thus leading to decreased cell growth and proliferation, hypoxia, and even cell death [178]. To maintain erythropoiesis and other iron-mediated vital cellular functions, 25 mg of iron is needed for daily use. However, dietary uptake of iron from intestinal sources only provides 1 to 2 mg of iron supply [179]. Therefore, other cellular mechanisms of iron regulation, such as iron release from the cellular iron storage protein, ferritin or recycling of iron from iron-containing biomolecules through the lysosome-mediated autophagy process, are extremely important and tightly regulated to provide iron needed for the biological systems [180].

Conversely, an excess of iron in biological systems leads to oxidative stress and damages biomolecules that harm the organism. Prolonged oxidative stress to biological systems causes inflammation, dysregulated cellular signaling pathways, and various pathogeneses, including neurodegenerative diseases (*e.g.*, Alzheimer's, Parkinson's and Huntington's diseases and Friedreich's ataxia) and cancer [181-185]. Increased physiological iron levels have also been reported to be associated with infection [186, 187].

The amount of total body iron in a healthy human being is about 50 mg/kg. This iron is derived from hemoglobin in erythrocytes and myoglobin in muscle cells [179, 188]. Humans lack mechanisms to eliminate iron, except through loss of hemoglobin during bleeding or defecation of apoptotic enterocytes and macrophages.

Since iron is important but dangerous at high or low levels, iron uptake and regulation is strictly controlled.

1.3.1. Cellular Iron Regulation

Following the release of iron from enterocytes and macrophages into the bloodstream, iron binds to transferrin (Tf), which is a plasma glycoprotein with two high affinity iron binding sites [189]. The fact that free iron binds to transferrin immediately after its release into the bloodstream prevents potential iron-induced toxicity in circulation. Fe^{3+} forms a complex with transferrin, which binds to transferrin receptor 1 (TfR1) for receptor-mediated endocytosis, resulting in iron delivery to endosomes/lysosomes [190]. In acidic late endosomes, Fe^{3+} is released from the transferrin and transferrin receptor complex; it is converted to Fe^{2+} by the enzyme ferrireductase, localized on the endosomal membrane. Fe^{2+} is then transported out of lysosomes through the divalent metal transporter 1 (DMT1) to form the labile or chelatable iron pool in the cytosol [191]. This iron is highly redox active and is distributed to several cellular destinations for storage or usage (Fig. 9). Cytosolic iron can be transported to ferritin, a cellular protein that sequesters and stores excess cytosolic free iron within cells to avoid iron-mediated ROS generation and cellular damage. Ferritin consists of heavy chain and light chain subunits, among which heavy chain has the ferroxidase activity to convert Fe^{2+} into Fe^{3+} and stores the whole complex as a ferric oxhydroxide mineral [192]. In addition to its location in the cytosol, ferritin is also found in the nucleus and mitochondria [193]. In addition, iron in the labile

iron pool can also be distributed for cellular usage (ex: nucleus for DNA synthesis) or be further transported to mitochondria through mitochondrial iron transporters (ex: mitoferrins) to support iron-sulfur, heme, and iron-containing enzyme synthesis in the mitochondria [194].

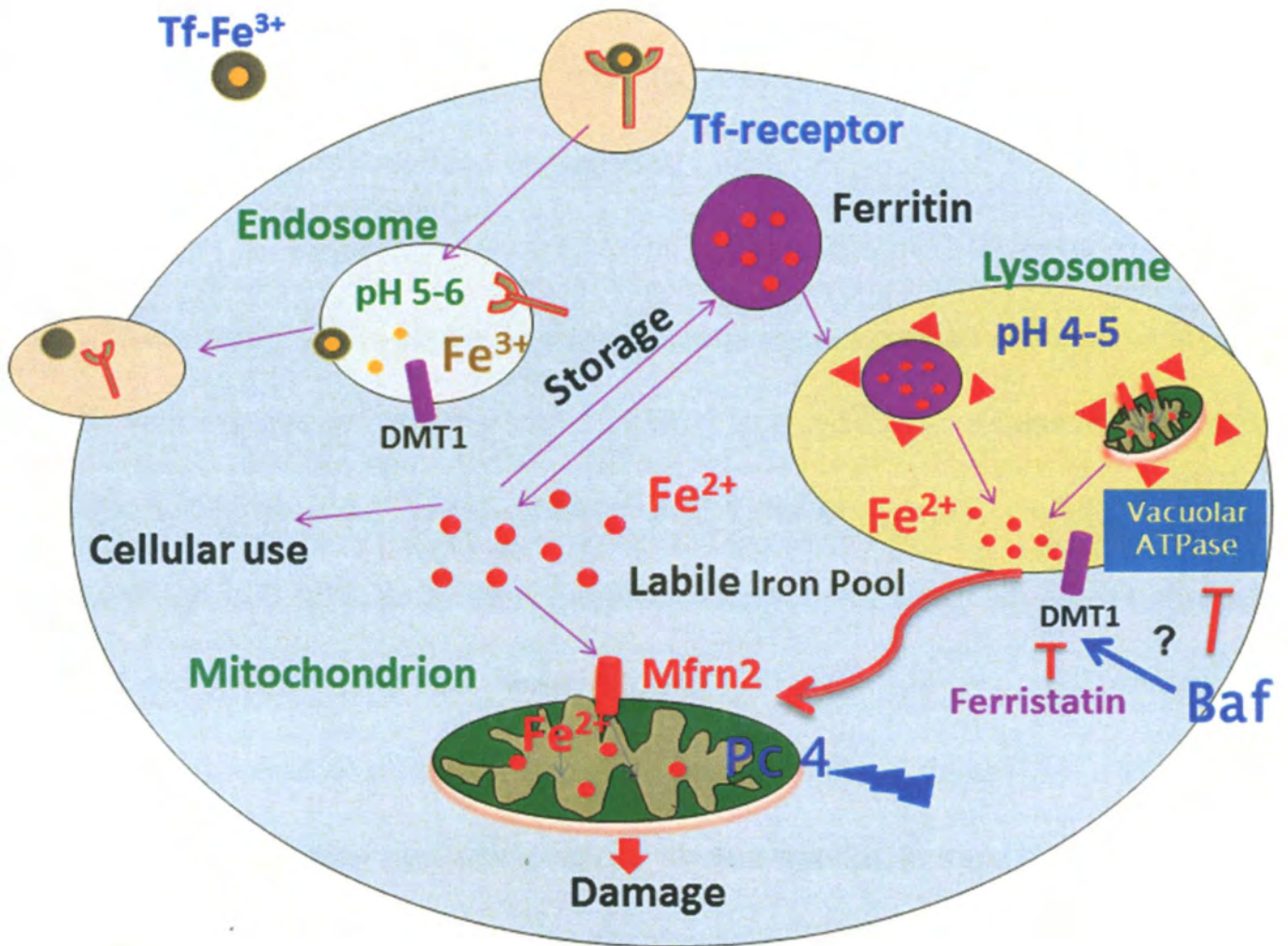


Figure 9. Cellular iron regulation and the interplay between cellular organelles.

For cellular iron export, the iron exporter ferroportin mediates Fe^{2+} efflux from enterocytes and macrophages into the plasma to maintain systemic iron homeostasis. This process is negatively regulated by a liver-derived peptide hormone hepcidin, which is excreted from the liver into circulation and interacts with the ferroportin in response to high intracellular iron level by promoting ferroportin phosphorylation, internalization, and endocytosis degradation [195].

In addition to iron uptake and export, intracellular iron levels are also regulated by the iron regulatory proteins 1 and 2 (IRP1 and IRP2) to maintain the balance of cellular iron homeostasis [194]. IRPs act as cellular iron sensors to detect the changes in cellular iron level and interact with iron-responsive elements (IREs) to regulate iron-related protein synthesis, including TfR1, DMT1, ferritin, mitochondrial aconitase, and 5-aminolevulinate synthase at the translational level [196, 197]. Cellular iron-regulated proteins that are involved in iron uptake, storage, transport and metabolism are all under control of the IRPs and IREs in response to the cellular iron condition. When cellular labile iron levels are decreased, the IRPs bind to iron-response elements (IREs) within the 5'-untranslated region (5'-UTR) of ferritin mRNA to inhibit the initiation of ferritin protein translation and down-regulates its expression. Simultaneously, IRPs bind to IREs within the 3'-UTR of the TfR1 to stabilize and protect its mRNA from being cleaved and degraded by the endonucleolytic enzymes and thus increase the expression of the TfR1 to restore cytosolic iron levels. Conversely, cytosolic labile iron levels are increased, IRPs bind to IREs with-

in the 5'-UTR of TfR1 and 3'-UTR of ferritin to reduce the free iron uptake and facilitate the iron being stored into ferritin to decrease the cellular iron levels and restore iron homeostasis.

Mitochondrial Iron Regulation

Cellular iron homeostasis is maintained through the interplay among cytosolic, mitochondrial, and lysosomal environments [180]. After Fe^{2+} is released from endosomes into the cytosol through the DMT1 to form the labile iron pool, Fe^{2+} can be transported into mitochondria through the mitochondrial iron transporters to supply the iron needed for mitochondrial heme and iron-sulfur cluster synthesis or iron storage in mitochondrial ferritin.

Although the mechanism of mitochondrial iron regulation is not yet well characterized, two proteins on the mitochondrial inner membrane have been identified that participate in mitochondrial iron uptake: mitoferrin 1 (Mfrn1) and mitoferrin 2 (Mfrn2). Mfrn1 expresses in erythroid cells whereas Mfrn2 expresses in non-erythroid cells [198, 199]. Mfrn1 has been reported to increase its half-life during erythropoiesis but the half-life of Mfrn2 remains the same in developing erythroid cells [199]. Mfrn2 has three isoforms, which include a full length and two truncated forms (Fig. 10). Although all three isoforms of the Mfrn2 [200] are able to localize to mitochondria, so far all the functional studies of Mfrn2 are based on the full length isoform, considered the canonical isoform.

Isoform -1 (364 bp)

Isoform -2 (177 bp)

Isoform -3 (176 bp) NPAE → MALL

Figure 10. Mfrn2 isoforms.

1.4 Aim and Outline of the Project

The aim of this project is to study a mechanism based strategy to enhance the efficacy of photodynamic therapy. In this project, we used the photosensitizer Pc 4. Pc 4 has recently completed a Phase I clinical trial for cutaneous neoplasms and is currently in a Phase I trial for psoriasis. Head and neck cancer is a disease model which has been effectively treated with PDT using other photosensitizers such as foscan and porfimer sodium. Our aim was to determine how lysosomes contribute to PDT induced by the mitochondria-targeted photosensitizer Pc 4. Specifically, we focused on the role of lysosomal iron in PDT's mechanism.

Chapter 2

Role of Iron in Pc 4-PDT-Treated Head and Neck Cancer Cell Lines

Hypothesis

Iron released from lysosomes enhances mitochondria-mediated cell killing during Pc 4-PDT.

Introduction

Head and neck squamous cell carcinomas (HNSCC) rank as the 6th most common cancers worldwide and lead to 350,000 deaths each year [3]. Despite advances in treatment, 5-year survival of patients with HNSCC has not significantly improved over the past several decades. First-line treatments are surgery, radiation, chemotherapy, and a combination of these modalities. However, many patients develop chemo- and radioresistance, and only 50-60% of the patients treated with radiation and chemotherapy are cured of their disease. Surgery is not an attractive mode of treatment since disfigurement dramatically affects quality of life. Therefore, better treatment modalities are needed to combat this devastating disease.

PDT is an FDA-approved, minimally invasive treatment modality that utilizes light in the presence of oxygen to activate photosensitizing agents and produce cell death. Currently, PDT has been shown to successfully treat early stages of HNSCC in the oral cavity, pharynx, and larynx [115-120]. Because the photosensitizers used in PDT do not target the nucleus but other cellular organelles (*e.g.*, mitochondria, lysosomes, ER, plasma membrane), PDT does not cause mutagenic or carcinogenic effects [77]. Together with its tumor selectivity and lack of systemic toxicity, PDT

can be repeatedly used to treat patients to achieve maximal therapeutic effects. In addition, PDT is a non-invasive therapy and can be combined with other traditional therapies to maximize treatment outcomes, making it a very promising cancer treatment modality [77, 114, 201-203]

Phthalocyanine 4 (Pc 4) is a second generation porphyrin-based photosensitizer used in PDT. Pc 4 has a strong absorption peak at 670 nm wavelength, allowing for penetration deep into tissue and a high quantum yield which efficiently generates $^1\text{O}_2$. Our laboratory has previously shown that Pc 4 localizes to cellular membranes of the mitochondria, ER, and golgi and causes mitochondria-mediated apoptotic cell death [204]. Pc 4 is a potent photosensitizer and has been applied with promising results for malignant and non-malignant treatments in vitro, in vivo, and clinically. Including 43 cancer patients who had actinic keratoses, Bowen's disease, squamous cell carcinoma, basal cell carcinoma, or mycosis fungoides, a recent phase I clinical trial showed promising effects to induce apoptotic cell death without causing any safety or toxicity issues [98].

Studies from other groups have shown that bafilomycin, a proton pump ATPase inhibitor, collapses the pH gradient of lysosomes and releases iron from lysosomes into the cytosol, causing iron accumulation in mitochondria [205]. In line with this, our group showed that bafilomycin enhanced Pc 4-PDT killing in A431 epidermal carcinoma cells through lysosomal iron release to cause mitochondrial de-

polarization and onset of apoptotic cell death [92]. These findings suggested the role of lysosomal iron in mitochondria-mediated PDT cytotoxicity.

In this study, our aim was to determine how lysosomes contribute to PDT induced by mitochondria-targeted photosensitizers such as Pc 4. Specifically, we focused on the role of lysosomal iron in PDT killing. In cells and tissues, two pools of iron exist. The first pool is “non-chelatable” iron, which is sequestered in ferritin and in structural components of proteins (*e.g.*, heme, iron-sulfur complexes) and cannot be removed by iron chelators like desferrioxamine (DFO). The second pool is “chelatable” iron, which represents free iron and iron bound loosely to a wide variety of anionic intracellular molecules [205]. Chelatable iron is accessible to DFO and other iron chelators. Chelatable iron and other transition metals, such as copper, catalyze formation of highly reactive hydroxyl radical (OH^\bullet) from H_2O_2 and $\text{O}_2^{\bullet-}$ and damage DNA, proteins, and membranes [206].

Lysosomes are a source of rapidly mobilized chelatable iron that, when released into the cytosol, is rapidly taken up by mitochondria through the calcium uniporter [205]. Inside mitochondria, this iron is available to catalyze toxic ROS cascades. Therefore, we hypothesized that iron translocation from lysosomes to mitochondria would enhance PDT-induced cell killing with mitochondria-targeted photosensitizers.

Materials and Methods

Cell Culture. Human head and neck squamous carcinoma cell lines (UMSCC1, UMSCC14 and UMSCC22A) were a gift from Dr. Besim Ogretmen (Medical University of South Carolina). Human A431 epidermoid carcinoma cells were obtained from the American Type Culture Collection. Cells were cultured in Dulbecco's Modified Eagle's Medium (DMEM) (Gibco) supplemented with 10% fetal bovine serum (FBS) and penicillin/streptomycin (complete culture medium) in a humidified 37°C incubator at 5% CO₂/95% air.

Cellular Pc 4 Uptake. The phthalocyanine photosensitizer Pc 4 was obtained from Dr. Malcolm Kenney (Case Western Reserve University) [97]. A stock solution of 0.5 mM was made in dimethyl formamide and diluted into complete culture medium. Cells (360,000/dish) were cultured on 60-mm Petri dishes in complete culture medium for 24 h. Subsequently, cells were incubated with Pc 4 concentrations, as indicated, for 18 h and then washed twice with PBS and lysed in 0.5% sodium dodecyl sulfate (SDS). Cell lysates were collected and fluorescence was measured with a fluorometer (Photon Technology International, Birmingham, NJ) using 610 nm excitation and 630-720 nm emission. A calibration curve was constructed by adding known concentrations of Pc 4 to the lysates.

Subcellular Localization of Pc 4. Cells were cultured onto 35-mm glass-bottomed Petri dishes (MatTek Corporation, Ashland, MA) at 150,000 cells/dish and incubated

for 24 h. Subsequently, UMSCC1, UMSCC14A and UMACC22A cells were loaded with Pc 4, as indicated, for 18 h. Medium was aspirated and changed to fresh medium supplemented with Insulin-Transferrin-Selenium-X (ITX) reagent [insulin (10 $\mu\text{g/ml}$), transferrin (5.5 $\mu\text{g/ml}$), selenium (6.7 ng/ml), ethanolamine (0.2 mg/ml)] (Gibco), and omitting FBS. To assess co-localization of Pc 4 with mitochondria, cells were loaded with 500 nM rhodamine 123 (Rh123) for 20 min. Medium was changed with fresh medium containing 50 nM Rh123. Dishes were placed in an environmental chamber at 37°C on the stage of Zeiss LSM 510 laser scanning confocal microscope (Zeiss, Germany). A 63 X N.A. 1.4 oil immersion planapochromat objective was used for all experiments. Rh123 and Pc 4 fluorescence was imaged using 488 nm excitation/500–530 nm emission and 543 nm excitation/560 nm long pass emission, respectively.

Photodynamic Therapy. Cell cultures were incubated with the desired concentration of Pc 4 for 18 h before exposure to 390 mJ/cm^2 red light ($\lambda = 670 \text{ nm}$) at 37°C from an Intense-HPD 7404 diode laser (North Brunswick, NJ). Subsequently after exposure to red light, cells were incubated for various periods of time prior to analysis.

Assessment of Cell Death. Cell death was assessed by propidium iodide (PI) using a multi-well fluorescence plate reader, as previously described [207]. Briefly, cells were cultured on 96-well plates (6,000 cells/well) for 24 h in complete culture medi-

um. Pc 4 in the presence or absence of DFO (1 mM), sDFO (1 mM) and Ru360 (10 μ M) were present during the last 18 h of the incubation, where indicated. Subsequently, medium was replaced with fresh medium supplemented with ITX reagent and PI (30 μ M) but without FBS. Bafilomycin (50 nM) was added as indicated. One h after drug addition but before irradiation, PI fluorescence was measured using 530 nm excitation (25 nm band pass) and 620 nm emission (40 nm band pass) filters. PI fluorescence was then measured at frequent intervals for 8 h. Between measurements, microtiter plates were placed in a 37°C incubator. At the end of the experiment, digitonin (200 μ M) was added to each well to permeabilize all cells and label all nuclei with PI. Percentage viability (V) was calculated as $V = 100(B-X)/(B-A)$, where A is initial fluorescence, B is fluorescence after addition of digitonin, and X is fluorescence after any given time. Cell viability determined by PI fluorometry is essentially the same as cell viability determined by trypan blue exclusion [207].

Apoptosis was determined from nuclear morphology after PI staining in the presence of digitonin. At indicated time points, floating and adherent cells were collected, centrifuged and resuspended in PBS containing 100 μ M digitonin and 30 μ M PI. Digitonin permeabilizes the plasma membrane and allows PI to enter cells and stain all nuclei. Thus, PI staining in the presence of digitonin is equivalent to staining with Hoechst and DAPI, the two fluorescent dyes most commonly used to assess apoptosis by nuclear morphology. Apoptotic nuclei were scored as apoptotic based on nuclear condensation and fragmentation and counted with a 40X microscope ob-

jective using a rhodamine filter set and expressed as a percentage of total cells. At least 200 cells were counted from three different microscopic fields for each sample.

Caspase 3/7 Activity. Caspase-3/7 activity was measured using a Caspase-Glo™ 3/7 kit (Promega, Madison, WI) according to the manufacturer's instructions. At indicated time points, cultured cells were scraped into a test tube followed by centrifugation. The pellet was resuspended and lysed with RIPA (150 mM NaCl, 1 mM EGTA, 1% sodium deoxycholate, 1% Triton X-100, 50 mM Tris-Cl, pH 7.4) buffer. Caspase-Glo™ 3/7 reagent and the lysate were mixed in 1:1 ratio, and luminescence was measured with a luminometer. The resulting luminescence was proportional to caspase activity.

Clonogenic Assay. Cells (330,000/dish) were cultured on 60-mm Petri dishes for 24 h. Subsequently, cells were loaded with 25 nM Pc 4 for 16-18 h. One hour prior to irradiation, 50 nM bafilomycin was added, as indicated. Immediately after irradiation, cells were harvested by trypsinization. Aliquots of cell suspensions were plated onto 60-mm Petri dishes in amounts sufficient to yield 50-100 colonies per dish. After 14 days in complete culture medium, colonies were stained with 0.1% crystal violet in 20% ethanol and counted by eye.

Lysosomal Integrity. To assess the lysosomal integrity, cells were incubated with 0.2 mg/ml of Alexa-488 dextran (10 kDa) for 18 h. Alexa-488 dextran is taken up

by cells via endocytosis. Alexa-488 fluorescence was imaged by confocal microscopy (488 nm excitation/500-530 nm emission). Bright green dots co-localized with lysosome-specific fluorophores (data not shown), such as LysoTracker Red, indicating that Alexa-488 dextran can be used as an endosomal/lysosomal marker. To assess LysoTracker Red release from lysosomes, cells were incubated with LysoTracker Red (500 nM) for 20 min at 37°C in complete culture medium. Medium was replaced with fresh medium supplemented with 200 nM LysoTracker. LysoTracker Red fluorescence was imaged by confocal microscopy (543 nm excitation/560 nm long pass emission).

Statistical Analysis. Data are calculated as means \pm SEM from at least three independent experiments performed in triplicate. Pairwise comparison was performed by two-tailed *t*-test using InStat2 software (GraphPAD, San Diego, CA). A *p* value < 0.05 was considered to be statistically significant.

Results

Cellular Uptake and Subcellular Localization of Pc 4 in Head and Neck Cancer Cells

Pc 4 is a hydrophobic photosensitizer that diffuses freely across the plasma membrane and binds to membranes of intracellular organelles [204]. Three different head and neck cancer cell lines were incubated with different concentrations of Pc 4, as indicated in Fig. 2-1A. Cellular Pc 4 uptake was determined by cell lysates. The 3 cell lines took up Pc 4 differently in the order of UMSCC22A, UMSCC14A, UMSCC1 (Fig. 2-1A). To achieve an equal cellular Pc 4 uptake among cell lines, UMSCC14A and UMSCC1 cells required higher loading concentrations of Pc 4 to yield the same Pc 4 uptake as UMSCC22A cells (Fig. 2-1A). Subcellular localization of Pc 4 was determined at equal cellular Pc 4 content (1.5 pmol/mg) using confocal microscopy. To determine co-localization of Pc 4 with mitochondria, cells were loaded with rhodamine 123, a mitochondria-specific probe. In all three cell lines, overall Pc 4 pattern and co-localization of Pc 4 with rhodamine 123 was similar (Fig. 2-1B).

Head and Neck Cancer Cells Respond Differently to PDT

After determination of the Pc 4 loading concentrations that resulted in equal cellular Pc 4 uptake between 3 different head and neck cancer cells, we determined their individual sensitivity to Pc 4-PDT. Sensitivity to Pc 4-PDT was determined at 3 different levels of cellular Pc 4 content. All 3 cell lines were resistant to PDT at the Pc 4 uptake of 0.8 pmol Pc 4/mg protein (Fig. 2-2A). At the Pc 4 uptake of 1.5

pmol Pc 4/mg protein, Pc 4-PDT had minimal toxicity in UMSCC1 and UMSCC14A cells (Fig. 2-2A). In contrast, UMSCC22A cells were more sensitive, and cell viability was decreased to 15% after 8 h (Fig. 2-2B). At even higher Pc 4-PDT dosages (2.8 pmol Pc 4/mg protein), differences in sensitivity between cell lines were diminished (Fig. 2-2C). Thus, we identified the Pc 4-PDT resistant and responsive head and neck cancer cells at 1.5 pmol Pc 4/mg protein. Since UMSCC1 and UMSCC14A cells behaved similarly regarding sensitivity to PDT, we decided to concentrate on UMSCC1 and UMSCC22A in further experiments. Results shown in (Fig 2-1 and Fig 2-2) demonstrated that head and neck cancer cells responded differently to the Pc 4-PDT while the difference in sensitivity cannot be explained by equivalent cellular uptake and similar patterns of Pc 4 subcellular localization.

Bafilomycin Enhances PDT Killing in Both Resistant and Responsive Cell Lines

It has been known that lysosomes can be an alternative target in cases of failed mitochondrial targeting therapy. Therefore, our lab took the pharmacology approach by combining the bafilomycin, an inhibitor of the vacuolar proton-pumping ATPase (H^+ -ATPase), which collapses lysosome pH and releases lysosomal iron to the mitochondria [205], with the mitochondria localized Pc 4-PDT. Results showed that bafilomycin enhances mitochondria-mediated Pc 4-PDT killing in A431 cells as shown in (Fig 2-3A) as well as results obtained from another lysosomal alkalization agent, chloroquine which is a weak base and accumulates into lysosomal acidic

vesicles to raise their pH. Chloroquine has the same biological effect as bafilomycin. Neither chloroquine nor bafilomycin alone with PDT induced cell killing but, when combined with Pc 4-PDT, both enhanced Pc 4-PDT cytotoxicity (Fig. 2-3A). In addition, the effects of bafilomycin on Pc 4-PDT treated A431 cancer cells were further confirmed by clonogenic assay, which measures the effect of a reagent on cancer cell survival and proliferation (Fig. 2-3B). Bafilomycin plus Pc 4-PDT treated A431 cells showed decreased proliferation and survival compared to the Pc 4-PDT.

Cell death type by bafilomycin enhanced Pc 4-PDT killing was further determined by PI nuclear morphology staining and caspase activity assay. The PI fluorometry assay monitors failure of the plasma membrane permeability barrier, an event that occurs during necrosis and late stage apoptosis, the latter often named secondary necrosis. To determine further the mode of cell death, apoptosis and caspase 3/7 activity were monitored. Both caspase-3/7 activity and apoptotic death were enhanced by bafilomycin after Pc 4-PDT treatment. Moreover, the pan caspase inhibitor z-VAD completely blocked Pc 4 plus bafilomycin-induced caspase activation and apoptosis (Fig. 2-4). Overall, the results indicate that bafilomycin enhances mitochondria targeted Pc 4-PDT cytotoxicity but alone is nontoxic.

We assessed the effect of bafilomycin on PDT-induced cell killing in the UM-SCC1 and UMSCC22 head and neck cancer cell lines. At 0.8 pmol Pc 4/mg protein, Pc 4-PDT alone or in combination with bafilomycin induced minimal toxicity in

UMSCC1 cells (Fig. 2-5A). Bafilomycin alone or light alone caused no toxicity (data not shown). At higher Pc 4 loading (1.5 pmol Pc 4/mg protein), its combination with bafilomycin caused 100% cell death after 5 h exposure to Pc 4-PDT (Fig. 2-5A) in UMSCC1 cells.

In UMSCC22A cells, 0.8 pmol Pc 4/mg protein caused no toxicity during PDT, but its combination with bafilomycin greatly enhanced cell killing and decreased viability from 93% (Pc 4-PDT alone) to 17% (Pc 4-PDT plus bafilomycin) (Fig. 2-5B). At even higher Pc 4 loading (1.5 pmol Pc 4/mg protein), Pc 4-PDT greatly induced cell killing, and bafilomycin did not further enhance it since the UMSCC22 cells are already very sensitive to the higher Pc 4 dose (1.5 pmol Pc 4/mg protein) alone. When another lysosomal alkalization reagent, chloroquine, was applied to further observe the dysregulated pH effect of lysosome on Pc 4-PDT, we obtained similar PDT-enhanced cytotoxicity results (data not shown).

These results suggest that, for those in whom mitochondrial targeted PDT therapy has shown failure or resistance, lysosomal alkalization agents represent a feasible combination adjuvant to increase PDT treatment efficacy.

Iron Chelators and Ru360 Protect Against Bafilomycin-Enhanced PDT Killing

Studies from hepatocytes demonstrate that bafilomycin releases iron from lysosomes to the cytosol [205]. Therefore, we characterized whether chelation of iron would protect against bafilomycin-enhanced cell killing during PDT. Cells were pretreated with DFO (1mM) for 18 h before bafilomycin and subsequent irradiation. In UMSCC1 cells at 1.5 pmol Pc 4/mg protein, DFO increased cell viability from 0 to 37% after 5 h (Fig. 4A). starch-DFO (sDFO) (1mM), which is taken up by endocytosis and specifically chelates endosomal/lysosomal iron, protected against cell killing after Pc 4-PDT to an even greater extent than DFO, increasing viability from 0 to 52% after 5 h (Fig. 2-6A). Ru360 is a highly specific inhibitor of the mitochondrial electrogenic calcium uniporter [205]. When cytosolic Fe^{2+} increases, the calcium uniporter transports iron into mitochondria [92]. Ru360 (10 μ M) blocked bafilomycin-enhanced PDT killing increasing viability from 0 to 79% after 5 h in UMSCC1 cells (Fig. 2-6A).

Similarly, in MUSCC22A cells, DFO and sDFO greatly protected against bafilomycin-enhanced PDT (0.8 pmol Pc 4/mg protein) toxicity, increasing viability from 17% to 69% and 60% in the presence of DFO and sDFO, respectively, after 8 h (Fig. 2-6B). Again, Ru360 provided even greater protection, with viability increasing from 17 to 87%. Cytoprotection by iron chelators indicates that bafilomycin-induced toxicity during PDT is mediated by the release of lysosomal iron to the cyto-

sol. Toxicity was likely related to increased mitochondrial iron uptake, since Ru360 greatly blocked toxicity.

Lysosomal Iron Augments Bafilomycin plus Pc 4-PDT-Mediated Cell Killing

Results from another group [205] and the iron chelators and calcium uniporter inhibitor tested in these experiments both suggested that bafilomycin enhanced Pc 4-PDT killing through lysosomal iron release and mitochondrial iron uptake, as shown in Fig. 2-6. To further assess whether iron participates in cell killing after Pc 4-PDT, we pre-incubated A431 cells with 30 μ M ammonium iron (III) citrate (Fe^{3+}) for 24 h before Pc 4 loading. Fe^{3+} binds to transferrin, which is taken up by cells through receptor-mediated endocytosis, resulting in increased lysosomal iron. After Fe^{3+} loading, cells were loaded with Pc 4 followed by bafilomycin or vehicle and light irradiation. At the low concentration of Pc 4 used, PDT in the absence and presence of Fe^{3+} caused virtually no toxicity (Fig. 2-7). However, in the presence of bafilomycin, Fe^{3+} nearly doubled the rate of bafilomycin Pc 4-PDT-induced killing, decreasing viability to 25% from 47% at 12 h after PDT. This result indicated that iron taken up into the lysosome and released into the cytosol by bafilomycin contributes to the increased PDT killing effect.

Bafilomycin Enhanced Pc4-PDT Killing through Lysosomal Iron Release without Causing Lysosomal Membrane Permeability

To determine whether bafilomycin-enhanced mitochondrial dysfunction after PDT was dependent on lysosomal membrane breakdown, cells were preloaded with Fe^{3+} , Alexa-488 dextran (10 kDa), and Pc 4 (25 nM). Alexa-488 dextran is taken up by endocytosis to label endosomes/lysosomes as bright fluorescent dots (Fig. 2-8A, Pc 4+Fe). Subsequent 1 h exposure of bafilomycin did not change endosomal /lysosomal integrity (Fig. 2-8A, +Baf). After 2 h of irradiation (Fig. 2-8A, +light), when mitochondrial depolarization was maximal, there was no change in Alexa-488 dextran fluorescence (Fig. 2-8A, +Baf+Light), mitochondria depolarization image is not shown). This result indicated that bafilomycin released lysosomal iron to cause mitochondrial depolarization without breaking the lysosomal membrane; otherwise, the small 10 kDa Alexa-488 dye would have leaked out and decreased the lysosomal labeling intensity. On the other hand, to further confirm that bafilomycin collapsed lysosomal pH gradient, cells were loaded with LysoTracker Red (500 nM) and subsequently exposed to bafilomycin. LysoTracker Red is a weak base and accumulates into acidic organelles such as lysosomes [208]. Inhibition of the vacuolar proton-pumping ATPase with bafilomycin is well established to collapse lysosomal pH gradients and induce lysosomal alkalinization where the LysoTracker Red can no longer be retained in increased pH environment. Result from (Fig. 2-8B) showed that release of LysoTracker Red after bafilomycin in our experiments confirmed that bafilomycin does collapse the lysosomal pH in the treated cells as expected (Fig. 2-

8B). At the same time, we also loaded lysosomes with Alexa-488 dextran (10 kDa) in other dishes. After 1 h exposure to bafilomycin, lysosomes retained Alexa-488 dextran but released LysoTracker Red (compare Fig. 2-8 A with B).

Bright LysoTracker Red-labeled spots disappeared after bafilomycin administration, indicating lysosomal alkalization (Fig. 2-8B). These results indicate that bafilomycin-enhanced mitochondrial dysfunction was not due to endosomal/lysosomal membrane breakdown but rather was caused by collapse of the pH gradient in these organelles, which promotes release of lysosomal chelatable iron into the cytosol. Taken together, these findings suggest that lysosomal alkalization by bafilomycin released iron without causing the generalized lysosomal membrane permeabilization. Additionally, imaging of Alexa-488 dextran did not show evidence of lysosomal swelling after bafilomycin, which would be expected as a colloid osmotic effect if the membrane became nonspecifically permeable to smaller molecular weight solutes. Indeed, nonspecific permeabilization to small or large molecular weight solutes has never been described for bafilomycin. Rather bafilomycin is a very specific and high affinity inhibitor of the lysosomal proton pump [209].

Ferristatin Protects Cells against Bafilomycin-Mediated PDT Toxicity

Although the mechanism by which bafilomycin releases iron from lysosomes was unclear until these results, findings from our lab and others have clearly showed that bafilomycin releases lysosomal iron without physically damaging the lysosomal membrane [92, 205]. In normal physiology, cells store ferrous iron in endosomes/lysosomes and move iron out of lysosomes through the DMT1 [210]. This phenomenon suggests a possible lysosomal iron releasing mechanism by bafilomycin through the DMT1.

With the attempt to study the putative role of bafilomycin in releasing lysosomal iron into the cytosol by DMT1, a pharmacologic approach was taken by applying ferristatin, an inhibitor of DMT1 [211] to bafilomycin-treated Pc 4-PDT. PDT results from UMSCC22A cells showed that ferristatin markedly protected cells against bafilomycin-enhanced PDT toxicity (Fig. 2-9) if pre-incubated more than 4 h prior to bafilomycin addition. Moreover, ferristatin failed to protect if it was added after bafilomycin (not shown), which had therefore already released lysosomal iron. These findings strongly support and suggest the possible mechanism of lysosomal iron release by bafilomycin via DMT1 (Fig. 2-9).

Chloroquine Retards Regrowth of Tumors after PDT

Our *in vitro* data show that bafilomycin greatly enhances Pc 4-PDT efficacy in Mfrn2-expressing cells. Thus, we hypothesized that adjuvant bafilomycin or chloroquine would enhance tumor response to Pc 4-PDT, especially in high Mfrn2-expressing tumors. Instead of bafilomycin, we used chloroquine in this study. Chloroquine showed the same enhanced PDT killing effects as bafilomycin in cancer cell lines (Fig. 2-3A). Chloroquine acts similarly to bafilomycin in collapsing the lysosomal pH gradient and releasing iron from the lysosomes [92]. Moreover, the advantage of chloroquine over bafilomycin for *in vivo* experiments is that chloroquine is already approved for human use by the FDA and has a long safe use record in humans. Xenografts were created with UMSCC22A cells in nude mice and subjected to Pc 4-PDT. Tumor size continued to increase progressively after exposure to light without the photosensitizer (light only) or light plus chloroquine (CHQ) without the photosensitizer. By contrast, with the photosensitizer, tumors disappeared within the first 4 days post-PDT. Subsequently, tumors in the Pc 4 group started to regrow (Pc4). Chloroquine, however, significantly ($p=0.011$) delayed tumor regrowth (Pc4+CHQ) as plotted in Kaplan-Meier form (Fig. 2-10). These pilot data provide proof of principle that chloroquine can enhance the efficacy of PDT *in vivo*.

Discussion

Mitochondrial apoptotic cell death is considered an efficient approach for cancer therapy. However, cancer cells constantly develop mutations within molecules that participate in the apoptotic cell death pathway, resulting in ineffective cancer treatment [212]. Accumulating literature reports that lysosomes can be alternative cellular targeting organelles to enhance therapy [213, 214]. Using a pharmacologic approach, we determined how lysosomes contribute to PDT-induced by mitochondria-targeted photosensitizers, such as Pc 4. Our results show that bafilomycin greatly accelerates mitochondria-specific Pc 4-PDT-mediated cell killing. Although bafilomycin acts on lysosomes, its toxic effects were manifested in mitochondria by accelerated depolarization after PDT, resulting in caspase 3/7 activation and apoptotic death. The findings indicate cross talk between lysosomes and mitochondria during PDT.

The endosomal/lysosomal compartment continuously receives iron by transferrin receptor-mediated endocytosis and by autophagic digestion of iron-containing proteins [180, 194]. Thus, lysosomes are a reservoir of chelatable, redox-active Fe^{2+} . Fe^{2+} reacts with H_2O_2 to generate highly reactive and toxic OH^\bullet . During Pc 4-PDT, a large proportion of ROS formation occurs inside mitochondria and leads to the onset of a mitochondrial permeability transition, as documented by increased mitochondrial dichlorofluorescein fluorescence and the movement of calcein across the mitochondrial inner membrane [204].

The alkalization of lysosomes/endosomes with bafilomycin enhanced Pc 4-PDT-mediated cell killing (Fig. 2-3 and Fig. 2-5). However, bafilomycin did not induce lysosomal membrane breakdown after Pc 4-PDT, as assessed by retention of 10 kDa Alexa-488 dextran with lysosomes (Fig. 2-8A). Alexa-488 dextran fluorescence is pH-independent, and, therefore, the loss of Alexa-488 dextran fluorescence signifies lysosomal disintegration specifically rather than indicating a change in lysosomal pH. These results indicate that lysosomal membranes remained intact during bafilomycin plus PDT treatment (Fig. 2-8A). Since lysosomal membrane permeabilization did not occur, the possibility of cathepsins and other proteases to be released from lysosomes and contribute to PDT cytotoxicity was ruled out.

Fe^{3+} forms a complex with transferrin, which binds to transferrin receptors for receptor-mediated endocytosis, resulting in iron delivery to endosomes/lysosomes. The observation that pre-incubation of cells with ammonium iron (III) citrate enhanced killing after bafilomycin plus Pc 4-PDT treatment and that *s*DFO prevented this cell killing is consistent with the conclusion that bafilomycin mobilizes iron from lysosomes into the cytosol. Similar results were obtained in a recent study with HeLa cells, where FeCl_3 enhanced ionizing radiation-induced killing that was prevented by iron chelation [215].

Our results established that lysosomal iron release mediates bafilomycin-mediated enhanced killing during PDT. However, the mechanism by which bafilomycin releases iron from lysosomes remains unclear. The release of iron occurred

without physical damage to lysosomal membranes (Fig. 2-8A). In normal cell physiology, Fe^{2+} stored in endosomes/lysosomes moves out of lysosomes through the DMT1 [211]. Therefore, we assessed the possibility of lysosomal iron to be released by bafilomycin through DMT1. Ferristatin, an inhibitor of DMT1 [216, 217] markedly protected against bafilomycin-enhanced toxicity (Fig. 2-9). Ferristatin failed to protect if it was added after bafilomycin (not shown) and thus after lysosomal iron release. These results support the conclusion that iron release after bafilomycin occurs *via* DMT1. Evidently these results need to be confirmed using a knock-down/knockout approach.

Fe^{2+} reacts with H_2O_2 to form OH^\bullet , a highly reactive form of ROS [194]. Bafilomycin by itself was not sufficient to induce cell killing (data not shown). Rather, mild oxidative stress induced by low dose Pc 4-PDT combined with bafilomycin was needed to induce cell killing (Fig. 2-3). The iron chelators DFO and sDFO protected against PDT plus bafilomycin-induced mitochondrial depolarization and killing (Fig. 2-6, and Fig. 3-4A) [92]. DFO is highly polar and poorly permeates through membranes, and therefore millimolar concentrations were required to have the protection effect. DFO may also be taken up by endocytosis resulting in its accumulation in endosomes/lysosomes [180]. Consequently, cytoprotection with DFO may be explained by chelation of redox-active iron in lysosomes. sDFO also prevented PDT plus bafilomycin-induced cell killing (Fig. 2-6), indicating that lyso-

somes/endosomes release redox-active iron after bafilomycin and that DFO and sDFO prevent this release by chelating the intraluminal iron store of these organelles.

Protection by lysosomal iron chelation against mitochondrial depolarization [92] after PDT suggests that mitochondrial iron uptake may be responsible for bafilomycin-enhanced killing. Mitochondria accumulate Fe^{2+} , but not Fe^{3+} , electrogenically *via* the MCU [218, 219]. The highly specific inhibitor of MCU, Ru360, also protected against bafilomycin-enhanced PDT toxicity (Fig. 2-6). Although Ru360 and iron chelators blocked cell killing, Ru360 was somewhat more effective in protecting against cell killing (Fig. 2-6). Thus, mitochondrial iron uptake seems to be a key event in bafilomycin-enhanced PDT toxicity.

Besides chelating iron, DFO also stabilizes HIF-1 α in normoxic cells [220]. HIF-1 α activates several protective signaling pathways that potentially could explain cytoprotection by iron chelation. Although DFO and sDFO did stabilize HIF-1 α protein levels, Ru360 did not (Fig. 2-11) [92]. Since Ru360 protected against cell killing even better than DFO/sDFO (Fig. 2-6) [92], HIF-1 α is not likely responsible for cytoprotection.

Bafilomycin is frequently used to inhibit autophagy by collapsing lysosomal pH gradients and thereby blocking fusion of autophagosomes with lysosomes [221]. Consistently with an effect on autophagy, bafilomycin alone and Pc 4-PDT plus bafilomycin increased cellular LC-3 II protein levels as assessed by Western blotting, presumably by inhibiting fusion of autophagosomes with lysosomes (Fig. 2-12).

Thus, bafilomycin inhibited autophagic flux, which may explain the increased PDT killing with bafilomycin. However, iron chelators and Ru360 protected cells against Pc 4-PDT plus bafilomycin toxicity, but neither iron chelators nor Ru360 altered LC-3 II protein levels (Fig. 2-12). Thus, it seems unlikely that enhanced survival by iron chelators and Ru360 acts through enhancing autophagy. Rather, iron chelators and Ru360 prevented cell killing induced by bafilomycin during PDT (Fig. 2-6).

In conclusion, we established a link between lysosomal alkalization and mitochondrial depolarization during PDT (Fig. 2-13) [92]. Strategies to engage lysosomes in cell death pathways have potential to enhance tumor cell killing. Our results here demonstrate that strategies to collapse the lysosomal pH gradient without lysosomal membrane breakdown are sufficient to induce iron-dependent cell killing. Lysosomal perturbation by bafilomycin effectively enhances cell killing during PDT. Pc 4-PDT has completed a Phase I clinical trial for cutaneous neoplasms [98] and is currently in a Phase I trial for psoriasis. The results of this study suggest that agents that disturb lysosomal function could potentially be used clinically as an adjuvant treatment with mitochondria-targeted photosensitizers.

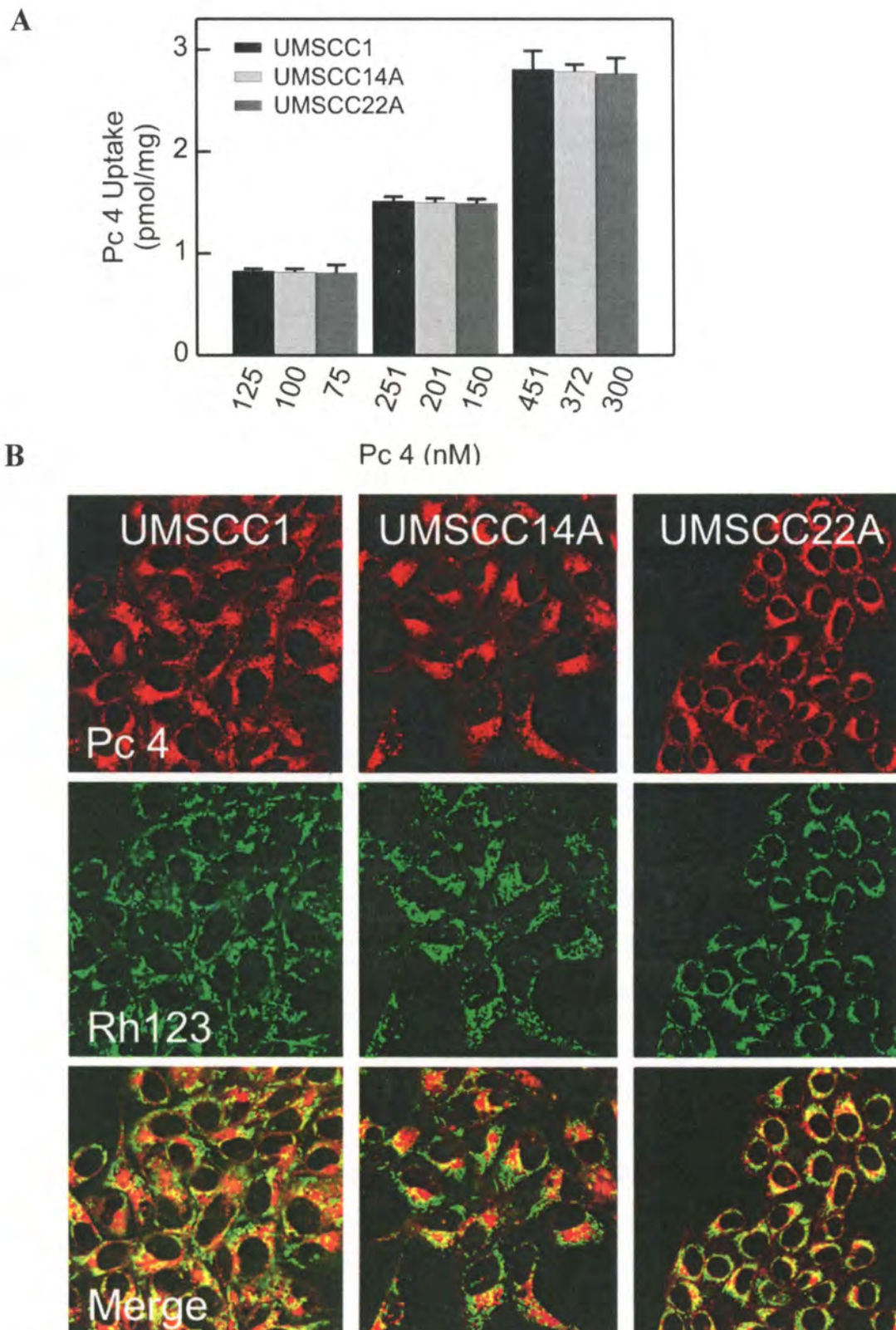


Figure 2-1. Cellular uptake and sub-cellular localization of Pc 4 in head and neck cancer cells. UMSCC1, UMSCC14 and UMSCC22A cells have (A) equivalent cellular Pc 4 uptake under the loading of Pc 4 at concentration of 75-300, 100-375, and 125-451 nM, respectively. Values were normalized to protein content and results represent three independent experiments (mean \pm SEM). (B) Similar Pc 4 cellular localization patterns. Images are representative of three independent experiments.

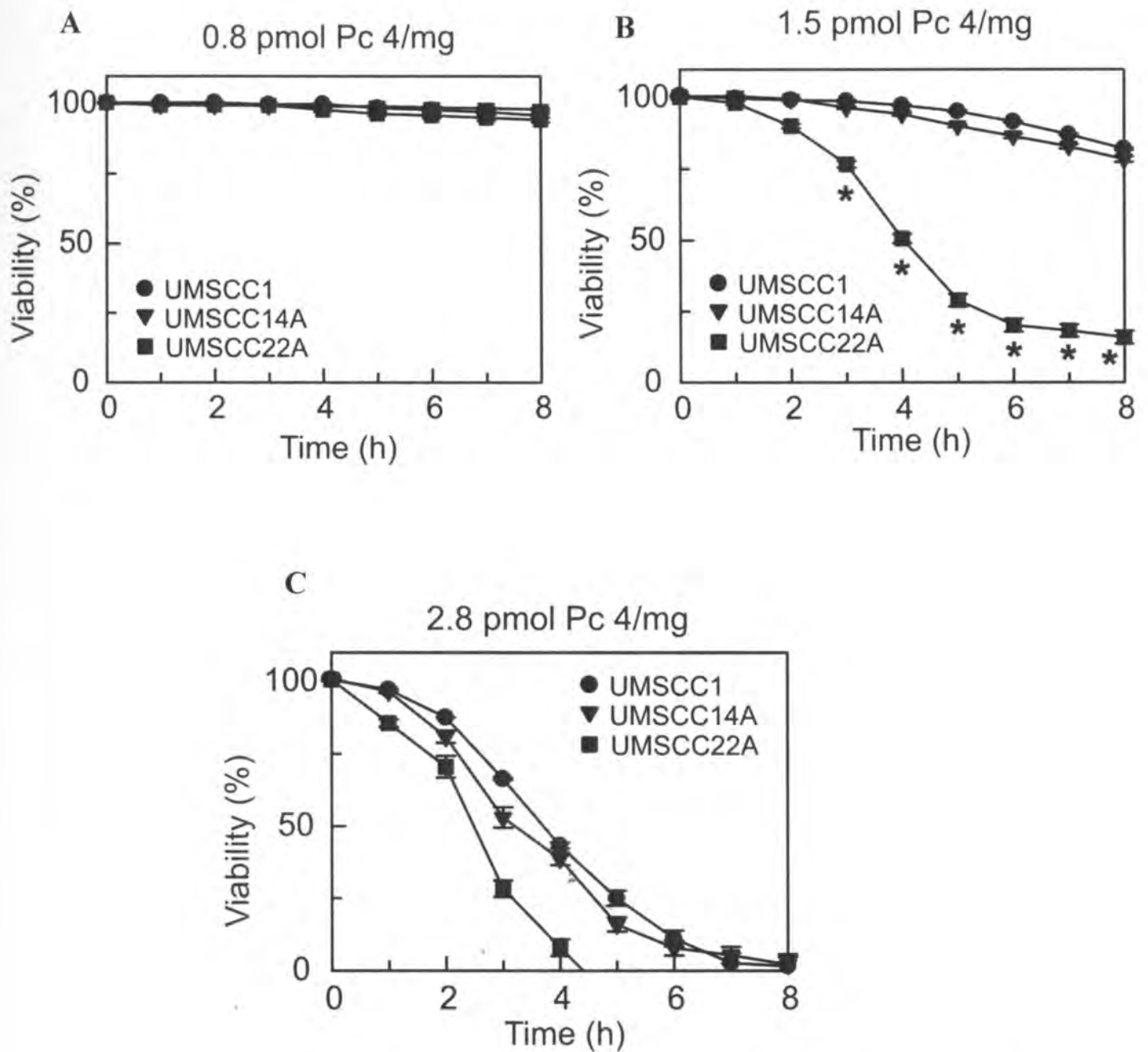


Figure 2-2. Head and neck cancer cells respond differently to PDT. UM-SCC1 and UM-SCC 22A cells respond to PDT dose at (A) 0.8 (B) 1.5 and (C) 2.8 pmol Pc 4/mg protein, as described in Fig. 2-1A. After 18 h, medium was changed to fresh medium supplemented with ITX reagent and PI (30 μ M) but omitting FBS. Cells were exposed to light as described in Materials and Methods. Viability was assessed by PI exclusion using fluorometry. Results are expressed as percent viability at 0 h. Data represent three independent experiments (mean \pm SEM) performed in quadruplicate. *, $p < 0.0001$ compared to UM-SCC1 and UM-SCC 22A.

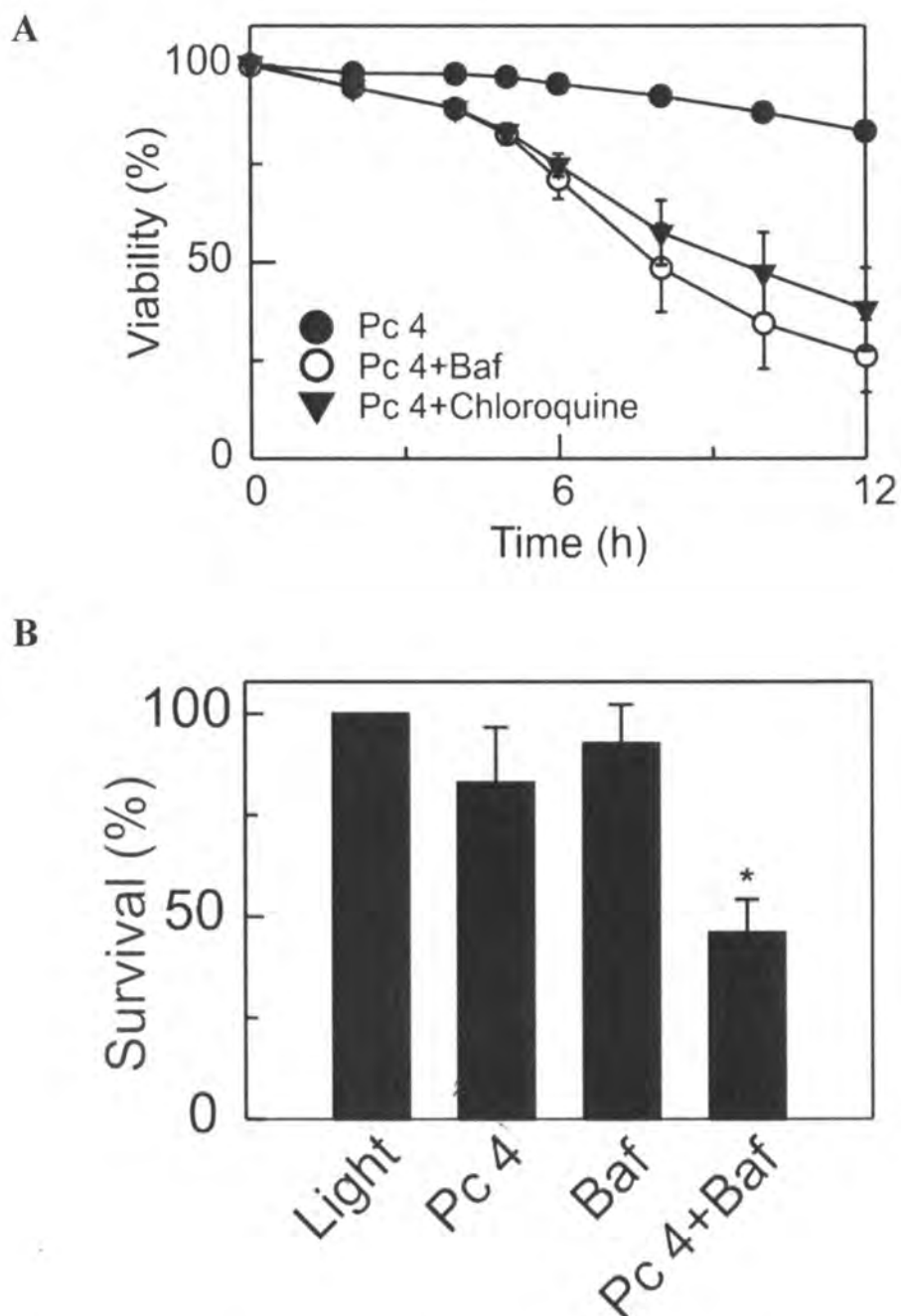


Figure 2-3. Chloroquine enhances Pc 4-PDT-induced A431 cell killing. (A) Both bafilomycin and chloroquine enhance Pc 4-PDT cytotoxicity. 50 nM bafilomycin or 50 μ M chloroquine was added 1 h before irradiation, and cell viability was monitored with PI fluorometry. Results are expressed as percent viability of 0 h. Data represent three independent experiments performed in quadruplicate. **(B)** Cells (330,000 cells/6-cm Petri dish) were treated and irradiated as in A. Subsequently, cells were trypsinized and plated on 6-cm Petri dishes. After 14 days, colonies were stained with crystal violet and counted. Results are expressed as percent colonies of light-treated cultures. Data represent three or more independent experiments performed in triplicate. *, $p < 0.05$ compared to Pc 4 (one-tailed t -test).

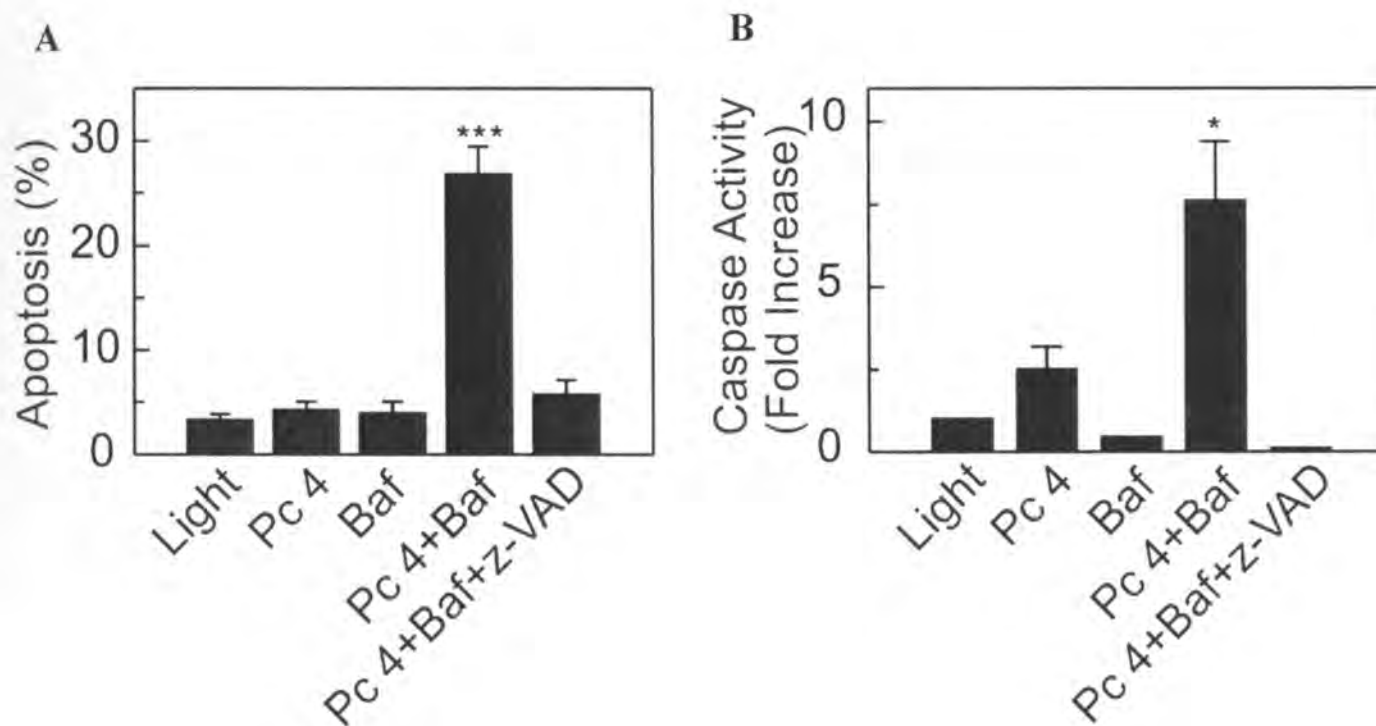
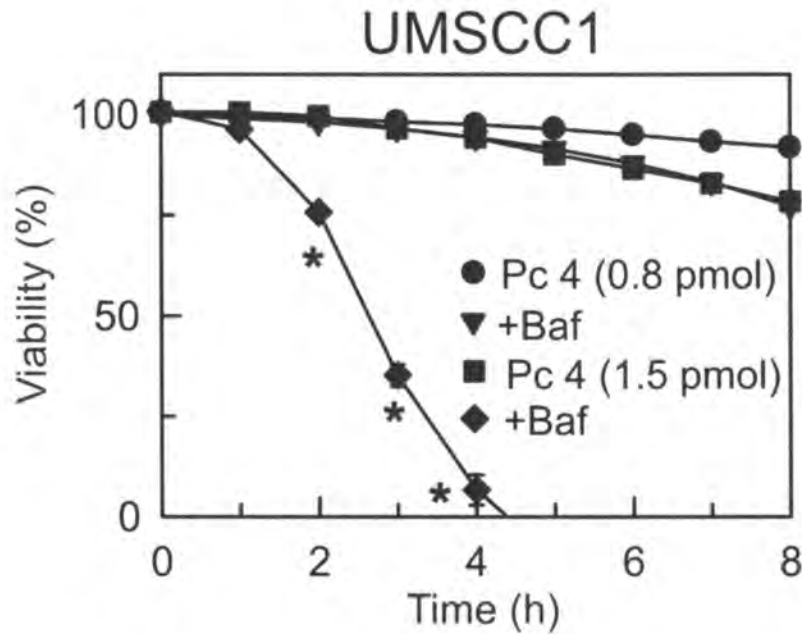


Figure 2-4. Bafilomycin enhances Pc 4-PDT killing in A431 cancer cells through apoptotic death. (A) cells were plated on 96-well plates (6,000 cells/well) and treated as described in experimental procedures. z-VAD (10 μ M) was added, as indicated, 1 h prior to irradiation. Four h after irradiation, apoptotic nuclei were scored with a fluorescence microscope as described in materials and methods. At least 200 cells were counted from three different microscopic fields for each treatment group. Results are expressed as percent apoptotic nuclei. Data represent three independent experiments (mean \pm SEM) performed in triplicate. ***, $p < 0.005$ compared to Pc 4. (B) cells were plated on 6-well plates (120,000 cells/well) and treated as described in A. Four h after irradiation, cell lysates were prepared as described in Materials and Methods. Caspase 3/7 activity was normalized for protein content, and results are expressed as fold increase from light-treated cells. Data represent three independent experiments (mean \pm SEM) performed in triplicate. *, $p < 0.05$ compared to Pc 4 (one-tailed t-test).

A



B

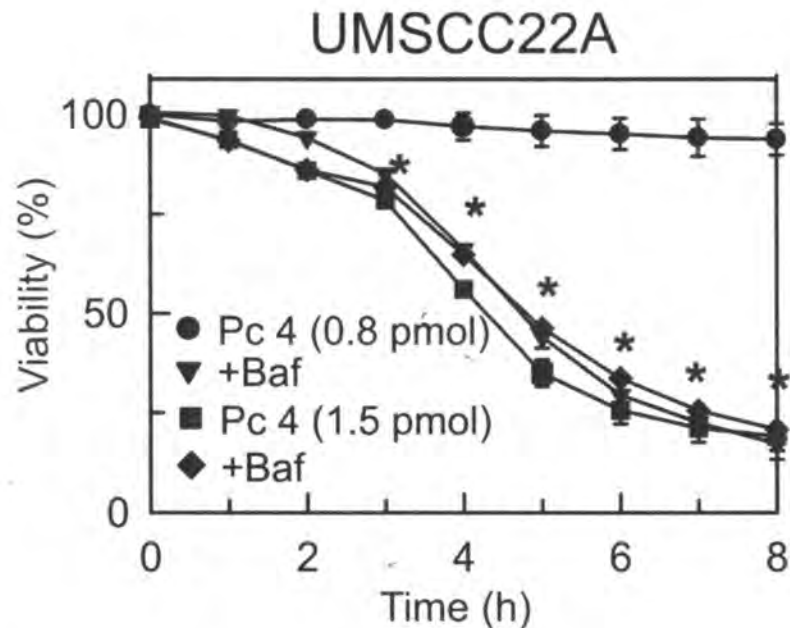
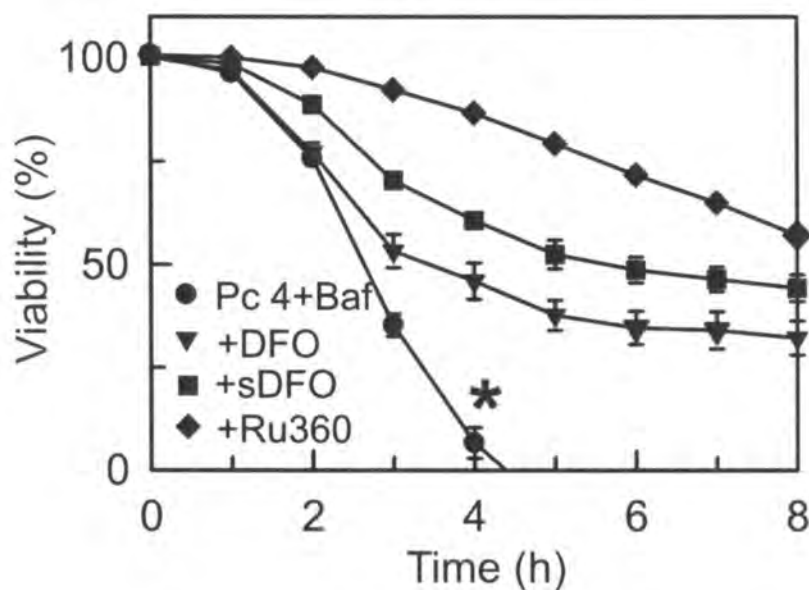


Figure 2-5. Bafilomycin enhances PDT killing in both resistant and responsive cell lines. UMSCC1 (A) and UMSCC22A (B) cells (6,000 cells) were cultured on 96-well plates for 24 h. Cells were incubated with Pc 4 to yield to 0.8 and 1.5 pmol/Pc 4/mg protein, as described in Fig. 2-1A. After 18 h, medium was changed to fresh medium supplemented with ITX reagent and PI (30 μ M) but omitting FBS, followed by incubation with bafilomycin (50 nM) (Baf) for 1 h, where indicated. Subsequently, cells were exposed to light, as described in Materials and Methods. Viability was assessed by PI exclusion. Data represent three independent experiments (mean \pm SEM) performed in quadruplicate. *, $p < 0.0001$ compared to Pc 4-PDT treatment alone.

A UMSCC1 (1.5 pmol Pc 4/mg)



B

UMSCC22 A (0.8 pmol Pc 4/mg)

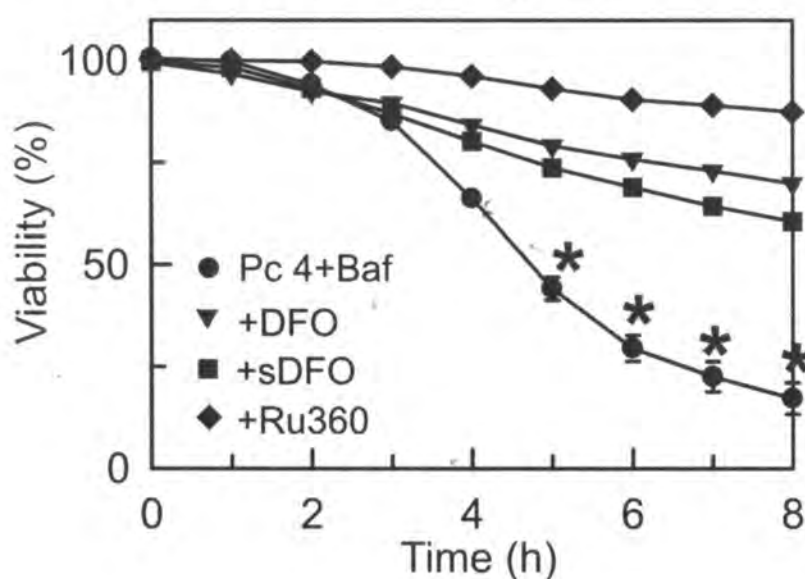


Figure 2-6. Iron chelators and Ru360 protect against bafilomycin-enhanced PDT killing. UMSCC1 (A) and UMSCC22A (B) cells were loaded with Pc 4 in the presence and absence of iron chelators DFO (1 mM) and sDFO (1 mM), and the inhibitor of the calcium uniporter Ru360 (10 μ M) for 18 h. Cells were irradiated and cell killing was assessed with PI exclusion, as described in materials and methods. Values are mean \pm SEM from 3 independent experiments. *, $p < 0.05$ compared to Pc 4+Baf.

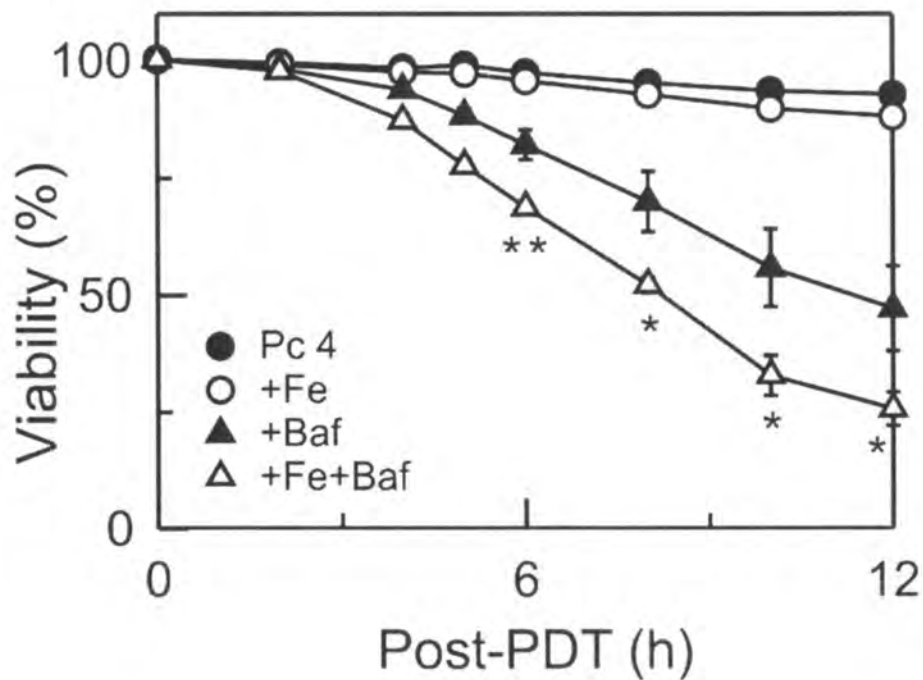


Figure 2-7. Iron enhances Pc 4-PDT-induced A431 cell killing. Cells were cultured in medium containing 30 μM ammonium iron (III) citrate (Fe) for 24 h, as indicated. Subsequently, Fe^{3+} was washed out and cells were incubated with 25 nM Pc 4 for 18 h. Medium was replaced with medium supplemented with Insulin-Transferrin-Selenium-X Reagent and omitting FBS. Bafilomycin (50 nM) was added, as indicated. Cell viability was monitored with PI fluorometry. Data represent three independent experiments (mean \pm SEM) performed in quadruplicate. *, $p < 0.05$; **, $p < 0.01$ compared to Pc 4 + Baf.

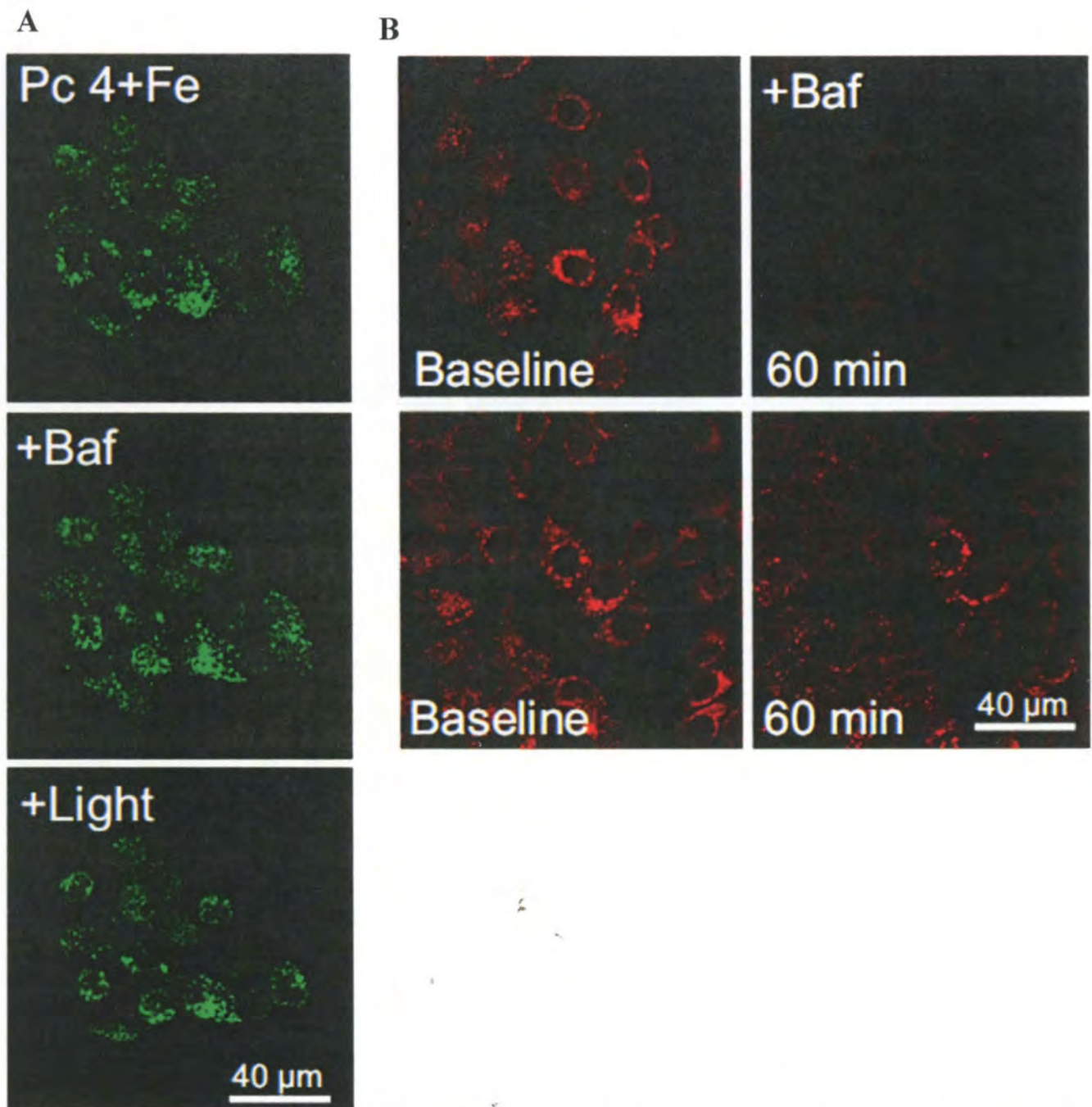


Figure 2-8. Lysosomal membrane permeability after bafilomycin and Pc 4-PDT in A431 cells. (A) cells were plated on glass-bottomed Petri dishes (150,000 cells/dish) in the presence of Fe. After 24 h, medium was replaced with fresh medium containing 25 nM Pc 4 and Alexa-488 dextran (10 kDa, 0.2 mg/ml). After 18 h, medium was replaced with fresh medium supplemented with ITX reagent and omitting FBS. Dishes were placed on a confocal microscope stage at 37°C. Images were obtained after Pc 4 and Fe (Pc 4+Fe), after 1 h exposure to bafilomycin (+Baf) and after 2 h exposure to light (+Baf+Light). (B) cells were loaded with LysoTracker Red (500 nM) for 20 min. Medium was replaced with fresh medium supplemented with 200 nM LysoTracker Red. After collecting a baseline image, bafilomycin (50 nM) was added and the images were taken after 60 min (upper panel). Lower panel shows untreated cells imaged before and after 60 min. Images in A and B are representative of three independent experiments.

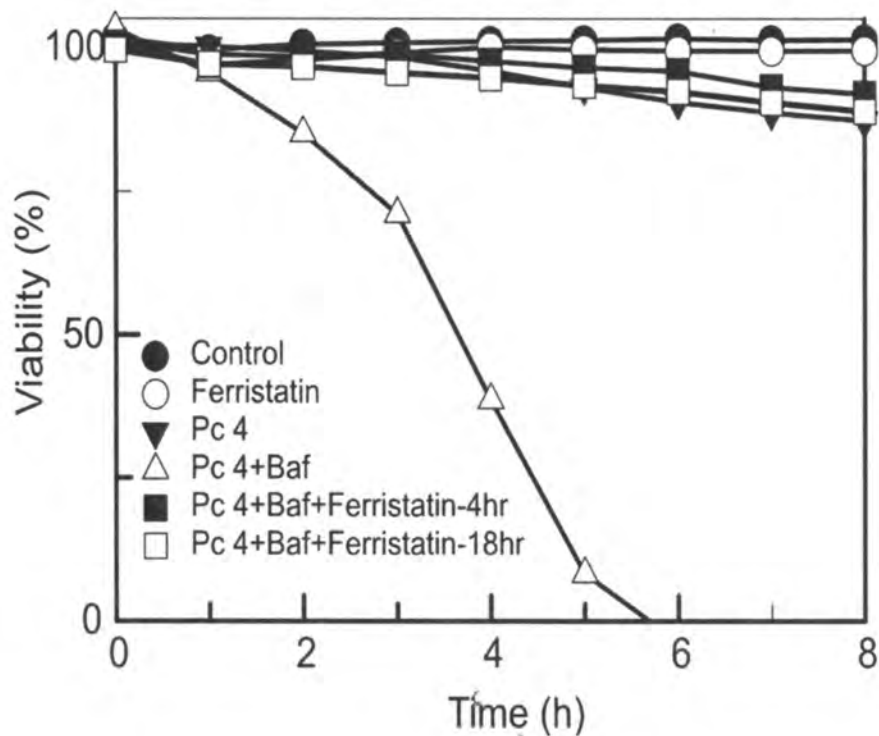


Figure 2-9. Ferristatin protects UMSCC22A cells against bafilomycin enhanced Pc 4-PDT cytotoxicity. UMSCC22A cells were plated on 96 well (15,000/ well) plate for 24 h. Subsequently, cells were loaded with 0.8 pmole Pc 4/mg for 18h in complete DMEM medium with the ferristatin 4 h or 18 h. Medium were then replaced with ITX medium with bafilomycin (50 nM) for 1 h prior to light exposure. Viability was assessed by PI exclusion.

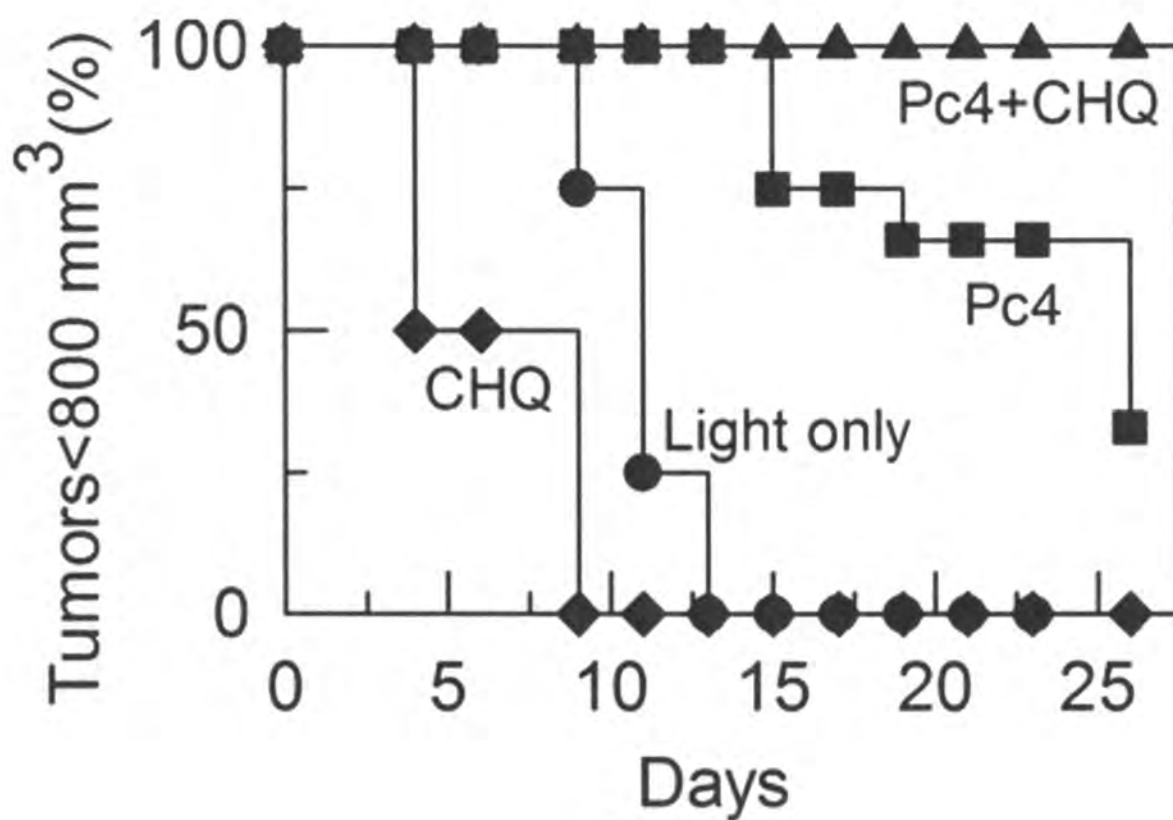


Figure 2-10. Effect of CHQ on tumor regrowth after Pc 4-PDT. UMSCC22A cell xenografts were created in flanks of nude mice (3×10^6 cells in right flank). Once tumors reached 60-100 mm³, Pc 4 (0.5 mg/kg) was administered via tail vein. After 48 h, CHQ (30 mg/kg, i.p.) was administered, as indicated. Four h later, tumors were irradiated (50 J/cm²). Post-PDT, tumor volume was measured with a digital caliper. The estimated difference and 95% confidence interval for Pc 4+CHQ vs. Pc 4 was statistically significant ($p = 0.011$).

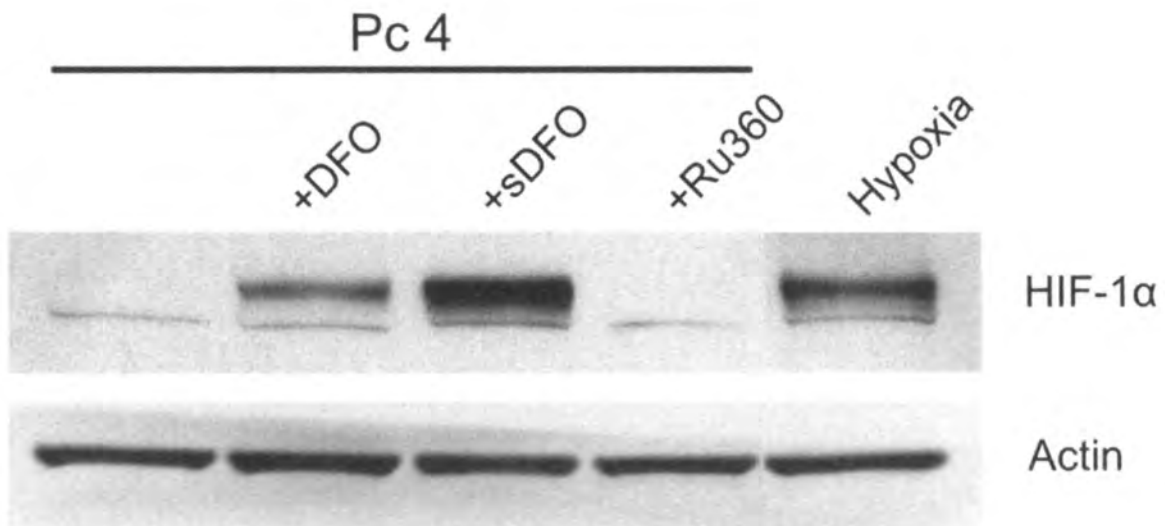


Figure 2-11. Effect of iron chelators and Ru360 on HIF-1 α protein levels. A431 cells were incubated with Pc 4 (25 nM) in the presence and absence of DFO (1 mM), sDFO (1mM) and Ru360 (10 μ M) for 18 h, and cell lysates were subjected to Western blotting. Cells were also exposed to hypoxia (0.5% O₂) for 6 h as a positive control. Actin was used as a loading control. Blots are representative of three independent lysates.

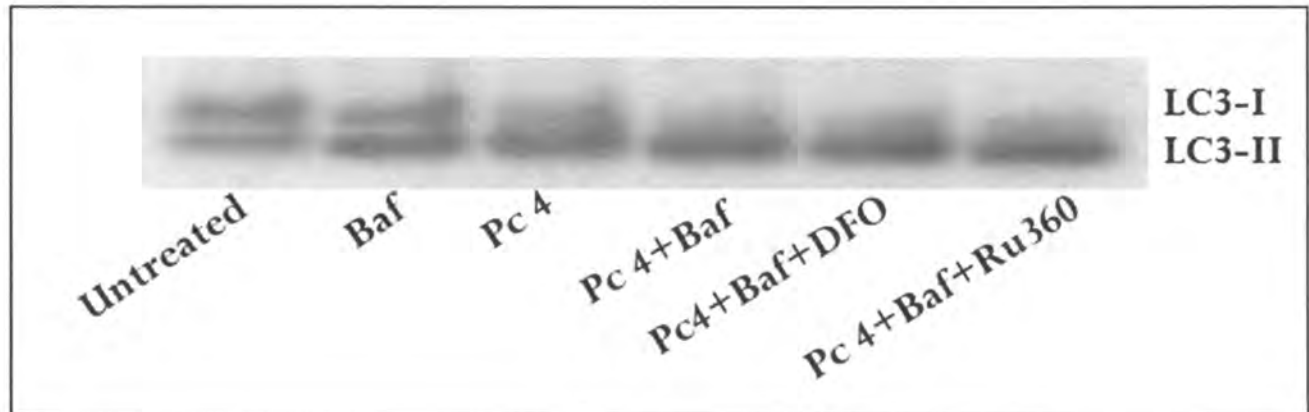


Figure 2-12. Effect of DFO and Ru360 on autophagy during bafilomycin plus Pc 4-PDT. UMSCC22A cells were plated on 6-well (300,000/well) plates for 24 h. Subsequently, cells were loaded with 0.8 pmole Pc 4/mg in the presence of DFO (1 mM) and Ru360 (10 μ M) for 18 h in complete medium. Medium was then replaced with ITX medium supplemented with bafilomycin (50 nM) in the presence and absence of DFO or Ru360 for 1 h prior to light exposure. Cell lysates were prepared after 45 min post-PDT treatment and probed with LC3 antibody.

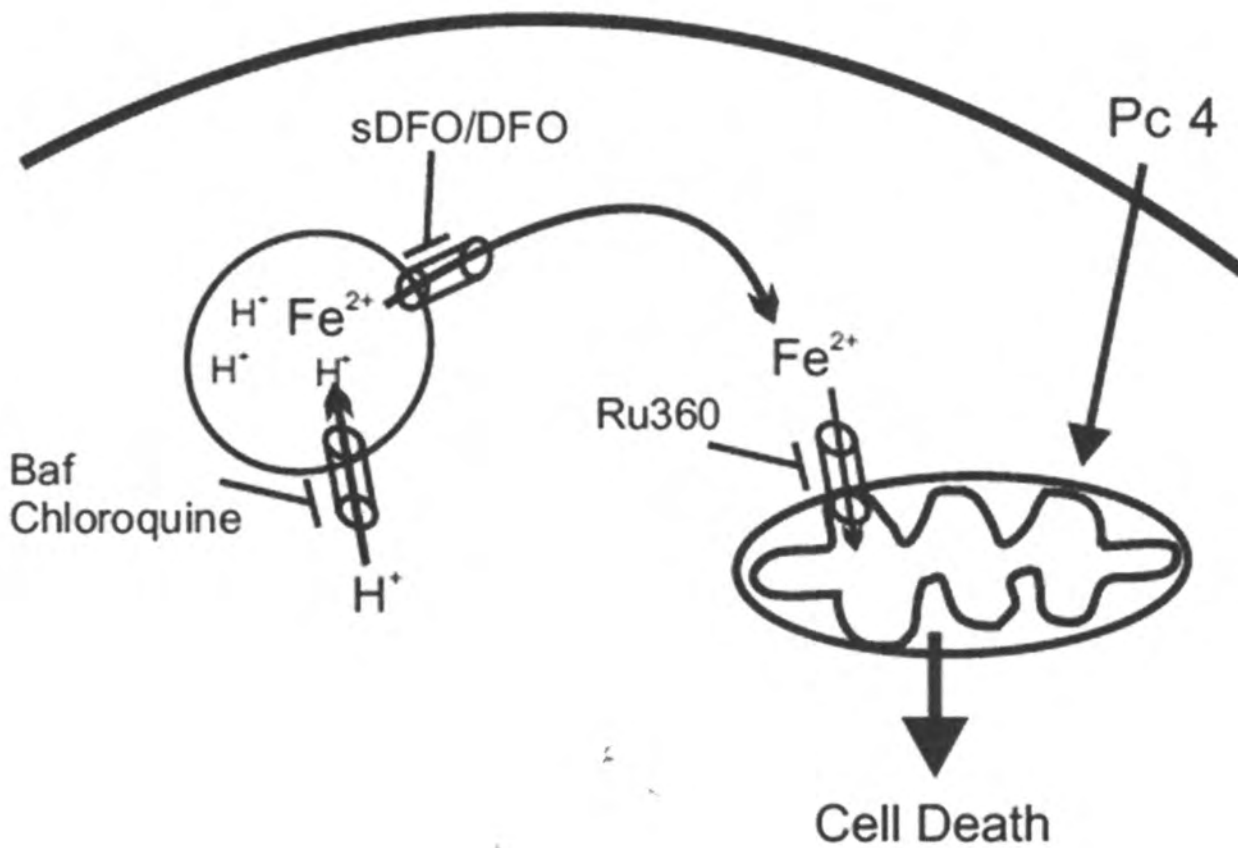


Figure 2-13. Proposed model for interplay between lysosomes and mitochondria during PDT.

Chapter 3

Role of Mitochondrial Iron Transporter Mitoferrin2 in Pc 4-PDT Treatment

Hypothesis

HNSCC cells expressing higher levels of Mfrn2 are more sensitive to PDT and particularly to bafilomycin-enhanced killing during PDT.

Introduction

In physiological conditions, cytosolic free iron concentration is low. However, in pathological conditions chelatable iron released from lysosomes can dramatically increase cytosolic iron concentration [194, 205]. Free iron is rapidly taken up by mitochondria through the MCU [205, 218, 219, 222]. MCU was recently characterized as a 40 kDa mitochondrial membrane protein with channel activity [218, 219]. Besides Ca^{2+} , MCU can also transport Fe^{2+} into mitochondria in a situation where cytosolic Fe^{2+} is elevated [222].

In addition, another mitochondrial protein, Mfrn has been recently described as an iron transporter across the inner mitochondrial membrane [223-225]. Mfrn2 protein has two functional analogues: Mfrn 1 (Mfrn1) and Mfrn 2 (Mfrn2). Mfrn1 (SLC25A37) is a 38 kDa protein that is highly expressed in erythroid cells and in low levels in other tissues, whereas Mfrn2 (SLC25A28), a 39 kDa protein, is expressed in non-erythroid tissue [199, 226-228]. Mfrn transports iron into mitochondria to supply iron required for biosynthesis of heme and iron-sulfur clusters [229]. During erythropoiesis, half-life of Mfrn1 increases in developing erythroid cells whereas half-life of Mfrn2 remains the same [227]. Mfrn1 deficiency in developing

zebrafish erythroid cells results in deficient iron delivery and defective heme synthesis that cannot be rescued by ectopic expression of Mfrn2 owing to different cellular regulation of these two Mfrn proteins [223]. Mfrn1 is also stabilized by Abcb10, a mitochondrial inner membrane ATP-binding cassette transporter. Abcb10 and Mfrn1 form a complex, which further interacts with ferrochelatase to form an oligomeric complex that enhances mitochondrial iron importation during erythropoiesis [230]. To date, no molecules have been identified to form a complex or interact with Mfrn2.

Mfrn2 belongs to family of the mitochondrial carrier family (MCF) and transports iron from cytosol into mitochondria. Mfrn2 locates on the chromosome 10q 24 and contains four exons which encode a full length 364-aa protein with six transmembrane domains. Splice variant isoform2 and its four amino substituent isoform3 (NPAE → MALL) encode a 177-aa and 176-aa proteins, respectively, with three transmembrane domains [200]. Mfrn2 full length isoform and the truncated isoform 2 are able to transport to mitochondria [199]. However, all the functional studies with respect to iron transport into mitochondria are performed with full length Mfrn2 and therefore the full length Mfrn2 is the canonical isoform. Mfrn2 is expressed in placenta, lung, kidney, pancreas, liver, brain, skeletal muscle and heart tissues [200].

In chapter 2, we demonstrated that bafilomycin releases iron from lysosomes to cytosol and enhances Pc 4-PDT-mediated cytotoxicity in both the head and neck responsive and resistant cell lines. In this study, we explored the potential contribu-

tion of Mfn2 to PDT-mediated mitochondrial dysfunction and cytotoxicity after releasing lysosomal iron by bafilomycin. The findings implicate that lysosomal iron release and mitochondrial iron uptake through Mfn2 act synergistically to induce PDT-mediated and iron-dependent mitochondrial dysfunction and subsequent cell killing. To our knowledge, this is the first study to show a causal link between Mfn2 and mitochondrial dysfunction in a pathological condition.

Materials and Methods

Cell Culture. The human head and neck squamous carcinoma cell lines (UMSCC1, UMSCC14A and UMSCC22A) were a gift from Dr. Besim Ogretmen (Medical University of South Carolina). Cells were cultured in Dulbecco's Modified Eagle's Medium (DMEM) (Gibco) supplemented with 10% fetal bovine serum (FBS) and penicillin/streptomycin (complete culture medium) in a humidified 37°C incubator at 5% CO₂/95% air.

Photodynamic Therapy. Cell cultures were incubated with the desired concentration of Pc 4 for 18 h before exposure to 390 mJ/cm² red light ($\lambda = 670$ nm) at 37°C from an Intense-HPD 7404 diode laser (North Brunswick, NJ). Subsequently after exposure to red light, cells were incubated for various periods of time prior to analysis

Assessment of Cell Death. Cell death was assessed by propidium iodide (PI) using a multi-well fluorescence plate reader, as previously described [207]. Briefly, cells were cultured on 96-well plates (6,000 cells/well) for 24 h in complete culture medium. Pc 4 in the presence or absence of DFO (1 mM), sDFO (1 mM) and Ru360 (10 μ M) were present during the last 18 h of the incubation, where indicated. Subsequently, medium was replaced with fresh medium supplemented with ITX reagent and PI (30 μ M) but without FBS. Bafilomycin (50 nM) was added as indicated.

One h after drug addition but before irradiation, PI fluorescence was measured using 530 nm excitation (25 nm band pass) and 620 nm emission (40 nm band pass) filters. PI fluorescence was then measured at frequent intervals for 8 h. Between measurements, microtiter plates were placed in a 37°C incubator. At the end of the experiment, digitonin (200 µM) was added to each well to permeabilize all cells and label all nuclei with PI. Cell viability determined by PI fluorometry is essentially the same as cell viability determined by trypan blue exclusion [207].

RNAi Knockdown. UMSCC22A cells (3×10^6) were transfected with human Mfrn2 and non-target siRNA (25 nM, Ambion) using Lipofectamine RNAiMAX transfection reagent (Invitrogen) with a reversed transfection method on 10-cm Petri dishes. After 3 days, cells were trypsinized and plated on 24-well plates (50,000 cells) for the second reversed siRNA transfection. After 3 days, cells were loaded with Pc 4 in complete culture medium for 18 h for the experiments.

Quantitative Real Time PCR. Total mRNA was extracted from cell lysates using a RNeasy Mini Kit (Qiagen) following the manufacturer's instructions. Quantitative real time PCR (RT PCR) was performed by a two-step procedure. cDNA was synthesized by a iScript cDNA Synthesis kit (Bio-Rad) and PCR was carried out using iQSYBR Green Supermix (Bio-Rad). Each PCR reaction contained 1 µl of the total 100 µl cDNA product from 1µg of total mRNA through RT process with 250 nM of both forward and reverse primer. The PCR reaction was performed using the follow-

ing protocol: 1 cycle of 3 min at 95°C for initial activation of the enzyme followed by 40 cycles of 10 s at 95°C for denaturation, and 45 s at 55°C for annealing and extension. After completion of the reaction, the PCR products were subjected to a melting curve analysis with 1 cycle of 1 min at 95°C to help denature and 1 min of 55°C followed by 80 cycles of 55°C. Relative Mfrn gene expression was quantified by r18S as a reference gene expression control. Primers for Mfrn1 and Mfrn2 were adopted from Harvard Gene Bank as follows: Mfrn1 (ID: 7706150a1)-fw, 5'-TAGCCAACGGGATAGCTGG-3'; Mfrn1-rv, 5'-GTGGTGTAGCTCCGGTAGAAG-3' (178 base pairs). Mfrn2 (ID: 28703800a1)-fw, 5'-CTGCGTGATGTACCCCATCG-3'; Mfrn2-rv, 5'-CCTGTTGCTGTGACGTTTCAG-3' (159base pairs). 18S-fw, 5'-GAGGGAGCCTGAGAAACGG-3'; 18S-rv, 5'-GTCGGGAGTGGGTAAATTTGC-3' (68 base pairs).

Western Blot Analysis. Total cell extracts were prepared in ice-cold RIPA lysis buffer [150 mM NaCl, 1 mM EGTA, 1% sodium deoxycholate, 1% Triton X-100, 0.1% SDS, 1% NP40, 50 mM Tris-Cl, pH 7.4] supplemented with a cocktail of protease inhibitors (Roche Diagnostics). Lysates were centrifuged, and resulting supernatants were quantified for the total protein content by Bradford (Bio-Rad). Equivalent amounts of protein were diluted in sample buffer (Invitrogen) supplemented with 10% SDS and 10% β-mercaptoethanol, and resolved on NuPAGE® Tris-bis polyacrylamide gel (4%-12% SDS-PAGE) (Invitrogen). Proteins were transferred

and immobilized on PVDF membranes (Millipore) and probed with anti-Mfn2 (1:500) (Abcam), anti-TOM20 (1:1000) (Santa Cruz), and anti- β -tubulin (1:1000) (Sigma). Membranes were developed by the enhanced chemiluminescence detection system (Pierce). Band intensities of the membranes were quantified using a Carestream 4000 PRO image station (Woodbridge, CT).

Mitochondrial Iron Uptake. Cells plated in 24-well plates were washed 3 times with intracellular buffer (ICB) containing (in mM): 120 KCl, 10 NaCl, 2 MgCl₂, 2.5 KH₂PO₄, 20 HEPES buffer, pH 7.4, 0.02 EGTA, 5 Na₂ succinate, 2 ATP, 3 glutathione, 1 μ M rotenone, 2 μ M thapsigargin, 5 μ M oligomycin, and 1 μ g/ml protease inhibitors pepstatin, antipain, and leupeptin leaving last wash. Ten μ M digitonin was added to last wash. After 10 min, buffer was substituted with ICB containing 5 μ M calcein, but no EGTA or digitonin and incubated for 5 min. Calcein fluorescence (excitation 495 nm emission 515 nm) was assayed every 0.5 sec for 120 sec using a BMG Novostar fluorescence plate reader. After 1 sec, 5 μ M FeSO₄ was added.

Statistical Analysis. Data are calculated as means \pm SEM from at least three independent experiments performed in triplicate. Pairwise comparison was performed by two-tailed *t*-test using InStat2 software (GraphPAD, San Diego, CA). A *p* value < 0.05 was considered to be statistically significant.

Results

Differential Endogenous Mfrn-2 Gene and Protein Expression in Head and Neck Cancer Cells

In non-erythroid cells, Mfrn2 is an iron transporter localized on inner mitochondrial membrane that transports iron from cytosol into mitochondria [229]. Since bafilomycin-induced toxicity during PDT is likely related to mitochondrial iron uptake, we assessed Mfrn2 expression in head and neck cancer cells. PDT-sensitive cells (UMSCC22A) expressed 2 fold higher Mfrn2 mRNA measured by quantitative PCR compared to PDT-resistant (UMSCC1 and UMSCC14A) cells. As expected, all head and neck cancer cells expressed very little Mfrn1 (Fig. 3-1A). Conversely, human K562 erythromyeloblastoid leukemia cells expressed high levels of Mfrn1 and less Mfrn2 (Fig. 3-1A). UMSCC22A expressed 2 fold higher Mfrn2 protein levels compared to UMSCC1 and UMSCC14A, and K562 cells expressed low Mfrn2 (Fig. 3-1B-C). Samples from all cell lines contained equal amounts of the mitochondria-specific protein TOM20 (Fig. 3-1C). Thus, the difference in Mfrn2 protein expression between the cell lines cannot be explained by differences in mitochondrial proteins in lysates.

Next we determined whether cells expressing more Mfrn2 were capable of transporting iron faster from the cytosol to mitochondria compared to cells with less Mfrn2. Mitochondrial iron uptake was measured in digitonin-permeabilized cells using calcein fluorescence. Indeed, UMSCC22A cells showed higher rates of mito-

chondrial Fe^{2+} uptake compared to UMSCC1 cells (0.27 *versus* 0.08 μmol Fe^{2+} /min/mg protein) (Fig. 3-2).

Downregulation of Mfrn2 Results in Decreased Mitochondrial Fe^{2+} Uptake

The results in Fig. 3-2 demonstrate the causal correlation of Mfrn2 expression and mitochondrial Fe^{2+} uptake in head and neck cancer cells. Therefore, we reasoned that downregulation of Mfrn2 in UMSCC22A cells should result in decreased mitochondrial Fe^{2+} uptake. Knockdown of Mfrn2 in UMSCC22A cells using siRNA resulted in 88% decrease in Mfrn2 mRNA expression (Fig. 3-3 A) and 56% decrease in protein expression (Fig. 3-3B). As expected, knockdown of Mfrn2 also decreased rates of mitochondrial Fe^{2+} uptake by 79% compared to cells transfected with non-target siRNA (0.31 μmol /min/mg *versus* 0.07 μmol /min/mg protein) (Fig. 3-3C). Taken together, the data are consistent with the conclusion that increased mitochondrial iron transport through Mfrn2 at least partly explains the differential sensitivity of head and neck cancer cell lines to bafilomycin-enhanced toxicity to PDT. Furthermore, Mfrn2 is likely a protein responsible for mitochondrial iron transport in cells.

Downregulation of Mfrn2 Delays Mitochondrial Depolarization and Cell Death after PDT plus Bafilomycin

Iron by participating in Fenton chemistry and increasing ROS production can induce mitochondrial dysfunction. Therefore, we assessed the effects of Mfrn2 knockdown on mitochondrial membrane potential and cell viability in high Mfrn2 expressing UMSCC22A cells. At 0 min, bright pseudocolored red and yellow spheroids represented high TMRM fluorescence intensities in polarized mitochondria (Fig. 3-4 A). After exposure to PDT (0.8 pmol Pc 4/mg protein) plus bafilomycin, bright spheroids rapidly disappeared in cells transfected with non-target siRNA (siControl) so that after 15 min, most of TMRM had leaked out from mitochondria, indicating mitochondrial depolarization. After 30 min, virtually all polarized mitochondria disappeared (Fig. 3-4 A top panel). Conversely, in Mfrn2 knockdown cells, some of the bright fluorescent spheroids remained even after 30 min (Fig. 3-4 A bottom panel). The average TMRM fluorescence after background subtraction under conditions described in panel A was determined every 5 min for 30 min. Results are expressed as percent TMRM fluorescence of 0 min (Fig. 3-4 B). Data are means calculated from analyses of 74-80 cells per treatment group obtained from three independent experiments (mean \pm SEM). *, $p < 0.05$ compared to control siRNA. Moreover, Mfrn2 knockdown increased cell viability from 0 to 56% after 8 h (Fig. 3-4 C). The results implicate Mfrn2-mediated mitochondrial iron uptake as a key step in bafilomycin-enhanced mitochondrial depolarization and subsequent cell death after PDT.

Increased Expression of Mfrn2 Enhances Cell Death in Resistant Head and Neck Cancer Cells after PDT Plus Bafilomycin

To further confirm the role of Mfrn2 in PDT response, we overexpressed the Mfrn2 in low Mfrn2 expressing UMSCC1 cells. First Mfrn2-GFP-overexpressed UMSCC1 cells were loaded with MitoTracker Red to observe the cellular localization of the ectopic expressed protein. Confocal images revealed co-localization of GFP and MitoTracker Red, indicating that GFP-Mfrn2 localizes to mitochondria (Fig. 3-5A). Next GFP-Mfrn2 protein levels were observed with both GFP and Mfrn2 antibodies by Western blotting. We detected GFP-Mfrn2 protein with both antibodies (Fig. 3-5B). Next we assessed the effect of GFP-Mfrn2 on cell killing during PDT. In GFP and GFP-Mfrn2 expressing UMSCC1 cells, Pc 4-PDT alone decreased viability to 75% 8 h post-PDT (Fig. 3-6). In GFP expressing cells, bafilomycin enhanced Pc 4-PDT-induced cell killing decreasing viability from 75% to 45% at 6 h post-PDT. In GFP-Mfrn2 expressing cells, however, viability decreased from 75% to 0%. These results further confirm our results with knockdown cells and implicate Mfrn2-mediated mitochondrial iron uptake as a key step in bafilomycin-enhanced cell death after PDT.

Discussion

Main findings of this study provide mechanistic information regarding the contribution of lysosomal chelatable iron to mitochondrial dysfunction and cell death in HNSCC cells during PDT. Our results indicate that lysosomal iron release and mitochondrial iron uptake through Mfrn2 act synergistically to induce PDT-mediated and iron-dependent mitochondrial dysfunction and subsequent cell killing in head and neck cancer cells. To our knowledge, this is the first study to show a causal link between Mfrn2 and mitochondrial dysfunction in a pathological condition.

Our results demonstrate that Ru360, a potent inhibitor of the MCU, markedly protected against bafilomycin-mediated PDT toxicity (Fig. 2-6). For years, Ca^{2+} uptake across the inner mitochondrial membrane has been known to be mediated by the MCU. However, it was until recently when MCU was identified as a 40 kDa protein that is localized to inner mitochondrial membrane. The protein contains two transmembrane domains and shows channel activity [218, 219]. However, transport of Fe^{2+} into mitochondria through MCU occurs in pathological situation when cytosolic free Fe^{2+} , but not Fe^{3+} , is increased [222]. Therefore, Ru360 protection against bafilomycin toxicity during PDT may be explained by prevention of Fe^{2+} uptake into mitochondria through MCU.

Although MCU may serve as an iron transporter across mitochondrial membranes during pathological conditions, other iron transporters have been identified as well. Mfrn1 is highly expressed in erythroid cells but in low levels in other tissues

[223]. In non-erythroid cells, Mfrn2 is expressed as three isoforms, a canonical full-length 39 kDa isoform and 2 alternative splicing isoforms [200]. So far only a full-length Mfrn2 has been shown to transport iron from the cytosol to mitochondria [199]. Thus, contributions of the other isoforms to the mitochondrial iron import remain to be determined. There is no sequence homology between MCU and Mfrn2 [218, 219]. All three head and neck cancer cell lines expressed very little Mfrn1 (Fig. 3-1A). Interestingly, the cell lines that were more resistant (UMSCC1 and UMSCC14A) to PDT and bafilomycin toxicity also expressed less Mfrn2 mRNA and protein than UMSCC22A, a sensitive cell line (Fig. 3-1A-B). Furthermore, mitochondria in permeabilized UMSCC22A cells took up Fe^{2+} at a 3.0 fold faster rate compared to UMSCC1 cells (Fig. 3-2). These findings suggest a causal link between mitochondrial Fe^{2+} uptake through Mfrn2 and cytotoxicity.

Downregulation of Mfrn2 decreased rate of mitochondrial Fe^{2+} uptake and delayed mitochondrial depolarization and subsequent cell death after PDT plus bafilomycin (Fig. 3-4A). Our results provide the first evidence how Mfrn2 by regulating mitochondrial Fe^{2+} uptake may contribute to cytotoxicity during PDT. The finding that Ru360 provided protection against bafilomycin-enhanced PDT toxicity also suggests that MCU may be responsible for mitochondrial Fe^{2+} uptake. Alternatively, interaction of MCU and Mfrn2 may be required for mitochondrial Fe^{2+} transport. This would explain why Ru360 provided such a great protection against bafilomycin-enhanced PDT toxicity (Fig. 2-6). Baughman and co-workers were not able to show interaction between MCU and Mfrn2 in physiological conditions from their co-

immunoprecipitation [218, 219]. It may be possible that interaction of these proteins is favored by high Fe^{2+} . Further studies are needed to answer these questions. Our *in vitro* data show that bafilomycin greatly enhances Pc 4-PDT efficacy in Mfrn2-expressing cells. The question remains whether this phenomenon also occurs *in vivo*. To address this question we performed a pilot study in nude mice. Xenografts were created with high Mfrn2-expressing UMSCC22A cells and subjected to PDT (Fig. 2-10). Instead using bafilomycin, we employed FDA-approved chloroquine in our animal experiment. After one single PDT dose, tumors disappeared within the first 4 days post-PDT. Chloroquine addition, however, significantly delayed tumor regrowth. It would be interesting to find out the outcome if we give a second PDT dose after tumors have begun to grow. A second treatment of chloroquine and Pc 4-PDT may result in greater tumor regression in mice bearing high Mfrn2 expressing tumors, or may result in a higher level of tumor free mice.

In summary, the data support the conclusion that lysosomal iron release and mitochondrial iron uptake act synergistically to induce PDT-mediated and iron-dependent mitochondrial dysfunction and subsequent cell killing (Fig. 3-7). Iron released from lysosomes is taken up by mitochondria through Mfrn2. Downregulation of Mfrn2 prevents mitochondrial iron uptake, and delays mitochondrial depolarization and cell death. Furthermore, Mfrn2 represents a possible predictive biomarker, since HNSCC expressing more Mfrn2 may benefit more from PDT.

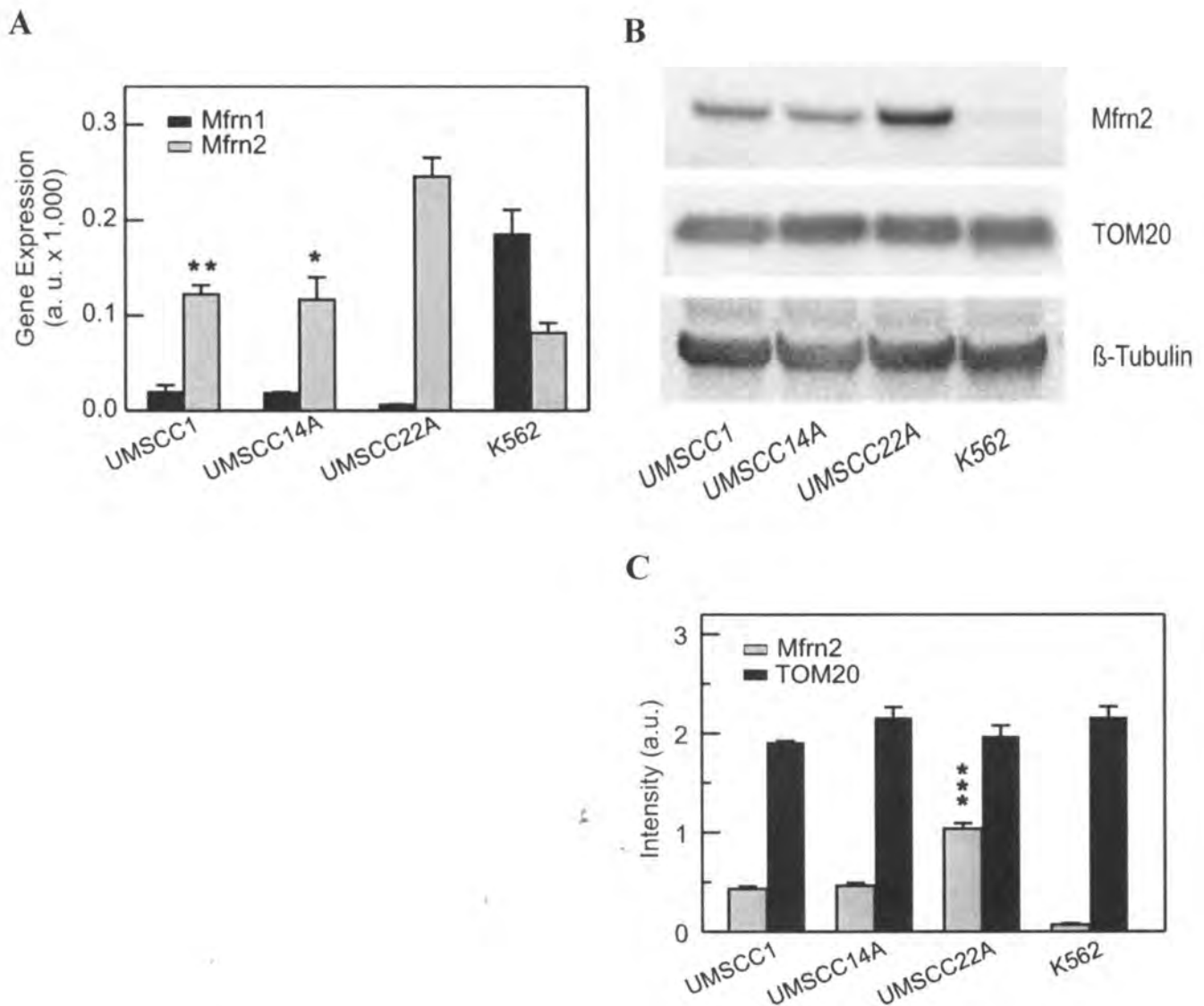


Figure 3-1. Differential endogenous Mfrn2 gene and protein expression in head and neck cancer cells. Cells were cultured on 6-well plates for 24 h. **(A)** total RNA was isolated, as described in Materials and Methods. Mfrn1 and Mfrn2 mRNA were quantified by real time PCR. Values are expressed as arbitrary units (a.u.) normalized to the housekeeping rRNA 18S. Data represent the mean \pm SEM from three independent lysates. *, $p < 0.01$ and **, $p < 0.001$ compared to UMSCC22A. **(B)** cell lysates were analyzed by Western blotting for Mfrn2, TOM20 and β -tubulin. Blots shown are representative of 3 independent experiments. **(C)** Band intensities were quantified and normalized to β -tubulin. Values are expressed as arbitrary units (a.u.). Data represent the mean \pm SEM from three independent lysates. ***, $p < 0.001$ compared to UMSCC1 and UMSCC22A.

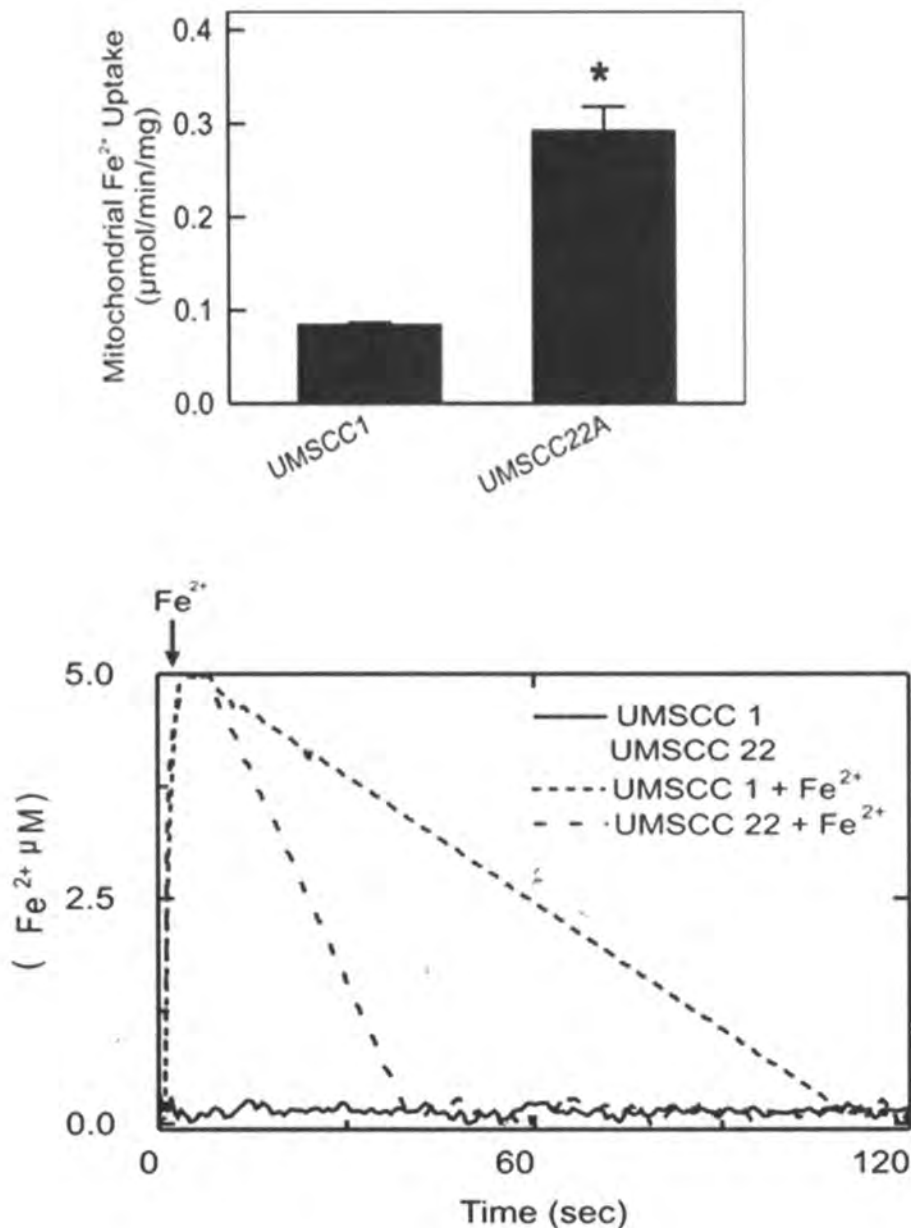


Figure 3-2. Differential mitochondria iron uptake in head and neck cancer cells. UMSCC1 (100,000) and UMSCC22A (200,000) cells were cultured on 24-well plates for 24 h. Subsequently, culture medium was changed to the IBC and rates of the mitochondrial Fe²⁺ uptake were measured in digitonin-permeabilized cells, as described in materials and methods. Values are expressed as Fe²⁺ uptake/min/mg protein. Data represent the mean ± SEM from three independent experiments performed in triplicate. *, $p < 0.01$ compared to UMSCC1.

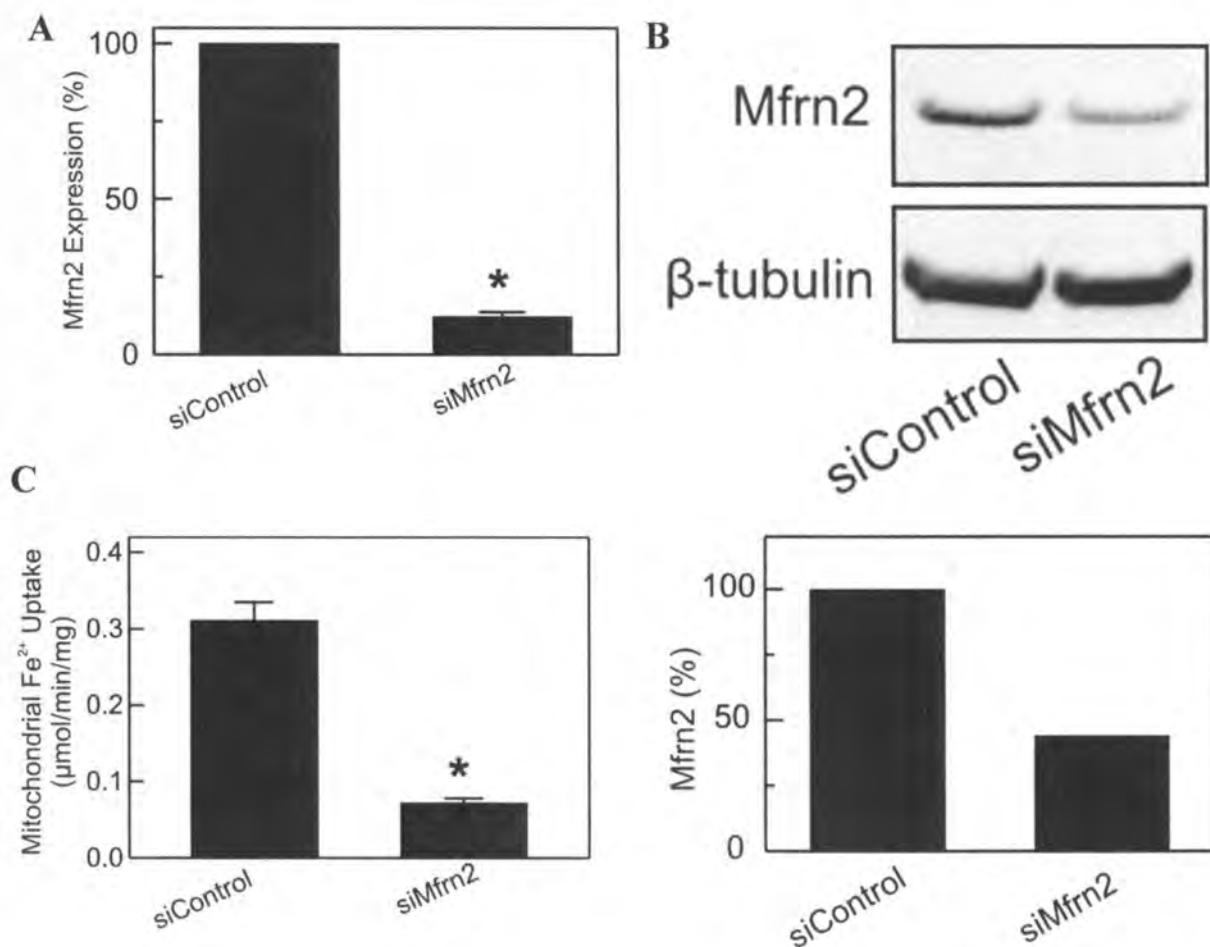
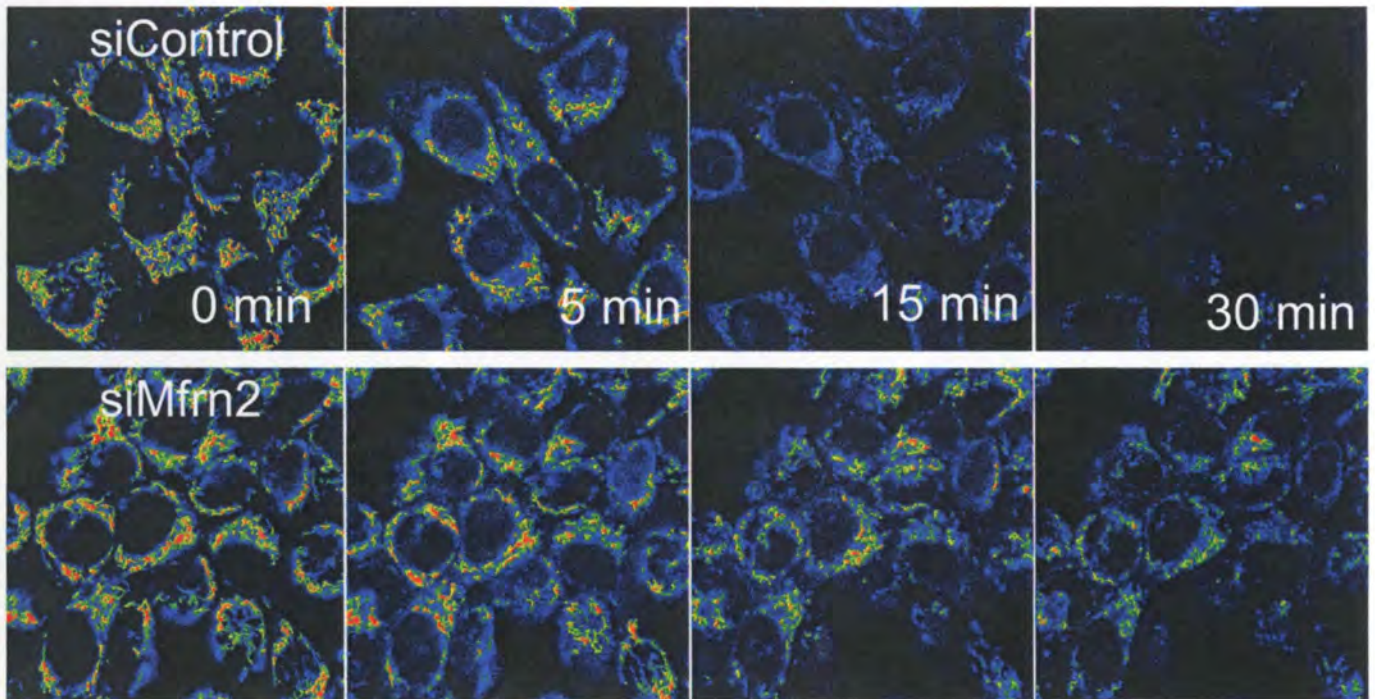
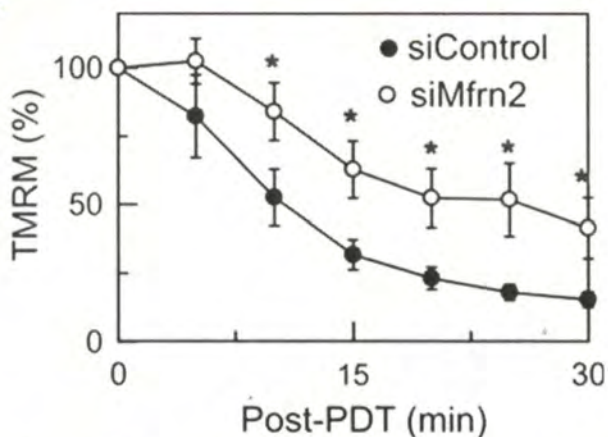


Figure 3-3. Mfrn2 knockdown decreases mitochondrial iron uptake. UM-SCC22A cells were transfected with Mfrn2 and non-target (siControl) siRNA for 6 days, as described in Materials and Methods. **(A)** total mRNA was isolated and analyzed for Mfrn2 expression by real time PCR. Mfrn2 mRNA was normalized to internal control rRNA 18S. Values are expressed as percent of siControl values. Data represent the mean \pm SEM from three independent experiments. **(B)** cell lysates were analyzed by Western blotting for Mfrn2 and β -tubulin. Representative Western blot is shown. Band intensities were quantified and normalized to β -tubulin. Results are expressed as percent of siControl. **(C)** mitochondrial Fe²⁺ uptake was measured in digitonin-permeabilized cells, as described in Materials and Methods. Values are expressed as Fe²⁺ uptake/min/mg protein. Data represent the mean \pm SEM from three independent experiments performed in triplicate. *, $p < 0.01$ compared to siControl.

A



B



C

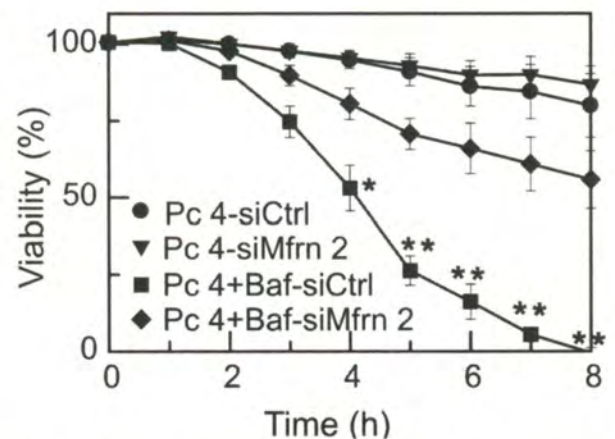


Figure 3-4. Mfrn2 knockdown confers sensitive cells resistant to PDT. (A) UM-SCC22A cells were transfected with Mfrn2 and non-target siRNA for 6 days, as described in Materials and Methods. Subsequently, cells were trypsinized and cultured (150,000/dish) on glass-bottomed Petri dishes for 24 h. Cells were incubated with Pc 4 (0.8 pmol Pc 4/mg protein) for 18 h in complete culture medium. Cells were loaded with 250 nM TMRM and subsequently incubated with TMRM (50 nM) and bafilomycin (50 nM) for 1 h before irradiation. Red fluorescence of TMRM was imaged with laser scanning confocal microscopy before (0 min) and every 5 min after irradiation for 30 min. Representative images from three independent experiments. Images were pseudocolored using a lookup table from 0 to 255 pixel intensities (B) average TMRM fluorescence after background subtraction under conditions described in panel A was determined every 5 min for 30 min. Results are expressed as percent TMRM fluorescence of 0 min. Data are means calculated from analyses of 74-80 cells per treatment group obtained from three independent experiments (mean \pm SEM). *, $p < 0.05$ compared to control siRNA. (C) cells were plated on 96-well plates and treated under same conditions as in panel A. Viability was monitored by PI fluorometry. Results are expressed as percent viability of 0 min. Data represent three independent experiments (mean \pm SEM) performed in quadruplicate. *, $p < 0.05$ and **, $p < 0.01$ compared to control siRNA.

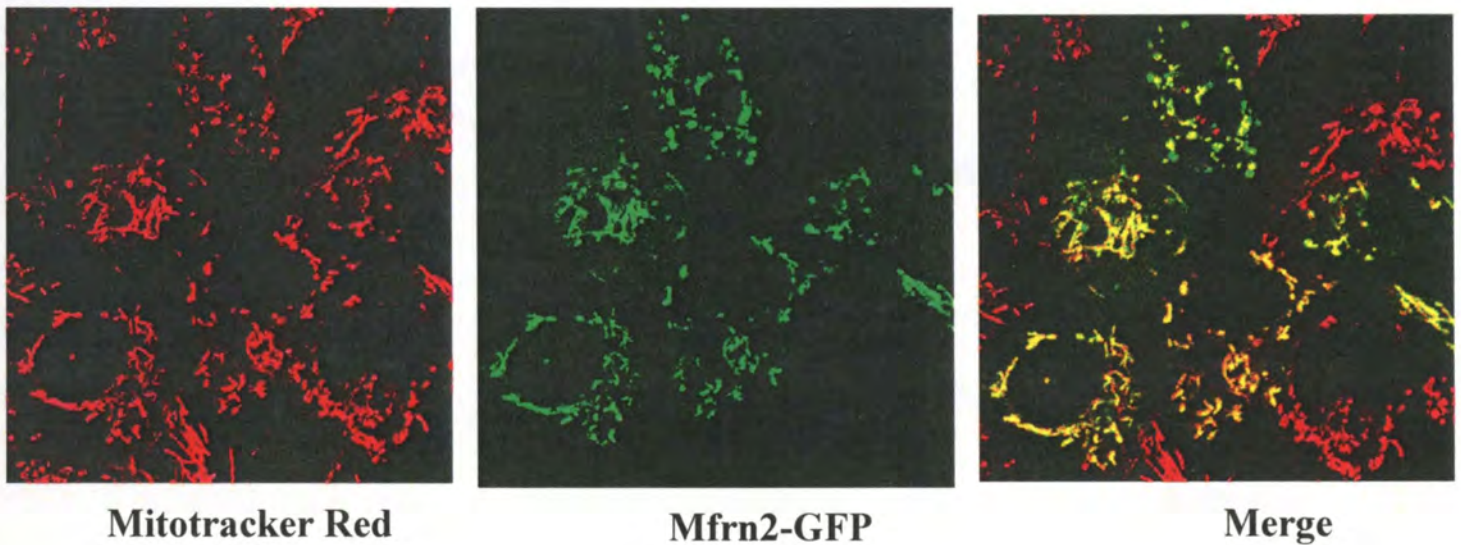
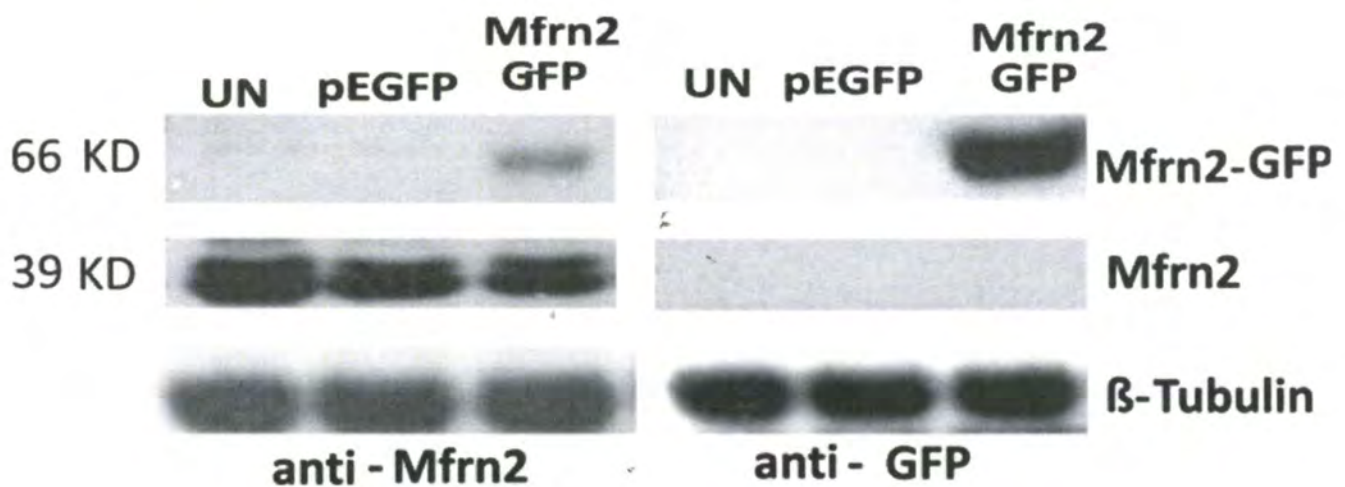
A**B**

Figure 3-5. Localization and protein expression of the overexpressed Mfrn2-GFP in the resistant UMSCC1 cells. (A) UMSCC1 cells were transiently transfected with Mfrn2-GFP plasmid. Sub-cellular localization of the overexpressed Mfrn2 protein was observed with confocal microscopy. Red: MitoTracker Red, Yellow: co-localization of MitoTracker Red and GFP. Mfrn2-GFP protein is imported to mitochondria. (B) Mfrn2-GFP plasmid was transfected into the resistant UMSCC1 cells. After transfection (72 h), cell lysates were probed for GFP, Mfrn2 and β -tubulin, respectively as indicated.

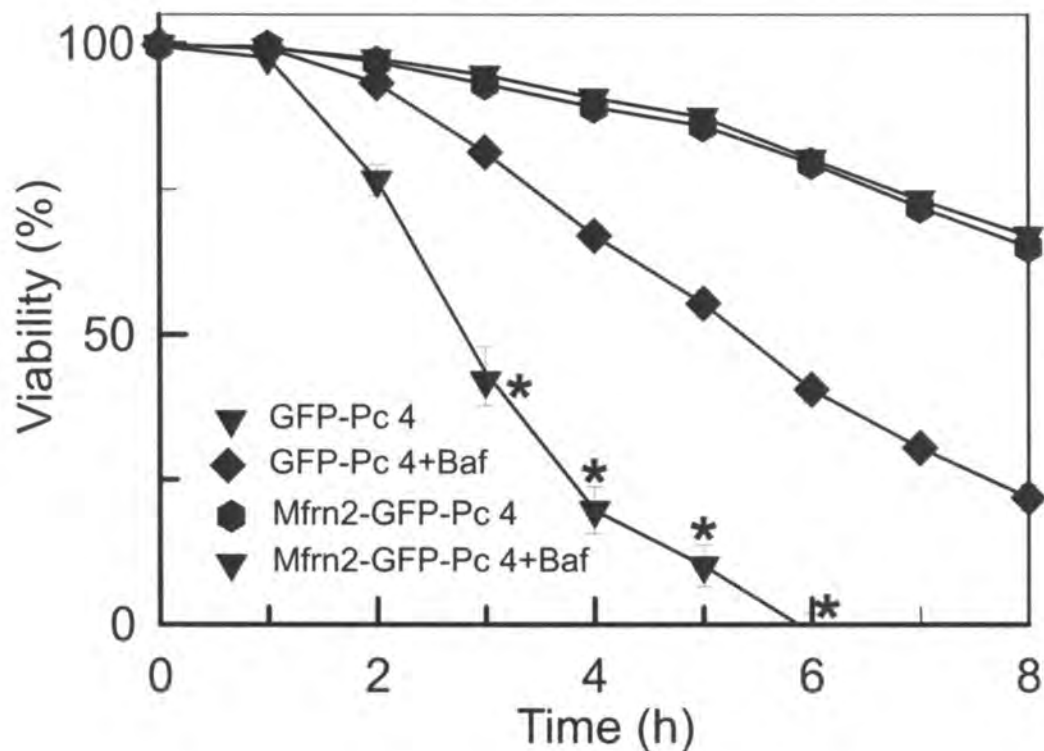


Figure 3-6. Increased Mfrn2 protein expression sensitizes resistant UMSCC1 cells to bafilomycin Pc 4-PDT. UMSCC1 cells were transiently transfected with Mfrn2-GFP and GFP plasmid respectively when cells reach 90% cell confluency at 60 mm dish for 24 h. Then cells were split on 96 well plate with 6000 cells/well for 24 h. Cells were loaded with 1.5 pmole Pc 4/mg for 18h in the complete DMEM medium. Subsequently, cells were changed into ITX with 50 nM bafilomycin for 1h prior to light exposure. Viability was monitored by PI fluorometry. Results are expressed as percent viability of 0 min. Data represent three independent experiments (mean \pm SEM) performed in quadruplicate. *, $p < 0.05$ compared to control GFP plasmid transfected UMSCC1 under baf+Pc 4-PDT treatment.

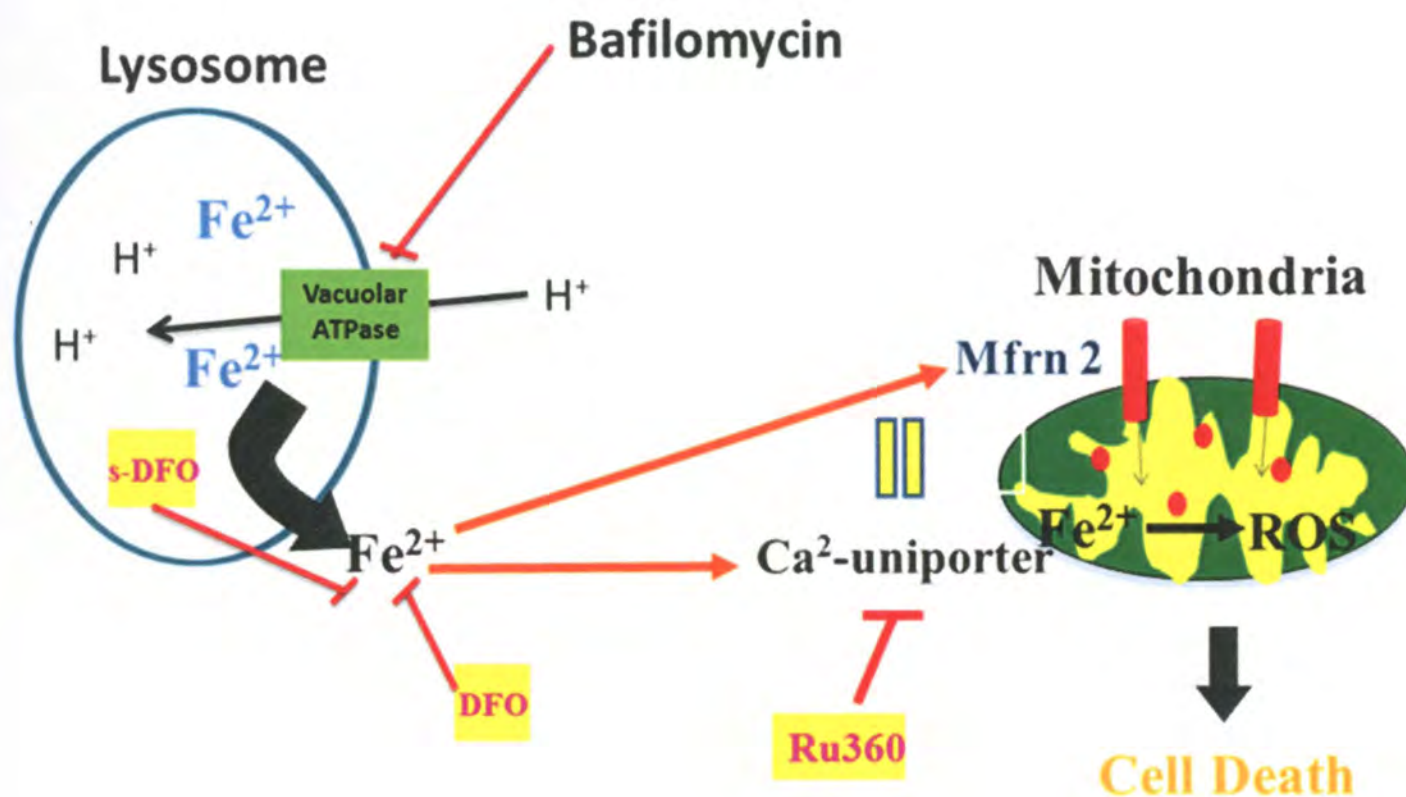


Figure 3-7. Proposed mechanism of interplay between lysosome and mitochondria and role of iron and Mfrn2 contribute to PDT-induced cell death. Pc 4-PDT induces mitochondrial ROS production resulting in apoptotic cell death. Bafilomycin (Baf) enhances Pc 4-PDT-mediated cell killing by releasing iron from lysosomes. Cytotoxicity is decreased by iron chelators DFO and sDFO, and Ru360 that prevent mitochondrial iron accumulation. Knock-down of Mfrn2 delays mitochondrial depolarization and cell death induced by bafilomycin during PDT.

Chapter 4

Summary and Future Directions

Summary and Future Directions

Mitochondria are frequently cellular targets for cancer therapy owing to their ability to trigger efficient apoptotic cell death. However, cancer cells frequently develop mutations against mitochondria targeted therapy. Therefore, lysosomes have gained more and more attention to serve as an alternative target organelle for defective mitochondria-mediated therapy. The main role of lysosomes is to accumulate various hydrolytic enzymes and redox-active mobile iron, and participate in the autophagic process. To date, most studies address the role of lysosomes in cell death with respect to increased lysosomal membrane permeability and subsequent release of hydrolytic proteases such as cathepsins. Some of the research has focused on the controversial role of autophagy in cell survival under various cellular stresses.

Our study shows that iron release from lysosomes into cytosol and then uptake by mitochondria is a way by which lysosomes enhance mitochondria-mediated therapy and cell death. We demonstrate that lysosomal iron release without lysosomal permeabilization is possibly regulated *via* DMT1. Furthermore, our results exclude the possibility that bafilomycin-enhanced PDT killing is mediated by inhibition of autophagy (data not shown). Cellular Mfn2 level is positively correlated with mitochondrial iron uptake. Higher Mfn2 protein levels confer cells sensitive to bafilomycin-enhanced Pc 4-PDT cytotoxicity. To our knowledge, this is the first study to show a causal link between Mfn2 and mitochondrial dysfunction in a pathological condition.

Role of DMT1 in lysosomal iron release after bafilomycin

Although bafilomycin and chloroquine have been shown to release iron from lysosomes into cytosol, the detailed mechanism by which bafilomycin releases iron from lysosomes remains unclear. The fact that ferristatin, an inhibitor of the DMT1, completely reversed bafilomycin-enhanced Pc 4-PDT cytotoxicity suggests DMT1 as a likely mechanism of lysosomal iron release with bafilomycin. Since ferristatin may have off-target effects, knockdown DMT1 using siRNA method could be further used to confirm results with ferristatin. DMT1 knockdown should protect against PDT toxicities (ROS formation, mitochondrial depolarization, cell death, etc.). Similar results are expected with knockdown of Mfrn2. However, since Mfrn2 knockdown did not produce 100% inhibition of Mfrn2 expression (Fig. 3-3B), some iron is still being taken up by mitochondria. Therefore, ferristatin/DMT1 knockdown in combination with Mfrn2 knockdown may be even more efficient in decreasing PDT toxicities than either treatment alone.

Mitochondrial iron regulation

Mechanisms underlying mitochondrial iron uptake are not completely known. Our results show that Mfrn2 regulates mitochondrial iron uptake in pathological situations such as PDT. MCU also transports iron into mitochondria when cytosolic iron concentration is increased [205, 222]. Ru360 is a highly specific inhibitor of the MCU. Ru360 and knockdown of Mfrn2 both prevented mitochondrial iron uptake

and protected cells from bafilomycin-enhanced PDT. It remains unclear whether Ru360 also blocks mitochondrial iron uptake through Mfn2. Also, the question remains whether interaction of Mfn2 and MCU is required for mitochondrial uptake. A recent study showed that Mfn2 and MCU are two distinct proteins and do not interact with each other [218, 219]. However, this experiment was performed in physiological conditions. It remains unclear whether increased cytosolic iron during pathological conditions induces interaction of these proteins.

Mfn2 has six transmembrane helices and MCU has two transmembrane domains with a short amino acid link termed DIME motif between these two transmembrane helices [200, 218, 219]. Recent reports from two different groups concurrently demonstrated that MCU and Mfn2 are two distinct proteins and do not interact with each other, as assessed by immunoprecipitation [218, 219]. Ru360 is a specific inhibitor of MCU [205], and our results showed that Ru360 markedly protect against bafilomycin-enhanced mitochondrial depolarization and Pc 4-PDT killing (Fig. 3-6) [92]. This implies some interaction between Ru360 and MCU/Mfn2. Overexpression of MCU confers cells slightly resistant to Ru360 whereas mutation on the DIME linker motif confers cells remarkably resistant to Ru360 [219]. These findings suggest that the linker region between the two transmembrane helices of MCU is important for Ru360 sensitivity. Mfn2 may share Ru360 sensitivity with MCU through the DIME motif. Further studies are needed to address this issue.

Signaling pathways induced by bafilomycin-enhanced Pc 4-PDT

MAPK kinase pathways are frequently induced during mitochondrial stress [231, 232]. Iron released from lysosomes with bafilomycin and taken up by mitochondria *via* Mfn2 depolarizes mitochondria and causes onset of apoptotic cell death during PDT. We have performed preliminary experiments to determine whether JNK pathway is involved in PDT. Our preliminary results from Western blotting showed PDT plus bafilomycin-induced increase of phospho-JNK1/2 protein expression (data not shown). These findings suggest JNK to be a possible killing pathway induced during bafilomycin-enhanced Pc 4-PDT killing. Future experiments should be performed to confirm the role of JNK pathway in bafilomycin-enhanced Pc 4-PDT killing. The interesting question would be inside the cells whether JNK is activated in cytosol or mitochondria.

In vivo studies

Pc 4 is a potent photosensitizer and has shown promising efficacy without any safety issues in phase I clinical trial [98]. However, single drugs are unable to cure most cancers. The same limitation applies to PDT as a sole modality. Thus, combining PDT with other modalities to improve the therapeutic index has received much interest [201, 233, 234]. Furthermore, using PDT in solid tumors is challenging. Higher photosensitizer dosages may be required to achieve sufficient concentration deep in tumors. However, high dose photosensitizer may increase accumulation in normal tissues that might also be exposed to light (skin, eyes). Insufficient light pen-

etration, whether from surface-illumination or from implanted fibers, and decreased oxygen tension deep in poorly vascularized tumors can result in decreased formation of $^1\text{O}_2$ and other ROS, thereby diminishing the therapeutic effect of PDT. A primary determinant of PDT efficacy is the extent of ROS (including $^1\text{O}_2$) production. Thus, manipulations that increase intracellular ROS production within tumors during PDT should increase treatment efficacy.

Our pilot experiments show that adjuvant treatment with chloroquine enhanced tumor response to Pc 4-PDT especially in high Mfrn2 expressing tumors. These results suggest that Mfrn2 expression levels in tumors could be utilized as a biomarker predicting response to PDT. It would be interesting to measure Mfrn2 mRNA/protein levels in tumor samples from head and neck cancer patients and see how much variation is in Mfrn2 expression levels among patients. If there is a variation between samples, then patients with high Mfrn2 expressing tumors would benefit from adjuvant treatment of chloroquine during PDT.

Nanoparticles

Although PDT is an effective treatment it may have some off target effects, since systemic delivery of the photosensitizers distribute them throughout the body. An ideal situation would be to deliver the photosensitizer exclusively into tumors. Recent studies have focused on applying nanoparticles conjugated to Pc 4 to increase its cellular overall uptake and delivery [112]. Nanoparticles have also been decorated

with a small peptide of epidermal growth factor (EGF) that directs them to cancer cells overexpressing receptors for EGF [235, 236]. Since many tumors overexpress EGF receptors, this is an efficient way to deliver Pc 4 specifically into tumors. Therefore, future studies can be focused on Pc 4-conjugated nanoparticles that can be decorated with various cancer-specific molecules to enhance specificity of PDT *in vivo* studies.

Significance and Conclusion

To our knowledge, we are the first group to demonstrate that iron released from the lysosome and taken up into the mitochondria enhances mitochondrial Pc 4-PDT cytotoxicity [92]. In addition, our study here demonstrates that Mfn2 plays the essential role for PDT response in cancer cells. In conclusion, our results demonstrate that both the lysosomal event of iron release by bafilomycin and the mitochondrial event of iron uptake by Mfn2 are required as two hits to enhance Pc 4-PDT efficacy *in vitro*. Furthermore, our preliminary *in vivo* results also extend and confirm our *in vitro* finding of lysosomal alkalization reagents enhancing the PDT killing and impeding tumor regrowth. Taken together, we demonstrated that iron is an essential factor for mitochondrial PDT efficacy, and Mfn2 represents a possible biomarker for cancer response to Pc 4-PDT as well as a means to guide therapy choice during PDT treatment.

References

1. Kamangar, F., G.M. Dores, and W.F. Anderson, *Patterns of cancer incidence, mortality, and prevalence across five continents: defining priorities to reduce cancer disparities in different geographic regions of the world*. J Clin Oncol, 2006. 24(14): p. 2137-50.
2. de Souza, D.L., M.M. Perez, and M.P. Curado, *Predicted incidence of oral cavity, oropharyngeal, laryngeal, and hypopharyngeal cancer in Spain and implications for cancer control*. Cancer Epidemiol, 2011. 35(6): p. 510-4.
3. Parkin, D.M., et al., *Global cancer statistics, 2002*. CA Cancer J Clin, 2005. 55(2): p. 74-108.
4. Licitra, L. and E. Felip, *Squamous cell carcinoma of the head and neck: ESMO clinical recommendations for diagnosis, treatment and follow-up*. Ann Oncol, 2009. 20 Suppl 4: p. 121-2.
5. Silveira, N.J., et al., *Searching for molecular markers in head and neck squamous cell carcinomas (HNSCC) by statistical and bioinformatic analysis of larynx-derived SAGE libraries*. BMC Med Genomics, 2008. 1: p. 56.
6. Seiwert, T.Y. and E.E. Cohen, *State-of-the-art management of locally advanced head and neck cancer*. Br J Cancer, 2005. 92(8): p. 1341-8.
7. Chin, D., et al., *Novel markers for poor prognosis in head and neck cancer*. Int J Cancer, 2005. 113(5): p. 789-97.

8. Hashibe, M., et al., *Interaction between tobacco and alcohol use and the risk of head and neck cancer: pooled analysis in the International Head and Neck Cancer Epidemiology Consortium*. *Cancer Epidemiol Biomarkers Prev*, 2009. 18(2): p. 541-50.
9. Lopes, C.F., et al., *Concomitant consumption of marijuana, alcohol and tobacco in oral squamous cell carcinoma development and progression: Recent advances and challenges*. *Arch Oral Biol*, 2012.
10. Ogden, G.R. and A.J. Wight, *Aetiology of oral cancer: alcohol*. *Br J Oral Maxillofac Surg*, 1998. 36(4): p. 247-51.
11. Howie, N.M., et al., *Short-term exposure to alcohol increases the permeability of human oral mucosa*. *Oral Dis*, 2001. 7(6): p. 349-54.
12. Takayama, S. and K. Oota, *Induction of Malignant Tumors in Various Strains of Mice by Oral Administration of N-Nitrosodimethylamine and N-Nitrosodiethylamine*. *Gann*, 1965. 56: p. 189-99.
13. Saarinen, N.M., et al., *Role of dietary lignans in the reduction of breast cancer risk*. *Mol Nutr Food Res*, 2007. 51(7): p. 857-66.
14. Llewellyn, C.D., N.W. Johnson, and K.A. Warnakulasuriya, *Risk factors for squamous cell carcinoma of the oral cavity in young people--a comprehensive literature review*. *Oral Oncol*, 2001. 37(5): p. 401-18.
15. Taghavi, N. and I. Yazdi, *Type of food and risk of oral cancer*. *Arch Iran Med*, 2007. 10(2): p. 227-32.

16. Schwartz, J. and G. Shklar, *Regression of experimental oral carcinomas by local injection of beta-carotene and canthaxanthin*. Nutr Cancer, 1988. 11(1): p. 35-40.
17. Shklar, G., et al., *Prevention of experimental cancer and immunostimulation by vitamin E (immunosurveillance)*. J Oral Pathol Med, 1990. 19(2): p. 60-4.
18. Schwartz, J.L., et al., *The administration of beta carotene to prevent and regress oral carcinoma in the hamster cheek pouch and the associated enhancement of the immune response*. Adv Exp Med Biol, 1990. 262: p. 77-93.
19. Zain, R.B., *Cultural and dietary risk factors of oral cancer and precancer--a brief overview*. Oral Oncol, 2001. 37(3): p. 205-10.
20. Jia, W.H., et al., *Traditional Cantonese diet and nasopharyngeal carcinoma risk: a large-scale case-control study in Guangdong, China*. BMC Cancer, 2010. 10: p. 446.
21. Fong, L.Y., J.H. Ho, and D.P. Huang, *Preserved foods as possible cancer hazards: WA rats fed salted fish have mutagenic urine*. Int J Cancer, 1979. 23(4): p. 542-6.
22. Armstrong, R.W., et al., *Nasopharyngeal carcinoma in Malaysian Chinese: salted fish and other dietary exposures*. Int J Cancer, 1998. 77(2): p. 228-35.
23. Baker, S.R. and C.J. Krause, *Carcinoma of the lip*. Laryngoscope, 1980. 90(1): p. 19-27.

24. Inaba, T., [*Radiation induced carcinogenesis*]. *Nihon Rinsho*, 2012. 70(3): p. 421-6.
25. Nabaa, B., et al., *Assessment of Salivary Gland Dysfunction after Radioiodine Therapy for Thyroid Carcinoma Using Non-Contrast-Enhanced CT: The Significance of Changes in Volume and Attenuation of the Glands*. *AJNR Am J Neuroradiol*, 2012.
26. Tribius, S., et al., *HPV status in patients with head and neck of carcinoma of unknown primary site: HPV, tobacco smoking, and outcome*. *Oral Oncol*, 2012.
27. Smith, E.M., et al., *Complex etiology underlies risk and survival in head and neck cancer human papillomavirus, tobacco, and alcohol: a case for multifactor disease*. *J Oncol*, 2012. 2012: p. 571862.
28. Wagner, S., et al., [*Human papillomavirus (HPV) and head and neck cancer*]. *Hautarzt*, 2012. 63(1): p. 24-9.
29. Olthof, N.C., et al., *Next-generation treatment strategies for human papillomavirus-related head and neck squamous cell carcinoma: where do we go?* *Rev Med Virol*, 2012. 22(2): p. 88-105.
30. Ang, K.K. and E.M. Sturgis, *Human papillomavirus as a marker of the natural history and response to therapy of head and neck squamous cell carcinoma*. *Semin Radiat Oncol*, 2012. 22(2): p. 128-42.
31. Syrjanen, S., *Human papillomavirus (HPV) in head and neck cancer*. *J Clin Virol*, 2005. 32 Suppl 1: p. S59-66.

32. Psyrrri, A. and D. DiMaio, *Human papillomavirus in cervical and head-and-neck cancer*. Nat Clin Pract Oncol, 2008. 5(1): p. 24-31.
33. Fakhry, C. and M.L. Gillison, *Clinical implications of human papillomavirus in head and neck cancers*. J Clin Oncol, 2006. 24(17): p. 2606-11.
34. Smith, E.M., et al., *Age, sexual behavior and human papillomavirus infection in oral cavity and oropharyngeal cancers*. Int J Cancer, 2004. 108(5): p. 766-72.
35. Tezal, M., et al., *Local Inflammation and Human Papillomavirus Status of Head and Neck Cancers* *Local Inflammation and HPV in Head and Neck Cancer*. Arch Otolaryngol Head Neck Surg, 2012: p. 1-7.
36. Miller, D.L., M.D. Puricelli, and M.S. Stack, *Virology and molecular pathogenesis of HPV (human papillomavirus)-associated oropharyngeal squamous cell carcinoma*. Biochem J, 2012. 443(2): p. 339-53.
37. El-Mofty, S.K., *Human papillomavirus (HPV) related carcinomas of the upper aerodigestive tract*. Head Neck Pathol, 2007. 1(2): p. 181-5.
38. Mineta, H., et al., *Human papilloma virus (HPV) type 16 and 18 detected in head and neck squamous cell carcinoma*. Anticancer Res, 1998. 18(6B): p. 4765-8.
39. Naidu, A. and J.M. Wright, *The role of the human papillomavirus in oropharyngeal cancer*. J Mich Dent Assoc, 2011. 93(9): p. 44-8.

40. Lindel, K., et al., *Human papillomavirus positive squamous cell carcinoma of the oropharynx: a radiosensitive subgroup of head and neck carcinoma*. Cancer, 2001. 92(4): p. 805-13.
41. Wise-Draper, T.M., et al., *Future directions and treatment strategies for head and neck squamous cell carcinomas*. Transl Res, 2012.
42. Herrero, R., et al., *Human papillomavirus and oral cancer: the International Agency for Research on Cancer multicenter study*. J Natl Cancer Inst, 2003. 95(23): p. 1772-83.
43. Fakhry, C., et al., *Improved survival of patients with human papillomavirus-positive head and neck squamous cell carcinoma in a prospective clinical trial*. J Natl Cancer Inst, 2008. 100(4): p. 261-9.
44. Nichols, A.C., et al., *HPV-16 infection predicts treatment outcome in oropharyngeal squamous cell carcinoma*. Otolaryngol Head Neck Surg, 2009. 140(2): p. 228-34.
45. Haraf, D.J., et al., *Human papilloma virus and p53 in head and neck cancer: clinical correlates and survival*. Clin Cancer Res, 1996. 2(4): p. 755-62.
46. Gillison, M.L., et al., *Evidence for a causal association between human papillomavirus and a subset of head and neck cancers*. J Natl Cancer Inst, 2000. 92(9): p. 709-20.
47. Chen, C.A., et al., *Human papillomavirus DNA and p53 status in stage IB bulky cervical cancer*. J Cancer Res Clin Oncol, 1994. 120(11): p. 678-82.

48. Ishikawa, H., et al., *The effects of p53 status and human papillomavirus infection on the clinical outcome of patients with stage IIIB cervical carcinoma treated with radiation therapy alone*. *Cancer*, 2001. 91(1): p. 80-9.
49. Tse, K.P., et al., *The relationship between secretory leukocyte protease inhibitor expression and Epstein-Barr virus status among patients with nasopharyngeal carcinoma*. *Anticancer Res*, 2012. 32(4): p. 1299-307.
50. Adham, M., et al., *Nasopharyngeal carcinoma in Indonesia: epidemiology, incidence, signs, and symptoms at presentation*. *Chin J Cancer*, 2012.
51. Park, B.J., S.I. Chiosea, and J.R. Grandis, *Molecular changes in the multistage pathogenesis of head and neck cancer*. *Cancer Biomark*, 2010. 9(1-6): p. 325-39.
52. El-Naggar, A.K., *Pathobiology of head and neck squamous tumorigenesis*. *Curr Cancer Drug Targets*, 2007; 7(7): p. 606-12.
53. Haddad, R.I. and D.M. Shin, *Recent advances in head and neck cancer*. *N Engl J Med*, 2008. 359(11): p. 1143-54.
54. Agrawal, N., et al., *Exome sequencing of head and neck squamous cell carcinoma reveals inactivating mutations in NOTCH1*. *Science*, 2011. 333(6046): p. 1154-7.
55. Stransky, N., et al., *The mutational landscape of head and neck squamous cell carcinoma*. *Science*, 2011. 333(6046): p. 1157-60.

56. Howard, J.D., B. Lu, and C.H. Chung, *Therapeutic targets in head and neck squamous cell carcinoma: identification, evaluation, and clinical translation*. Oral Oncol, 2012. 48(1): p. 10-7.
57. Leemans, C.R., B.J. Braakhuis, and R.H. Brakenhoff, *The molecular biology of head and neck cancer*. Nat Rev Cancer, 2011. 11(1): p. 9-22.
58. Poeta, M.L., et al., *TP53 mutations and survival in squamous-cell carcinoma of the head and neck*. N Engl J Med, 2007. 357(25): p. 2552-61.
59. van Houten, V.M., et al., *Mutated p53 as a molecular marker for the diagnosis of head and neck cancer*. J Pathol, 2002. 198(4): p. 476-86.
60. Balz, V., et al., *Is the p53 inactivation frequency in squamous cell carcinomas of the head and neck underestimated? Analysis of p53 exons 2-11 and human papillomavirus 16/18 E6 transcripts in 123 unselected tumor specimens*. Cancer Res, 2003. 63(6): p. 1188-91.
61. Braakhuis, B.J., et al., *Genetic patterns in head and neck cancers that contain or lack transcriptionally active human papillomavirus*. J Natl Cancer Inst, 2004. 96(13): p. 998-1006.
62. Cmelak, A.J., *Current issues in combined modality therapy in locally advanced head and neck cancer*. Crit Rev Oncol Hematol, 2012.
63. van Dongen, G.A., et al., *Immuno-PET: a navigator in monoclonal antibody development and applications*. Oncologist, 2007. 12(12): p. 1379-89.
64. Vermorken, J.B., et al., *Platinum-based chemotherapy plus cetuximab in head and neck cancer*. N Engl J Med, 2008. 359(11): p. 1116-27.

65. Pignon, J.P., et al., *Chemotherapy added to locoregional treatment for head and neck squamous-cell carcinoma: three meta-analyses of updated individual data. MACH-NC Collaborative Group. Meta-Analysis of Chemotherapy on Head and Neck Cancer.* Lancet, 2000. 355(9208): p. 949-55.
66. Bourhis, J., et al., *Phase I/II study of cetuximab in combination with cisplatin or carboplatin and fluorouracil in patients with recurrent or metastatic squamous cell carcinoma of the head and neck.* J Clin Oncol, 2006. 24(18): p. 2866-72.
67. Bonner, J.A., et al., *Radiotherapy plus cetuximab for squamous-cell carcinoma of the head and neck.* N Engl J Med, 2006. 354(6): p. 567-78.
68. Graveland, A.P., et al., *Loss of heterozygosity at 9p and p53 immunopositivity in surgical margins predict local relapse in head and neck squamous cell carcinoma.* Int J Cancer, 2011. 128(8): p. 1852-9.
69. Watling, D.L., A.M. Gown, and M.D. Coltrera, *Overexpression of p53 in head and neck cancer.* Head Neck, 1992. 14(6): p. 437-44.
70. Peltonen, J.K., et al., *p53 in head and neck cancer: functional consequences and environmental implications of TP53 mutations.* Head Neck Oncol, 2010. 2: p. 36.
71. Erber, R., et al., *TP53 DNA contact mutations are selectively associated with allelic loss and have a strong clinical impact in head and neck cancer.* Oncogene, 1998. 16(13): p. 1671-9.

72. Skinner, H.D., et al., *TP53 disruptive mutations lead to head and neck cancer treatment failure through inhibition of radiation-induced senescence*. Clin Cancer Res, 2012. 18(1): p. 290-300.
73. Sandulache, V.C., et al., *Individualizing antimetabolic treatment strategies for head and neck squamous cell carcinoma based on TP53 mutational status*. Cancer, 2012. 118(3): p. 711-21.
74. Vassilev, L.T., *MDM2 inhibitors for cancer therapy*. Trends Mol Med, 2007. 13(1): p. 23-31.
75. *INGN 201: Ad-p53, Ad5CMV-p53, adenoviral p53, p53 gene therapy--introgen, RPR/INGN 201*. Drugs R D, 2007. 8(3): p. 176-87.
76. Nava, H.R., et al., *Photodynamic therapy (PDT) using HPPH for the treatment of precancerous lesions associated with barrett's esophagus*. Lasers Surg Med, 2011. 43(7): p. 705-12.
77. Agostinis, P., et al., *Photodynamic therapy of cancer: an update*. CA Cancer J Clin, 2011. 61(4): p. 250-81.
78. Ahn, M.Y., et al., *Pheophorbide a-mediated photodynamic therapy induces apoptotic cell death in murine oral squamous cell carcinoma in vitro and in vivo*. Oncol Rep, 2012. 27(6): p. 1772-8.
79. Baldea, I. and A.G. Filip, *Photodynamic therapy in melanoma - an update*. J Physiol Pharmacol, 2012. 63(2): p. 109-18.
80. Bader, M.J., et al., *Photodynamic Therapy of Bladder Cancer - A Phase I Study Using Hexaminolevulinate (HAL)*. Urol Oncol, 2012.

81. Johnson, R.P., et al., *Poly(L-histidine)-tagged 5-aminolevulinic acid prodrugs: new photosensitizing precursors of protoporphyrin IX for photodynamic colon cancer therapy*. Int J Nanomedicine, 2012. 7: p. 2497-512.
82. Goldberg, L.H., et al., *Evaluation of the chemopreventative effects of ALA PDT in patients with multiple actinic keratoses and a history of skin cancer*. J Drugs Dermatol, 2012. 11(5): p. 593-7.
83. Montazerabadi, A.R., et al., *Mitoxantrone as a prospective photosensitizer for photodynamic therapy of breast cancer*. Photodiagnosis Photodyn Ther, 2012. 9(1): p. 46-51.
84. Fateye, B., et al., *Combination of Phosphatidylinositol 3-Kinases Pathway Inhibitor and Photodynamic Therapy in Endothelial and Tumor Cells*. Photochem Photobiol, 2012.
85. Szliszka, E., et al., *Chlorin-based photodynamic therapy enhances the effect of tumor necrosis factor-related apoptosis-inducing ligand (TRAIL) in bladder cancer cells*. Med Sci Monit, 2012. 18(1): p. BR47-53.
86. Sakamoto, F.H., et al., *Surgical scar remodelling after photodynamic therapy using aminolaevulinic acid or its methylester: a retrospective, blinded study of patients with field cancerization*. Br J Dermatol, 2012. 166(2): p. 413-6.
87. Jeremic, G., et al., *Using photodynamic therapy as a neoadjuvant treatment in the surgical excision of nonmelanotic skin cancers: prospective study*. J Otolaryngol Head Neck Surg, 2011. 40 Suppl 1: p. S82-9.

88. O'Connor, A.E., W.M. Gallagher, and A.T. Byrne, *Porphyrin and nonporphyrin photosensitizers in oncology: preclinical and clinical advances in photodynamic therapy*. Photochem Photobiol, 2009. 85(5): p. 1053-74.
89. Robertson, C.A., D.H. Evans, and H. Abrahamse, *Photodynamic therapy (PDT): a short review on cellular mechanisms and cancer research applications for PDT*. J Photochem Photobiol B, 2009. 96(1): p. 1-8.
90. Dougherty, T.J., W.R. Potter, and K.R. Weishaupt, *The structure of the active component of hematoporphyrin derivative*. Prog Clin Biol Res, 1984. 170: p. 301-14.
91. Dolmans, D.E., D. Fukumura, and R.K. Jain, *Photodynamic therapy for cancer*. Nat Rev Cancer, 2003. 3(5): p. 380-7.
92. Saggu, S., et al., *Lysosomal signaling enhances mitochondria-mediated photodynamic therapy in A431 cancer cells: role of iron*. Photochem Photobiol, 2012. 88(2): p. 461-8.
93. Li, J.Z., et al., *Synthesis of novel long wavelength cationic chlorins via stereoselective aldol-like condensation*. Bioorg Med Chem Lett, 2012. 22(5): p. 1846-9.
94. Yoon, J.H., et al., *The enhanced anti-cancer effect of hexenyl ester of 5-aminolaevulinic acid photodynamic therapy in adriamycin-resistant compared to non-resistant breast cancer cells*. Lasers Surg Med, 2012. 44(1): p. 76-86.

95. Kubler, A., et al., [*Analysis of cost effectiveness of photodynamic therapy with Foscan (Foscan-PDT) in comparison with palliative chemotherapy in patients with advanced head-neck tumors in Germany*]. *Laryngorhinootologie*, 2005. 84(10): p. 725-32.
96. Wainwright, M., *Photodynamic therapy: the development of new photosensitisers*. *Anticancer Agents Med Chem*, 2008. 8(3): p. 280-91.
97. Rodriguez, M.E., et al., *Structural factors and mechanisms underlying the improved photodynamic cell killing with silicon phthalocyanine photosensitizers directed to lysosomes versus mitochondria*. *Photochem Photobiol*, 2009. 85(5): p. 1189-200.
98. Baron, E.D., et al., *Silicon phthalocyanine (Pc 4) photodynamic therapy is a safe modality for cutaneous neoplasms: results of a phase 1 clinical trial*. *Lasers Surg Med*, 2010. 42(10): p. 728-35.
99. Ben-Hur, E., et al., *Biodistribution and virus inactivation efficacy of a silicon phthalocyanine in red blood cell concentrates as a function of delivery vehicle*. *Photochem Photobiol*, 1995. 62(3): p. 575-9.
100. Oleinick, N.L., et al., *New phthalocyanine photosensitizers for photodynamic therapy*. *Photochem Photobiol*, 1993. 57(2): p. 242-7.
101. He, J., et al., *The synthesis, photophysical and photobiological properties and in vitro structure-activity relationships of a set of silicon phthalocyanine PDT photosensitizers*. *Photochem Photobiol*, 1997. 65(3): p. 581-6.

102. Anula, H.M., et al., *Synthesis and photophysical properties of silicon phthalocyanines with axial siloxy ligands bearing alkylamine termini*. J Phys Chem A, 2006. 110(15): p. 5215-23.
103. Molinari, A., et al., *m-THPC-mediated photodynamic therapy of malignant gliomas: assessment of a new transfection strategy*. Int J Cancer, 2007. 121(5): p. 1149-55.
104. Obwegeser, A., R. Jakober, and H. Kostron, *Uptake and kinetics of ¹⁴C-labelled meta-tetrahydroxyphenylchlorin and 5-aminolaevulinic acid in the C6 rat glioma model*. Br J Cancer, 1998. 78(6): p. 733-8.
105. Zimmermann, A., M. Ritsch-Marte, and H. Kostron, *mTHPC-mediated photodynamic diagnosis of malignant brain tumors*. Photochem Photobiol, 2001. 74(4): p. 611-6.
106. Kubler, A.C., et al., *Treatment of squamous cell carcinoma of the lip using Foscan-mediated photodynamic therapy*. Int J Oral Maxillofac Surg, 2001. 30(6): p. 504-9.
107. Morton, C.A., et al., *Comparison of red and green light in the treatment of Bowen's disease by photodynamic therapy*. Br J Dermatol, 2000. 143(4): p. 767-72.
108. Sakamoto, F.H., J.D. Lopes, and R.R. Anderson, *Photodynamic therapy for acne vulgaris: a critical review from basics to clinical practice: part I. Acne vulgaris: when and why consider photodynamic therapy?* J Am Acad Dermatol, 2010. 63(2): p. 183-93; quiz 193-4.

109. Svanberg, K., et al., *Photodynamic therapy of non-melanoma malignant tumours of the skin using topical delta-amino levulinic acid sensitization and laser irradiation*. Br J Dermatol, 1994. 130(6): p. 743-51.
110. Musiol, R., M. Serda, and J. Polanski, *Prodrugs in photodynamic anticancer therapy*. Curr Pharm Des, 2011. 17(32): p. 3548-59.
111. Master, A.M., et al., *EGFR-mediated intracellular delivery of Pc 4 nanoformulation for targeted photodynamic therapy of cancer: in vitro studies*. Nanomedicine, 2012. 8(5): p. 655-64.
112. Master, A.M., et al., *Delivery of the photosensitizer Pc 4 in PEG-PCL micelles for in vitro PDT studies*. J Pharm Sci, 2010. 99(5): p. 2386-98.
113. Jerjes, W., et al., *The surgical palliation of advanced head and neck cancer using photodynamic therapy*. Clin Oncol (R Coll Radiol), 2010. 22(9): p. 785-91.
114. Bredell, M.G., et al., *The application and challenges of clinical PD-PDT in the head and neck region: a short review*. J Photochem Photobiol B, 2010. 101(3): p. 185-90.
115. Biel, M.A., *Photodynamic therapy and the treatment of head and neck neoplasia*. Laryngoscope, 1998. 108(9): p. 1259-68.
116. Biel, M., *Advances in photodynamic therapy for the treatment of head and neck cancers*. Lasers Surg Med, 2006. 38(5): p. 349-55.

117. Keller, G.S., D.R. Doiron, and G.U. Fisher, *Photodynamic therapy in otolaryngology--head and neck surgery*. Arch Otolaryngol, 1985. 111(11): p. 758-61.
118. Feyh, J., et al., *Photodynamic therapy in head and neck surgery*. J Photochem Photobiol B, 1990. 7(2-4): p. 353-8.
119. Copper, M.P., et al., *Photodynamic therapy in the treatment of multiple primary tumours in the head and neck, located to the oral cavity and oropharynx*. Clin Otolaryngol, 2007. 32(3): p. 185-9.
120. D'Cruz, A.K., M.H. Robinson, and M.A. Biel, *mTHPC-mediated photodynamic therapy in patients with advanced, incurable head and neck cancer: a multicenter study of 128 patients*. Head Neck, 2004. 26(3): p. 232-40.
121. Grant, W.E., et al., *Photodynamic therapy of oral cancer: photosensitisation with systemic aminolaevulinic acid*. Lancet, 1993. 342(8864): p. 147-8.
122. Sieron, A., et al., *Photodynamic therapy of premalignant lesions and local recurrence of laryngeal and hypopharyngeal cancers*. Eur Arch Otorhinolaryngol, 2001. 258(7): p. 349-52.
123. Oleinick, N.L., R.L. Morris, and I. Belichenko, *The role of apoptosis in response to photodynamic therapy: what, where, why, and how*. Photochem Photobiol Sci, 2002. 1(1): p. 1-21.

124. Pazos, M.C. and H.B. Nader, *Effect of photodynamic therapy on the extracellular matrix and associated components*. Braz J Med Biol Res, 2007. 40(8): p. 1025-35.
125. Ochsner, M., *Light scattering of human skin: a comparison between zinc (II)-phthalocyanine and photofrin II*. J Photochem Photobiol B, 1996. 32(1-2): p. 3-9.
126. Plaetzer, K., et al., *Photophysics and photochemistry of photodynamic therapy: fundamental aspects*. Lasers Med Sci, 2009. 24(2): p. 259-68.
127. Juzeniene, A., K.P. Nielsen, and J. Moan, *Biophysical aspects of photodynamic therapy*. J Environ Pathol Toxicol Oncol, 2006. 25(1-2): p. 7-28.
128. Brancalion, L. and H. Moseley, *Laser and non-laser light sources for photodynamic therapy*. Lasers Med Sci, 2002. 17(3): p. 173-86.
129. Jarvi, M.T., M.S. Patterson, and B.C. Wilson, *Insights into photodynamic therapy dosimetry: simultaneous singlet oxygen luminescence and photosensitizer photobleaching measurements*. Biophys J, 2012. 102(3): p. 661-71.
130. Beyer, W., *Systems for light application and dosimetry in photodynamic therapy*. J Photochem Photobiol B, 1996. 36(2): p. 153-6.
131. Sitnik, T.M., J.A. Hampton, and B.W. Henderson, *Reduction of tumour oxygenation during and after photodynamic therapy in vivo: effects of fluence rate*. Br J Cancer, 1998. 77(9): p. 1386-94.

132. Curnow, A., J.C. Haller, and S.G. Bown, *Oxygen monitoring during 5-aminolaevulinic acid induced photodynamic therapy in normal rat colon. Comparison of continuous and fractionated light regimes.* J Photochem Photobiol B, 2000. 58(2-3): p. 149-55.
133. Maier, A., et al., *Combined photodynamic therapy and hyperbaric oxygenation in carcinoma of the esophagus and the esophago-gastric junction.* Eur J Cardiothorac Surg, 2000. 18(6): p. 649-54; discussion 654-5.
134. Tomaselli, F., et al., *Acute effects of combined photodynamic therapy and hyperbaric oxygenation in lung cancer--a clinical pilot study.* Lasers Surg Med, 2001. 28(5): p. 399-403.
135. Dysart, J.S. and M.S. Patterson, *Characterization of Photofrin photobleaching for singlet oxygen dose estimation during photodynamic therapy of MLL cells in vitro.* Phys Med Biol, 2005. 50(11): p. 2597-616.
136. Moan, J., et al., *Intracellular localization of photosensitizers.* Ciba Found Symp, 1989. 146: p. 95-107; discussion 107-11.
137. Ketabchi, A., et al., *Induction of apoptotic cell death by photodynamic therapy in human keratinocytes.* Arch Oral Biol, 1998. 43(2): p. 143-9.
138. Kessel, D. and M. Castelli, *Evidence that bcl-2 is the target of three photosensitizers that induce a rapid apoptotic response.* Photochem Photobiol, 2001. 74(2): p. 318-22.

139. Xue, L.Y., S.M. Chiu, and N.L. Oleinick, *Photochemical destruction of the Bcl-2 oncoprotein during photodynamic therapy with the phthalocyanine photosensitizer Pc 4*. *Oncogene*, 2001. 20(26): p. 3420-7.
140. Usuda, J., et al., *Domain-dependent photodamage to Bcl-2. A membrane anchorage region is needed to form the target of phthalocyanine photosensitization*. *J Biol Chem*, 2003. 278(3): p. 2021-9.
141. Buytaert, E., M. Dewaele, and P. Agostinis, *Molecular effectors of multiple cell death pathways initiated by photodynamic therapy*. *Biochim Biophys Acta*, 2007. 1776(1): p. 86-107.
142. Kessel, D., *Relocalization of cationic porphyrins during photodynamic therapy*. *Photochem Photobiol Sci*, 2002. 1(11): p. 837-40.
143. Vanlangenakker, N., et al., *Molecular mechanisms and pathophysiology of necrotic cell death*. *Curr Mol Med*, 2008. 8(3): p. 207-20.
144. Wu, W., P. Liu, and J. Li, *Necroptosis: an emerging form of programmed cell death*. *Crit Rev Oncol Hematol*, 2012. 82(3): p. 249-58.
145. Dewaele, M., H. Maes, and P. Agostinis, *ROS-mediated mechanisms of autophagy stimulation and their relevance in cancer therapy*. *Autophagy*, 2010. 6(7): p. 838-54.
146. Chiu, S.M., et al., *Bax is essential for mitochondrion-mediated apoptosis but not for cell death caused by photodynamic therapy*. *Br J Cancer*, 2003. 89(8): p. 1590-7.

147. Chiu, S.M., et al., *Photodynamic therapy-induced death of HCT 116 cells: Apoptosis with or without Bax expression*. *Apoptosis*, 2005. 10(6): p. 1357-68.
148. Kessel, D. and J.J. Reiners, Jr., *Apoptosis and autophagy after mitochondrial or endoplasmic reticulum photodamage*. *Photochem Photobiol*, 2007. 83(5): p. 1024-8.
149. Kessel, D., M.G. Vicente, and J.J. Reiners, Jr., *Initiation of apoptosis and autophagy by photodynamic therapy*. *Autophagy*, 2006. 2(4): p. 289-90.
150. Xue, L.Y., et al., *The death of human cancer cells following photodynamic therapy: apoptosis competence is necessary for Bcl-2 protection but not for induction of autophagy*. *Photochem Photobiol*, 2007. 83(5): p. 1016-23.
151. Huang, Z., et al., *Photodynamic therapy for treatment of solid tumors--potential and technical challenges*. *Technol Cancer Res Treat*, 2008. 7(4): p. 309-20.
152. Star, W.M., et al., *Destructive effect of photoradiation on the microcirculation of a rat mammary tumor growing in "sandwich" observation chambers*. *Prog Clin Biol Res*, 1984. 170: p. 637-45.
153. Chen, B., et al., *Vascular and cellular targeting for photodynamic therapy*. *Crit Rev Eukaryot Gene Expr*, 2006. 16(4): p. 279-305.
154. Fingar, V.H., *Vascular effects of photodynamic therapy*. *J Clin Laser Med Surg*, 1996. 14(5): p. 323-8.

155. Abels, C., *Targeting of the vascular system of solid tumours by photodynamic therapy (PDT)*. Photochem Photobiol Sci, 2004. 3(8): p. 765-71.
156. Korbelik, M., *PDT-associated host response and its role in the therapy outcome*. Lasers Surg Med, 2006. 38(5): p. 500-8.
157. Krosl, G., M. Korbelik, and G.J. Dougherty, *Induction of immune cell infiltration into murine SCCVII tumour by photofrin-based photodynamic therapy*. Br J Cancer, 1995. 71(3): p. 549-55.
158. Korbelik, M. and I. Cecic, *Contribution of myeloid and lymphoid host cells to the curative outcome of mouse sarcoma treatment by photodynamic therapy*. Cancer Lett, 1999. 137(1): p. 91-8.
159. Garg, A.D., et al., *DAMPs and PDT-mediated photo-oxidative stress: exploring the unknown*. Photochem Photobiol Sci, 2011. 10(5): p. 670-80.
160. Sun, J., et al., *Neutrophils as inflammatory and immune effectors in photodynamic therapy-treated mouse SCCVII tumours*. Photochem Photobiol Sci, 2002. 1(9): p. 690-5.
161. Gollnick, S.O., et al., *Role of cytokines in photodynamic therapy-induced local and systemic inflammation*. Br J Cancer, 2003. 88(11): p. 1772-9.
162. Abdel-Hady, E.S., et al., *Immunological and viral factors associated with the response of vulval intraepithelial neoplasia to photodynamic therapy*. Cancer Res, 2001. 61(1): p. 192-6.

163. Kabingu, E., et al., *CD8+ T cell-mediated control of distant tumours following local photodynamic therapy is independent of CD4+ T cells and dependent on natural killer cells*. Br J Cancer, 2007. 96(12): p. 1839-48.
164. Kessel, D. and C. Erickson, *Porphyrin photosensitization of multi-drug resistant cell types*. Photochem Photobiol, 1992. 55(3): p. 397-9.
165. Friedberg, J.S., et al., *A phase I study of Foscan-mediated photodynamic therapy and surgery in patients with mesothelioma*. Ann Thorac Surg, 2003. 75(3): p. 952-9.
166. Crescenzi, E., et al., *Photodynamic therapy with indocyanine green complements and enhances low-dose cisplatin cytotoxicity in MCF-7 breast cancer cells*. Mol Cancer Ther, 2004. 3(5): p. 537-44.
167. Pogue, B.W., et al., *Photodynamic therapy with verteporfin in the radiation-induced fibrosarcoma-1 tumor causes enhanced radiation sensitivity*. Cancer Res, 2003. 63(5): p. 1025-33.
168. Nahabedian, M.Y., et al., *Combination cytotoxic chemotherapy with cisplatin or doxorubicin and photodynamic therapy in murine tumors*. J Natl Cancer Inst, 1988. 80(10): p. 739-43.
169. Yang, P.W., et al., *The effects of Photofrin-mediated photodynamic therapy on the modulation of EGFR in esophageal squamous cell carcinoma cells*. Lasers Med Sci, 2012.

170. Golab, J., et al., *Erythropoietin restores the antitumor effectiveness of photodynamic therapy in mice with chemotherapy-induced anemia*. Clin Cancer Res, 2002. 8(5): p. 1265-70.
171. Peng, Q., et al., *Antitumor effect of 5-aminolevulinic acid-mediated photodynamic therapy can be enhanced by the use of a low dose of photofrin in human tumor xenografts*. Cancer Res, 2001. 61(15): p. 5824-32.
172. Hentze, M.W., M.U. Muckenthaler, and N.C. Andrews, *Balancing acts: molecular control of mammalian iron metabolism*. Cell, 2004. 117(3): p. 285-97.
173. MacKenzie, E.L., K. Iwasaki, and Y. Tsuji, *Intracellular iron transport and storage: from molecular mechanisms to health implications*. Antioxid Redox Signal, 2008. 10(6): p. 997-1030.
174. Papanikolaou, G. and K. Pantopoulos, *Iron metabolism and toxicity*. Toxicol Appl Pharmacol, 2005. 202(2): p. 199-211.
175. Rouault, T.A. and W.H. Tong, *Iron-sulphur cluster biogenesis and mitochondrial iron homeostasis*. Nat Rev Mol Cell Biol, 2005. 6(4): p. 345-51.
176. Lill, R. and U. Muhlenhoff, *Iron-sulfur protein biogenesis in eukaryotes: components and mechanisms*. Annu Rev Cell Dev Biol, 2006. 22: p. 457-86.
177. Almeida, A.M., et al., *Mitochondrial DNA damage associated with lipid peroxidation of the mitochondrial membrane induced by Fe²⁺-citrate*. An Acad Bras Cienc, 2006. 78(3): p. 505-14.

178. Beard, J., *Iron deficiency alters brain development and functioning*. J Nutr, 2003. 133(5 Suppl 1): p. 1468S-72S.
179. Munoz, M., I. Villar, and J.A. Garcia-Erce, *An update on iron physiology*. World J Gastroenterol, 2009. 15(37): p. 4617-26.
180. Kurz, T., A. Terman, and U.T. Brunk, *Autophagy, ageing and apoptosis: the role of oxidative stress and lysosomal iron*. Arch Biochem Biophys, 2007. 462(2): p. 220-30.
181. Bishop, G.M., et al., *Iron: a pathological mediator of Alzheimer disease?* Dev Neurosci, 2002. 24(2-3): p. 184-7.
182. Kaur, D. and J. Andersen, *Does cellular iron dysregulation play a causative role in Parkinson's disease?* Ageing Res Rev, 2004. 3(3): p. 327-43.
183. Trinder, D., et al., *Molecular pathogenesis of iron overload*. Gut, 2002. 51(2): p. 290-5.
184. Yu, Y., et al., *Iron chelators for the treatment of cancer*. Curr Med Chem, 2012. 19(17): p. 2689-702.
185. Brissot, P., et al., *Non-transferrin bound iron: A key role in iron overload and iron toxicity*. Biochim Biophys Acta, 2012. 1820(3): p. 403-10.
186. Zhou, T., et al., *Design of iron chelators with therapeutic application*. Dalton Trans, 2012. 41(21): p. 6371-89.
187. Oppenheimer, S.J., *Iron and infection in the tropics: paediatric clinical correlates*. Ann Trop Paediatr, 1998. 18 Suppl: p. S81-7.

188. Oudit, G.Y., et al., *Role of L-type Ca²⁺ channels in iron transport and iron-overload cardiomyopathy*. J Mol Med (Berl), 2006. 84(5): p. 349-64.
189. Aisen, P., A. Leibman, and J. Zweier, *Stoichiometric and site characteristics of the binding of iron to human transferrin*. J Biol Chem, 1978. 253(6): p. 1930-7.
190. Richardson, D.R. and P. Ponka, *The molecular mechanisms of the metabolism and transport of iron in normal and neoplastic cells*. Biochim Biophys Acta, 1997. 1331(1): p. 1-40.
191. Mackenzie, B., et al., *Divalent metal-ion transporter DMT1 mediates both H⁺-coupled Fe²⁺ transport and uncoupled fluxes*. Pflugers Arch, 2006. 451(4): p. 544-58.
192. Arosio, P., R. Ingrassia, and P. Cavadini, *Ferritins: a family of molecules for iron storage, antioxidation and more*. Biochim Biophys Acta, 2009. 1790(7): p. 589-99.
193. Santambrogio, P., et al., *Mitochondrial ferritin expression in adult mouse tissues*. J Histochem Cytochem, 2007. 55(11): p. 1129-37.
194. Kurz, T., J.W. Eaton, and U.T. Brunk, *The role of lysosomes in iron metabolism and recycling*. Int J Biochem Cell Biol, 2011. 43(12): p. 1686-97.
195. Nemeth, E., et al., *Hepcidin regulates cellular iron efflux by binding to ferroportin and inducing its internalization*. Science, 2004. 306(5704): p. 2090-3.

196. Hentze, M.W., et al., *Two to tango: regulation of Mammalian iron metabolism*. Cell, 2010. 142(1): p. 24-38.
197. Rouault, T.A., *The role of iron regulatory proteins in mammalian iron homeostasis and disease*. Nat Chem Biol, 2006. 2(8): p. 406-14.
198. Metzendorf, C., W. Wu, and M.I. Lind, *Overexpression of Drosophila mitoferrin in l(2)mbn cells results in dysregulation of Fer1HCH expression*. Biochem J, 2009. 421(3): p. 463-71.
199. Paradkar, P.N., et al., *Regulation of mitochondrial iron import through differential turnover of mitoferrin 1 and mitoferrin 2*. Mol Cell Biol, 2009. 29(4): p. 1007-16.
200. Li, F.Y., et al., *Characterization of a novel human putative mitochondrial transporter homologous to the yeast mitochondrial RNA splicing proteins 3 and 4*. FEBS Lett, 2001. 494(1-2): p. 79-84.
201. Pizova, K., et al., *Photodynamic therapy for enhancing antitumour immunity*. Biomed Pap Med Fac Univ Palacky Olomouc Czech Repub, 2012. 156(2): p. 93-102.
202. Yano, T., et al., *Phase I study of photodynamic therapy using talaporfin sodium and diode laser for local failure after chemoradiotherapy for esophageal cancer*. Radiat Oncol, 2012. 7: p. 113.
203. Li, P., et al., *Photodynamic therapy with hyperbranched poly(ether-ester) chlorin(e6) nanoparticles on human tongue carcinoma CAL-27 cells*. Photodiagnosis Photodyn Ther, 2012. 9(1): p. 76-82.

204. Lam, M., N.L. Oleinick, and A.L. Nieminen, *Photodynamic therapy-induced apoptosis in epidermoid carcinoma cells. Reactive oxygen species and mitochondrial inner membrane permeabilization*. J Biol Chem, 2001. 276(50): p. 47379-86.
205. Uchiyama, A., et al., *Translocation of iron from lysosomes into mitochondria is a key event during oxidative stress-induced hepatocellular injury*. Hepatology, 2008. 48(5): p. 1644-54.
206. Kuo, K.L., et al., *Intravenous iron exacerbates oxidative DNA damage in peripheral blood lymphocytes in chronic hemodialysis patients*. J Am Soc Nephrol, 2008. 19(9): p. 1817-26.
207. Nieminen, A.L., et al., *A novel cytotoxicity screening assay using a multiwell fluorescence scanner*. Toxicol Appl Pharmacol, 1992. 115(2): p. 147-55.
208. Griffiths, G., et al., *The mannose 6-phosphate receptor and the biogenesis of lysosomes*. Cell, 1988. 52(3): p. 329-41.
209. Gagliardi, S., M. Rees, and C. Farina, *Chemistry and structure activity relationships of bafilomycin A1, a potent and selective inhibitor of the vacuolar H⁺-ATPase*. Curr Med Chem, 1999. 6(12): p. 1197-212.
210. Gunshin, H., et al., *Cloning and characterization of a mammalian proton-coupled metal-ion transporter*. Nature, 1997. 388(6641): p. 482-8.
211. Lane, D.J., et al., *Two routes of iron accumulation in astrocytes: ascorbate-dependent ferrous iron uptake via the divalent metal transporter (DMT1) plus an independent route for ferric iron*. Biochem J, 2010. 432(1): p. 123-32.

212. Fulda, S., *Tumor resistance to apoptosis*. Int J Cancer, 2009. 124(3): p. 511-5.
213. Fehrenbacher, N. and M. Jaattela, *Lysosomes as targets for cancer therapy*. Cancer Res, 2005. 65(8): p. 2993-5.
214. Linder, S. and M.C. Shoshan, *Lysosomes and endoplasmic reticulum: targets for improved, selective anticancer therapy*. Drug Resist Updat, 2005. 8(4): p. 199-204.
215. Berndt, C., et al., *Chelation of lysosomal iron protects against ionizing radiation*. Biochem J, 2010. 432(2): p. 295-301.
216. Buckett, P.D. and M. Wessling-Resnick, *Small molecule inhibitors of divalent metal transporter-1*. Am J Physiol Gastrointest Liver Physiol, 2009. 296(4): p. G798-804.
217. Wetli, H.A., P.D. Buckett, and M. Wessling-Resnick, *Small-molecule screening identifies the selanazol drug ebselen as a potent inhibitor of DMT1-mediated iron uptake*. Chem Biol, 2006. 13(9): p. 965-72.
218. De Stefani, D., et al., *A forty-kilodalton protein of the inner membrane is the mitochondrial calcium uniporter*. Nature, 2011. 476(7360): p. 336-40.
219. Baughman, J.M., et al., *Integrative genomics identifies MCU as an essential component of the mitochondrial calcium uniporter*. Nature, 2011. 476(7360): p. 341-5.
220. Knowles, H.J., et al., *Effect of ascorbate on the activity of hypoxia-inducible factor in cancer cells*. Cancer Res, 2003. 63(8): p. 1764-8.

221. Yang, S., et al., *Pancreatic cancers require autophagy for tumor growth*. Genes Dev, 2011. 25(7): p. 717-29.
222. Flatmark, T. and I. Romslo, *Energy-dependent accumulation of iron by isolated rat liver mitochondria. Requirement of reducing equivalents and evidence for a unidirectional flux of Fe(II) across the inner membrane*. J Biol Chem, 1975. 250(16): p. 6433-8.
223. Shaw, G.C., et al., *Mitoferrin is essential for erythroid iron assimilation*. Nature, 2006. 440(7080): p. 96-100.
224. Satre, M., et al., *Mitochondrial carrier family: repertoire and peculiarities of the cellular slime mould Dictyostelium discoideum*. Biochimie, 2007. 89(9): p. 1058-69.
225. Froschauer, E.M., R.J. Schweyen, and G. Wiesenberger, *The yeast mitochondrial carrier proteins: Mrs3p/Mrs4p mediate iron transport across the inner mitochondrial membrane*. Biochim Biophys Acta, 2009. 1788(5): p. 1044-50.
226. Amigo, J.D., et al., *Identification of distal cis-regulatory elements at mouse mitoferrin loci using zebrafish transgenesis*. Mol Cell Biol, 2011. 31(7): p. 1344-56.
227. Troadec, M.B., et al., *Targeted deletion of the mouse Mitoferrin1 gene: from anemia to protoporphyria*. Blood, 2011. 117(20): p. 5494-502.

228. Ren, Y., et al., *Reduction of mitoferrin results in abnormal development and extended lifespan in Caenorhabditis elegans*. PLoS One, 2012. 7(1): p. e29666.
229. Richardson, D.R., et al., *Mitochondrial iron trafficking and the integration of iron metabolism between the mitochondrion and cytosol*. Proc Natl Acad Sci U S A, 2010. 107(24): p. 10775-82.
230. Chen, W., H.A. Dailey, and B.H. Paw, *Ferrochelatase forms an oligomeric complex with mitoferrin-1 and Abcb10 for erythroid heme biosynthesis*. Blood, 2010. 116(4): p. 628-30.
231. Bhattacharyya, S., J. Ghosh, and P.C. Sil, *Iron induces hepatocytes death via MAPK activation and mitochondria-dependent apoptotic pathway: Beneficial role of glycine*. Free Radic Res, 2012.
232. Verma, G. and M. Datta, *The critical role of JNK in the ER-mitochondrial crosstalk during apoptotic cell death*. J Cell Physiol, 2012. 227(5): p. 1791-5.
233. Lindenmann, J., et al., *Individualized, multimodal palliative treatment of inoperable esophageal cancer: clinical impact of photodynamic therapy resulting in prolonged survival*. Lasers Surg Med, 2012. 44(3): p. 189-98.
234. Tuncer, S., N. Kir, and C.L. Shields, *Dramatic regression of amelanotic choroidal melanoma with PDT following poor response to brachytherapy*. Ophthalmic Surg Lasers Imaging, 2012. 43(3): p. e38-40.

235. Kameyama, N., et al., *Photodynamic therapy using an anti-EGF receptor antibody complexed with verteporfin nanoparticles: a proof of concept study*. *Cancer Biother Radiopharm*, 2011. 26(6): p. 697-704.
236. Master, A.M., et al., *Optimization of a Nanomedicine-Based Silicon Phthalocyanine 4 Photodynamic Therapy (Pc 4-PDT) Strategy for Targeted Treatment of EGFR-Overexpressing Cancers*. *Mol Pharm*, 2012.